ANALYTICAL MODELS FOR FLOWING-FLUID TEMPERATURE DISTRIBUTION IN SINGLE-PHASE OIL RESERVOIRS ACCOUNTING FOR JOULE-THOMSON EFFECT

A Thesis

by

NATASHA CHEVARUNOTAI

Submitted to the Office of Graduate and Professional Studies of
Texas A&M University
in partial fulfillment of the requirements for the degree of

MASTER OF SCIENCE

Chair of Committee:	A. Rashid Hasan
Committee Members:	Peter P. Valko
	Jianxin Zhou
Head of Department:	A. Daniel Hill

December 2014

Major Subject: Petroleum Engineering

ABSTRACT

Modern downhole temperature measurements indicate that bottomhole fluid temperature could be significantly higher or lower than the original reservoir temperature, especially in 'more challenging' low-permeability reservoirs, where high pressure drawdown is expected during production. This recent finding contradicts the isothermal assumption originally made for typical conventional reservoirs. In a high-pressure drawdown environment, Joule-Thomson (J-T) phenomenon plays an important role in fluid temperature alteration in the reservoir.

In this study, we developed a robust analytical model to estimate the flowing-fluid-temperature distribution in the reservoir accounting for J-T heating or cooling effect. All significant heat-transfer mechanisms for fluid flow in the reservoir, including heat transfer due to conduction, convection, and heat transfer from over- and -under-burden formations to the reservoir, as well as temperature change due to J-T phenomena, are incorporated in this study. The proposed model is successfully validated with results from a rigorous numerical simulator using field data. In general, a more accurate flowing-fluid temperature calculation leads to better estimates of well productivity index, which is one of the key parameters in production optimization and field development planning.

Sensitivity analysis results show that production rate, reservoir permeability, fluid viscosity, and J-T coefficient are critical parameters in reservoir flowing-fluid temperature calculation. Findings from the sensitivity analysis allow us to make a

decision whether or not to acquire more data or to perform additional tests for a more reasonable outcome- the flowing-fluid temperature in the reservoir.

Bottomhole flowing-fluid temperature from the proposed analytical model can be further coupled with wellbore heat-transfer model to allow prediction of flowing-fluid temperature along the wellbore up to surface. The flowing-fluid temperature profile along the wellbore is normally very useful for well design and production optimization in production engineering, as well as for pressure-transient analysis.

DEDICATION

To my parents and sisters for their unconditional love and support.

ACKNOWLEDGEMENTS

I would like to take this opportunity to express my gratitude to my advisor, Dr. A. Rashid Hasan for his technical guidance and continuous support throughout the course of this research. I am very thankful for his kindness and willingness to always help me on both work and life during my years at Texas A&M University. I also would like to thank Dr. Peter P. Valko and Dr. Jianxin Zhou for serving as my committee members. Their recommendations and supports are greatly appreciated.

I would like to extend my sincere gratitude to my mentor, Shah Kabir from Hess Corporation, who always gave useful guidance and inspired me throughout the course of this study.

I also thank Chevron Thailand Exploration and Production, Ltd. for their financial support throughout my study at Texas A&M University.

Thanks to all of my friends at Texas A&M University for making my time here a great and memorable experience. I am very grateful for their friendship and support during my two years here.

Finally, I would like to express a sincere appreciation to my mother, father, and sisters, for supporting my decision and encouraging me to accomplish one of the key goals in my life, and to my fiancé, for his love, patience, and always believing in me.

NOMENCLATURE

A	flow area, ft^2, L^2
A_s	reservoir top-and-bottom surface area, ft^2, L^2
B_o	oil formation volume factor, bbl/STB
c_t	total compressibility, 1/psi, Lt^2/m
C_p	system specific heat capacity, Btu/lbm.°F, L^2/t^2T
C_{pf}	formation specific heat capacity, Btu/lbm.°F, L^2/t^2T
C_{po}	oil specific heat capacity, Btu/lbm.°F, L^2/t^2T
C_{pw}	water specific heat capacity, Btu/lbm.°F, L^2/t^2T
h	formation thickness, ft, L
h_c	heat transfer coefficient, Btu/hr.ft^2.°F, $m/t^3/T$
$\hat{H}$	enthalpy, lbm.ft^2/hr^2, mL^2/t^2
$\hat{H}_f$	enthalpy of formation, lbm.ft^2/hr^2, mL^2/t^2
$\hat{H}_o$	enthalpy of oil, lbm.ft^2/hr^2, mL^2/t^2
$\hat{H}_w$	enthalpy of water, lbm.ft^2/hr^2, mL^2/t
J	productivity index, STB/D.psi, L^4t/m
k	reservoir permeability, md, L^2
p	pressure, psi, m/Lt^2
p_b	bubble point pressure, psi, m/Lt^2
p_D	dimensionless pressure
p_e	pressure at reservoir external boundary, psi, m/Lt^2

p_i	initial reservoir pressure, psi, m/Lt^2
p_{wf}	flowing-fluid pressure at well bottom, psi, m/Lt^2
p_r	average reservoir pressure, psi, m/Lt^2
PI	productivity index, STB/D.psi, L^4t/m
q	volumetric flow rate, ft^3/hr, L^3/t
$p(r,t)$	pressure at particular radius and time, psi, m/Lt^2
$\dot{Q}$	net heat transfer rate between the system and surroundings, $Btu/hr.ft^2$, m/Lt^3
r	radius, ft, L
r_D	dimensionless radius
r_e	external reservoir radius, ft, L
r_{eD}	dimensioness external reservoir radius
r_w	wellbore radius, ft, L
S	saturation
S_o	oil saturation
S_w	water saturation
S_{wi}	irreducible water saturation
t	time, hr, t
t_D	dimensionless time
T	fluid temperature, °F, T
T_e	fluid temperature at reservoir external boundary, °F, T
T_i	initial reservoir temperature, °F, T

T_s	temperature of overburden and underburden formations, °F, T
T_{wf}	flowing-fluid temperature at well bottom, °F, T
$T(r,t)$	fluid temperature at particular radius and time, °F, T
$\vec{u}$	superficial velocity, ft/hr, L/t
u_r	fluid local velocity in radial direction, ft/hr, L/t
$\hat{U}$	fluid internal energy, lbm.ft^2/hr^2, mL^2/t^2
$\hat{V}$	specific volume, ft^3/lbm, L^3/m
λ	reservoir thermal conductivity, Btu/hr.ft.°F, TLt^2/m
μ	fluid viscosity, cp, m/Lt
ρ	density, lbm/ft^3, m/L^3
ρ_o	oil density, lbm/ft^3, m/L^3
ρ_w	water density, lbm/ft^3, m/L^3
ρ_f	formation density, lbm/ft^3, m/L^3
σ_o	Joule Thomson throttling coefficient of oil, Btu/lbm.psi, L^3/m
σ_w	Joule Thomson throttling coefficient of water, Btu/lbm.psi, L^3/m
$\vec{\tau}$	stress, lbf/ft^2, m/Lt^2
ϕ	porosity

TABLE OF CONTENTS

LIST OF FIGURES

FIGURE Page

FIGURE Page

LIST OF TABLES

CHAPTER I

INTRODUCTION

1.1 Introduction and Literature Review

Conventionally, a reservoir is assumed to be isothermal; that is, at a given depth, reservoir temperature is the same across the reservoir. Most of the time, temperature of the fluid entering at the perforations is assumed to be the same as that in the reservoir at a given depth and is treated as constant over time, regardless of changes in flow condition. Downhole temperature measurement during pressure transient tests in conventional reservoirs show that fluid flowing temperature at bottomhole does change when the well is flowing at different rates, but the changes are minimal and normally assumed to be negligible.

For many modern, deepwater reservoirs with significant drawdown, such as those in the Gulf of Mexico, neglecting temperature change along the radial direction may be unwise. There have been several studies on radial fluid-temperature distribution in the reservoir. Early attempts to establish fluid temperature model were mainly for heavy-oil reservoir management in thermal recovery operations to achieve maximum recovery. Most of the models developed for thermal recovery treated heat conduction and convection as main heat-transfer mechanisms in the reservoir. Fluid temperature change because of other energy transfer phenomena, such as Joule-Thomson effect, is rarely taken into account in this model category.

One of the earliest models for estimating temperature distribution in thermal recovery reservoirs was presented by Lauwerier (1955). He developed an analytical solution for fluid temperature in a 1D linear flow system. The main heat-transfer mechanisms in his study are heat conduction from a layer of hot water being injected into over- and under-burden layers and heat convection due to transportation of hot fluid into the reservoir. He assumed that water layer has the same temperature across the reservoir and that there is no conduction in the lateral direction. No viscous dissipation (Joule-Thomson (J-T) effect) is incorporated in his analysis since pressure drop; that is, fluid expansion across the reservoir is generally minimal in heavy-oil reservoirs.

By applying the same assumptions as Lauwerier, Malofeev (1960) solved the energy-balance equation in radial system and proposed an analytical solution for fluid temperature distribution in the reservoir for thermal operation. Satman et al. (1979) modified Lauwerier's original work and proposed new analytical solution where heat transfer coefficient variation over time, as opposed to constant thermal conductivity, was applied to evaluate heat transfer from injection fluid to surrounded strata.

Spillette (1965) compared assumptions and results of various analytical solutions for fluid temperature distribution in thermal-recovery reservoir (Avdomin, 1964a and 1964b, Lauwerier, 1955, Malofeev, 1960, and Rubenstein, 1959) in addition to proposing his own numerical solution developed for the same purpose. He successfully validated his solution with results derived from those earlier analytical models.

Development of more challenging reservoirs, such as deep and ultra-deep reservoirs at high pressures and high temperatures, tight gas and oil reservoirs, and

unconventional reservoirs, has been increasing over the past few decades. Also, several recent downhole data from wells which produce from those reservoirs show that bottomhole flowing-fluid temperature could be significantly changing overtime even though production rate is constant. In addition, bottomhole flowing-fluid temperature could be influenced by changing of production rates.

A significant change in bottomhole temperature from original reservoir temperature in these 'unconventional' production environments is caused by the Joule-Thomson (J-T) phenomenon. The J-T effect is a phenomenon where fluid temperature change is caused by an immediate expansion of fluid (fluid pressure drop along the reservoir and into the wellbore) at constant enthalpy without any work or heat transfer to surroundings. It is generally considered an adiabatic process.

The J-T heating or cooling was originally of interest in interpretation of production logs. Steffensen and Smith (1973) proposed an analytical solution for estimating the fluid's static and flowing temperature at bottomhole during steady-state flow by incorporating the J-T effect. They pointed out that main heat-transfer mechanisms of fluids in the reservoir during production and injection are heat convection and J-T heating (or cooling). Temperature change due to radial conduction is normally negligible. They also proposed that heat transfer between reservoir and under- and over-burden formations during steady-state flow is negligible; therefore, the 'heat transfer to over-burden' term was not included in their study. The heating and/or cooling effect of J-T are generally different for different fluid types: fluid is typically heated if liquid production exists, while fluid temperature normally declines for

production of gas. However, for high-pressure systems, gas expansion could lead to increase in temperature. Therefore, temperature differences measured during production logging could be used as an indicator to verify type of fluid flowing into the wellbore. More recently, Kabir et al. (2012), among others, showed how independent estimation of individual layer contributions may be made from temperature profiles in both gas and oil wells, with the J-T effect playing a major role.

Change of reservoir flowing-fluid temperature due to J-T effect is directly proportional to pressure drawdown along the flow direction. In conventional reservoirs, pressure drawdown during production may not be large enough to trigger the J-T effect. In contrast, high pressure drawdown is normally required to commercially produce from more challenging reservoirs; that is, deep, tight, high pressure, and unconventional. As a result, the impact of J-T effect to flowing fluid temperature is more prominent in these 'unconventional' systems. In some cases, fluid heating due to the J-T effect can easily translate to 20 to 30 ^{o}F higher than the fluid temperature at initial reservoir conditions.

In addition to pressure drawdown, J-T heating and cooling are influenced by J-T coefficient, which is dependent on type and compositions of the reservoir fluid. In low-pressure gas reservoirs, J-T coefficient is positive, resulting in cooling effect. Conversely, heating is normally observed in high-pressure oil reservoirs where J-T coefficient is negative.

In addition to typical heat-transfer processes in wellbore and reservoir; that is, conduction and convection, a good understanding of J-T 'heat up' or 'cool down' processes allows a more reasonable bottomhole fluid temperature estimation during

flowing conditions, especially in high-pressure, high-drawdown environments. Improved estimation of flowing-fluid temperature at the wellbore will allow more reasonable bottomhole pressure, as well as well productivity calculations. Also, a reasonable coupled reservoir/wellbore temperature model is very useful for inverse calculation of some reservoir and flow parameters; that is, flow rate, skin, reservoir permeability, etc.

Several authors studied fluid temperature distribution in the reservoir accounting for fluid temperature alteration due to J-T effect. Yoshioka et al. (2005, 2006) introduced coupled reservoir/wellbore analytical temperature model for horizontal well production in a single-phase reservoir, assuming steady state conditions. Radial conduction, convection, and temperature change due to J-T effect are incorporated in their model. With the availability of dynamic temperature data from distributed temperature sensors and the estimated reservoir properties, their approach can be used as a basis for inverse modeling for determining fluid flow profiles along a horizontal well.

Dawkrajai et al. (2006) developed a finite-difference coupled reservoir/wellbore numerical solution to estimate fluid temperature distribution in the reservoir for two-phase production in horizontal wells. This work is an extension of Yoshioka et al.'s work in 2005. Their numerical solution removes the steady-state temperature assumption and allows variation of reservoir and fluid properties in space and time.

An analytical model to evaluate fluid temperature distribution in single-phase oil reservoir during unsteady-state flow was proposed by Ramazanov and Nagimov (2007). In their model, they assumed that main heat transfer mechanisms in the reservoir are

convection and heat transfer due to fluid expansion; that is, the J-T effect. Radial conduction is assumed to be negligible. Subsequently, they proposed a numerical model for fluid-temperature distribution in the reservoir (Ramazanov et al., 2013) and validated it with their original analytical solution. Additionally, they proposed an improved numerical solution where radial conduction was included in system's energy balance equation. Results from their model with and without radial conduction showed that the impact of radial conduction to fluid temperature distribution in a reservoir is minimal when production rate remains constant. However, radial heat conduction could become significant once the flow rate is adjusted (decreased or increased) after the flowing-fluid is already heated up or cooled down.

Duru and Horne (2010) developed a semianalytical solution for the same problem, taking into account viscous dissipation (J-T heating or cooling), as well as heat conduction and convection. They applied Operator Splitting and Time Stepping (OSATS) semianalytical technique to solve the problem and split reservoir energy balance equation into two parts: convective transport and diffusion. They solved the convective transport portion analytically and solution from this part is subsequently used in the diffusion part. The diffusion part of the energy-balance equation was solved semianalytically; that is, the results from the first time-step are an initial condition for next time-step and so on. They also coupled the reservoir-temperature model with the wellbore heat-transfer model (Izgec et al., 2007) for an analysis of flowing-fluid temperature in a complete production system.

App (2009, 2010) developed a nonisothermal reservoir simulator for single-phase reservoir coupling mass and energy balance equations. He included all possible heat-transfer mechanisms in the reservoir with a comprehensive energy-balance equation of the system. While most of the work by other authors in this area generally assumes no heat transfer from reservoir to surroundings (adiabatic process), App's work incorporates heat transfer from reservoir to over- and under-burden formations. His model shows that heat loss to overburden strata is significant and becomes crucial when fluid is significantly heated up later in production period. He also discussed potential change of well productivity due to J-T heating (or cooling) in high-pressure, low-permeability reservoirs, where large drawdown occurs for maintaining commercial rates. The resultant J-T heating causes the fluid viscosity to decline, which, in turn, favors well productivity.

1.2 Problem Statement

Recently, development of more challenging reservoirs, such as deep/tight oil and gas, unconventional resources has increased dramatically across onshore and offshore environments. As discussed earlier, the flowing-fluid temperature in the reservoir can be significantly impacted by the J-T phenomenon because of large pressure drawdown in these 'unconventional' systems. Thus, inclusion of the J-T effect may be critical in predicting flowing-fluid temperature across the reservoir and at well bottom, especially in a high-pressure, high-drawdown environment.

Analytical solution of coupled energy and mass balance equations of fluids (and rock) in reservoir with a reasonable set of assumptions will allow better estimation of flowing-fluid temperature across the reservoir. A reasonable analytical transient solution will eventually allow fluid temperature calculation over production time with minimal computational cost.

Better assessment of flowing-fluid temperature in the reservoir also allows calculation of fluid viscosity change across the reservoir. Generally, fluid viscosity is a function of fluid pressure and temperature. Therefore, fluid viscosity variation could be very significant in a near-wellbore region, where temperature change from J-T effect is significant and pressure drawdown is large. As a result, a reasonable analytical solution to this problem is very useful to achieve more accurate well productivity estimation, especially in an environment where effect from J-T is prominent.

Analytical solution for flowing fluid temperature in reservoir can be coupled to wellbore temperature model to allow estimation of fluid temperature at any location in the wellbore: from perforation depth to surface. A reasonable estimation of wellbore temperature is very useful in well completion designs.

Inverse assessment of a complete system flowing-fluid temperature model will allow reasonable approximation of some reservoir properties, such as permeability and skin. In cases where fluid temperature from the distributed temperature sensors (DTS) is available, flow rates can be estimated by inverse modeling in a layered system.

1.3 Research Objectives

This study aims to develop a robust analytical transient model for flowing-fluid temperature distribution in single-phase oil reservoir with constant rate production. Joule-Thomson phenomenon is included as one of the main heat transfer mechanisms of fluid flow in the reservoir. The ultimate deliverable from the proposed model is an approach for fluid temperature estimation across the reservoir and at the well bottom. The estimated bottomhole temperature (BHT) can be coupled with wellbore heat-transfer model for further analysis in the case where downhole gauges are away from the perforation intervals, which is the norm in most deepwater completions.

Analytical solution for flowing-fluid temperature in reservoir is coupled with analytical inflow (pressure) equations for transient, steady state, or pseudosteady state producing conditions. A coupled reservoir-temperature-and-pressure model allows calculation of fluid viscosity variation across the reservoir throughout the production period. As a result, the secondary objective of this study is to estimate well productivity over time incorporating thermal effects in the reservoir. We also compare well productivity estimation from simulations of the constant fluid-viscosity case, isothermal case (allowing viscosity to depend on pressure only), and fully nonisothermal case (viscosity depending on pressure and temperature).

Sensitivity analysis in this study provides a better understanding of reservoir types and fluid environments, where the J-T phenomenon plays an important role in reservoir flowing-fluid temperature that eventually affects well productivity. Additionally, key independent variables that are critical to reservoir flowing-fluid

temperature estimation are addressed. Results from the sensitivity analysis can be used as a guide to put more focus on the assessment of these critical variables where nonisothermal condition is dominant.

CHAPTER II

MODEL DEVELOPMENT

2.1 Reservoir and Wellbore System

The reservoir system considered in this study is a 1-D radial reservoir where fluid flow occurs only in the radial direction. It is assumed that there is no flow vertically, or in z-direction. The only flowing fluid in the reservoir is understaurated oil. Formation water is considered irreducible water. Fig. 1 shows a schematic of the reservoir system used in this study. Let us note that fluid flow is in a 'negative' r-direction (-r) during production. In the model, wellbore is located at the center of a circular reservoir.

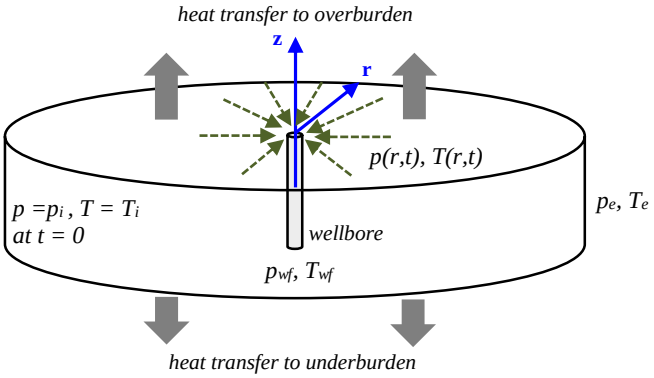

Fig. 1: Schematic of reservoir system in the study

The main goal of this study is to estimate fluid temperature distribution in the reservoir, as well as flowing-fluid temperature at well bottom, labeled as $T(r,t)$ and T_{wf} in Fig. 1 respectively. At the initial condition, T_i and p_i represent temperature and pressure

of reservoir fluid, whereas T_e and p_e are reservoir fluid temperature and pressure, respectively, at the reservoir boundary.

Generally, heat transfer mechanisms in the reservoir system are radial conduction, convection, and cooling or heating effect from the J-T phenomenon. In addition, heat transfer from the pay zone (reservoir of interest) to surroundings; that is, over- and under-burden formations, is included in this study.

2.2 Energy Balance in the Reservoir

A principle for estimation of fluid temperature distribution in the reservoir is conservation of energy in the reservoir system, which includes reservoir fluid and rock. Conservation of mass for reservoir fluids is also incorporated in this study to achieve a comprehensive energy balance equation of the system. We also assumed that reservoir is perfectly horizontal; thus, gravitational effect (change in fluid potential energy) is negligible.

The general form of thermal energy balance in terms of equation of change for internal energy can be written as Eq. 2.1 below:

$$\frac{\partial}{\partial t}\rho\widehat{U} = -\left(\nabla \cdot \rho\widehat{U}\vec{u}\right) - (\nabla \cdot \vec{q}) - p(\nabla \cdot \vec{u}) - (\vec{\tau}\colon \nabla\vec{u}) + \dot{Q} \qquad (2.1)$$

where $\widehat{U}$ is fluid internal energy, ρ is fluid and/or rock density, and $\vec{u}$ is fluid local velocity. The $\nabla \cdot$ term generally represents net input rate of energy per unit volume of the system. The first term on left side of Eq. 2.1 represents total rate of internal energy increase in the system. The first and second terms on right side of the same equation are net input rate of internal energy to the system caused by convective

transport (convection) and heat conduction respectively. The third term represents net reversible rate of internal energy increase due to fluid compression (pressure difference) while the fourth term is net irreversible rate of internal energy increase caused by fluid viscous dissipation. The fourth term is also referred as 'frictional' or 'viscous dissipation' term in this study.

In addition to heat conduction, convection, and J-T phenomena caused by fluid flow in the reservoir, energy transfer from surroundings (over- and under-burden formations) to the system (reservoir fluids and formation) is considered in this study. Therefore, a term representing net energy transfer rate between the system and surroundings, $\dot{Q}$, is added to our energy balance equation as the last term in Eq.2.1.

Eq.2.1 can also be written in terms of enthalpy, temperature, and pressure. The relationship between internal energy and enthalpy is presented in Eq.2.2 or Eq.2.3 below:

$$\widehat{U} = \widehat{H} - p\widehat{V} \tag{2.2}$$

$$\widehat{U} = \widehat{H} - \frac{p}{\rho} \tag{2.3}$$

while $\widehat{H}$ is enthalpy, p is fluid pressure, and $\widehat{V}$ is specific volume which is equal to $\frac{1}{\rho}$. Plugging Eq.2.3 into Eq. 2.1, we get

$$\frac{\partial}{\partial t}\rho\widehat{H} - \frac{\partial p}{\partial t} = -\left(\nabla \cdot \rho\widehat{H}\vec{u}\right) + \nabla \cdot \rho\vec{u} - (\nabla \cdot \vec{q}) - (\vec{\tau} : \nabla\vec{u}) - p(\nabla \cdot \vec{u}) + \dot{Q} \tag{2.4}$$

Substantial derivative of pressure is generally defined as

$$\frac{Dp}{Dt} = \frac{\partial p}{\partial t} + \vec{u} \cdot \nabla p \tag{2.5}$$

Hence, Eq.2.4 can also be written in term of substantial derivative of pressure as

$$\frac{\partial}{\partial t}\rho\widehat{H} + \nabla\cdot\rho\widehat{H}\vec{u} = -(\nabla\cdot\vec{q}) - (\vec{\tau}:\nabla\vec{u}) + \frac{Dp}{Dt} + \dot{Q} \tag{2.6}$$

According to Fourier's law of conduction, the first term on right side of Eq.2.6 can be replaced by

$$-\nabla\cdot\vec{q} = \nabla\cdot(\lambda\nabla T) \tag{2.7}$$

According to Newton's law of viscosity, for a 1-D cylindrical coordinate system where fluid is only flowing radially, the viscous dissipation term is

$$-(\vec{\tau}:\nabla\vec{u}) = 2\mu\left(\frac{\partial u_r}{\partial r}\right)^2 \tag{2.8}$$

Combining Eq.2.6, Eq.2.7, and Eq.2.8, we obtain a thermal energy balance equation for a 1-D radial flow as presented in Eq.2.9 below.

$$\frac{\partial}{\partial t}\rho\widehat{H} + \frac{1}{r}\frac{\partial}{\partial r}\left[r\rho\widehat{H}u_r\right] = \frac{1}{r}\frac{\partial}{\partial r}\left[\lambda r\frac{\partial T}{\partial r}\right] + 2\mu\left(\frac{\partial u_r}{\partial r}\right)^2 + \frac{Dp}{Dt} + \dot{Q} \tag{2.9}$$

Al-Hadhrami et al. (2003) showed that the viscous dissipation term in energy balance equation for 1-D radial flow in porous media can be approximated as $-u_r\frac{\partial p}{\partial r}$. Thus, we substitute an approximation of viscous dissipation term for the second term on right side of Eq.2.9 to get

$$\frac{\partial}{\partial t}\rho\widehat{H} + \frac{1}{r}\frac{\partial}{\partial r}\left[r\rho\widehat{H}u_r\right] = \frac{1}{r}\frac{\partial}{\partial r}\left[\lambda r\frac{\partial T}{\partial r}\right] - u_r\frac{\partial p}{\partial r} + \frac{Dp}{Dt} + \dot{Q} \tag{2.10}$$

Rearranging Eq.2.10, we get

$$\rho\frac{\partial\widehat{H}}{\partial t} + \widehat{H}\frac{\partial\rho}{\partial t} + \frac{1}{r}\frac{\partial}{\partial r}\left[r\rho\widehat{H}u_r\right] = \frac{1}{r}\frac{\partial}{\partial r}\left[\lambda r\frac{\partial T}{\partial r}\right] - u_r\frac{\partial p}{\partial r} + \frac{\partial p}{\partial t} + u_r\frac{\partial p}{\partial r} + \dot{Q} \tag{2.11}$$

Therefore,

$$\rho\frac{\partial\widehat{H}}{\partial t} + \widehat{H}\left[\frac{\partial p}{\partial t} + \frac{1}{r}\frac{\partial}{\partial r}(r\rho u_r)\right] = \frac{1}{r}\frac{\partial}{\partial r}\left[\lambda r\frac{\partial T}{\partial r}\right] + \frac{\partial p}{\partial t} + \dot{Q} \tag{2.12}$$

Conservation of mass is generally described in a form of

$$\frac{\partial p}{\partial t} + (\nabla \cdot \rho \vec{u}) = 0 \tag{2.13}$$

In a 1-D cylindrical coordinate (radial) system, mass conservation can be written as

$$\frac{\partial p}{\partial t} + \frac{1}{r}\frac{\partial}{\partial r}(r\rho u_r) = 0 \tag{2.14}$$

Substituting Eq.2.14 for the second term on left side of Eq.2.12, the thermal energy balance becomes

$$\rho \frac{\partial \hat{H}}{\partial t} = \frac{1}{r}\frac{\partial}{\partial r}\left[\lambda r \frac{\partial T}{\partial r}\right] + \frac{\partial p}{\partial t} + \dot{Q} \tag{2.15}$$

Enthalpy of reservoir fluids and rock can be defined in terms of pressure and temperature as presented in Eq.2.16 and Eq.2.17 below:

$$d\hat{H}_{o/w} = c_{po/w}dT + \sigma_{o/w}dp \tag{2.16}$$

$$d\hat{H}_f = c_{pf}dT \tag{2.17}$$

where c_p is specific heat capacity, and σ is Joule-Thomson throttling coefficient of each reservoir component. The subscripts o, w, and f represent oil, water, and formation (rock) respectively. We can see that enthalpy of formation depends only on specific heat capacity of reservoir rock while enthalpy of reservoir fluids is a function of both specific heat capacity and Joule-Thomson phenomenon.

We write enthalpy in terms of pressure and temperature for each reservoir component, i.e. oil, irreducible water, and formation rock, and plug all parameters into Eq.2.15 to get

$$\left[\emptyset s_o \rho_o c_{po} + \emptyset s_w \rho_w c_{pw} + (1-\emptyset)\rho_f c_{pf}\right]\frac{\partial T}{\partial t} + \rho_o u_r c_{po}\frac{\partial T}{\partial r} + \rho_o u_r \sigma_o \frac{\partial p}{\partial r} +$$

$$\left[\emptyset s_o \rho_o \sigma_o + \emptyset s_w \rho_w \sigma_w - 1\right]\frac{\partial p}{\partial t} = \frac{1}{r}\frac{\partial}{\partial r}\left[\lambda r \frac{\partial T}{\partial r}\right] + \dot{Q} \qquad (2.18)$$

Eq.2.18 is the comprehensive energy balance equation for our system. The first and second terms on left side of Eq.2.18 physically represent energy change due to temperature transient and convective transport respectively. The third term is energy change due to J-T effect whereas the following term represents energy change due to pressure transient in the reservoir. The first term on right side of Eq.2.18 is energy change from radial heat conduction and the last term represents rate of heat transfer across system boundary (to/from over- and under-burden formations).

In the case where heat transfer from system (pay zone) to over- and under-burden formations is minimal and can be neglected, the energy balance equation is reduced to

$$\left[\emptyset s_o \rho_o c_{po} + \emptyset s_w \rho_w c_{pw} + (1-\emptyset)\rho_f c_{pf}\right]\frac{\partial T}{\partial t} + \rho_o u_r c_{po}\frac{\partial T}{\partial r} + \rho_o u_r \sigma_o \frac{\partial p}{\partial r} +$$

$$\left[\emptyset s_o \rho_o \sigma_{po} + \emptyset s_w \rho_w \sigma_{pw} - 1\right]\frac{\partial p}{\partial t} = \frac{1}{r}\frac{\partial}{\partial r}\left[\lambda r \frac{\partial T}{\partial r}\right] \qquad (2.19)$$

Eq.2.18 and Eq.2.19 are fundamentally the same as the final form of thermal energy balance equation of the same system presented by App (2010). This equation is generally a basis for our proposed analytic model to evaluate flowing-fluid temperature distribution in the reservoir.

2.3 Model Assumptions

In this study, reservoir is assumed to be homogeneous i.e. reservoir properties are the same across the reservoir. In addition, those properties are assumed to be independent of time. In an original version of our proposed model (Section 2.4), all fluid properties are assumed to be constant over time across the reservoir. However, in the improved version (explained in details in Section 2.5), change in fluid viscosity based on reservoir pressure and temperature is allowed.

Other general assumptions for model development in this study are:

1. The only flowing fluid phase in reservoir is oil.
2. Reservoir is producing at a constant rate.
3. Original temperature of over- and under-burden formations is the same as reservoir temperature at initial condition. Their elevation differences from reservoir depth are negligible.
4. Over- and under-burden formations are infinite sources/sinks. Temperature of over- and under-burden formations remains at their original temperature even after heat transfer to/from reservoir occurs.
5. Radial heat conduction is negligible during constant rate production.

   This assumption is supported by a study by Ramazanov et al. (2013) where they presented that radial heat conduction causes insignificant impact to flowing fluid temperature in reservoir if production is maintained at a constant rate.
6. To simplify the problem for analytical solution, pressure transient term, $\frac{\partial p}{\partial t}$, is assumed to be negligible.

Generally, impact of pressure transient term to fluid temperature calculation is small compared to other terms in our comprehensive energy balance equation (Eq. 2.18). Results from the proposed solution shows that flowing fluid temperature calculated based on this assumption is reasonably close to the results obtained from a rigorous numerical model developed by App (2010). In general, temperature transient normally continues even after steady state or pseudo-steady state flow regime is reached. Therefore, this assumption is considered reasonable and eventually results in a good estimate of flowing-fluid temperature in the reservoir.

7. Fluid local velocity (superficial velocity) can be estimated from Darcy's equation:

$$q = -\frac{kA}{\mu}\frac{\partial p}{\partial r} = -\frac{2\pi rhk}{\mu}\frac{\partial p}{\partial r} \tag{2.20}$$

$$u_r = \frac{q}{A} = \frac{q}{2\pi rh} = -\frac{k}{\mu}\frac{\partial p}{\partial r} \tag{2.21}$$

Thus, $\frac{\partial p}{\partial r}$ term in the comprehensive energy balance equation, Eq.2.18 and Eq.2.19, can be written in terms of fluid velocity or flow rate as

$$\frac{\partial p}{\partial r} = -\frac{\mu}{k}u_r = -\frac{\mu q}{kA} = -\frac{\mu q}{2\pi rhk} \tag{2.22}$$

2.4 The Analytical Solutions

Analytical solutions to comprehensive energy balance equation are developed for estimation of flowing-fluid temperature distribution in the reservoir. The first solution presented in subsection 2.4.1 is derived from an assumption that there is no heat transfer between the system (reservoir) and surroundings. In contrast, the other solution shown in

subsection 2.4.2 incorporates heat transfer to and from the system, $\dot{Q}$, into our calculations.

2.4.1 Solution without heat transfer between reservoir and surroundings (Model I)

As described in Section 2.2, a comprehensive energy balance equation of our system without a consideration of heat transfer from pay zone to over/underburden formations can be written as

$$\left[\emptyset s_o \rho_o c_{po} + \emptyset s_w \rho_w c_{pw} + (1-\emptyset)\rho_f c_{pf}\right]\frac{\partial T}{\partial t} + \rho_o u_r c_{po}\frac{\partial T}{\partial r} + \rho_o u_r \sigma_o \frac{\partial p}{\partial r} +$$

$$\left[\emptyset s_o \rho_o \sigma_o + \emptyset s_w \rho_w \sigma_w - 1\right]\frac{\partial p}{\partial t} = \frac{1}{r}\frac{\partial}{\partial r}\left[\lambda r \frac{\partial T}{\partial r}\right] \quad (2.19)$$

Based on our assumptions, radial heat conduction during constant rate production is minimal; therefore, the term on right side of Eq.2.18 becomes zero. In addition, based on Eq.2.21 and Eq.2.22, we can rewrite fluid velocity,u_r, in term of flow rate as $\frac{q}{2\pi rh}$ and rewrite the $\frac{\partial p}{\partial r}$ term as $-\frac{\mu q}{2\pi rhk}$ respectively. Thus, Eq.2.19 becomes

$$\left[\emptyset s_o \rho_o c_{po} + \emptyset s_w \rho_w c_{pw} + (1-\emptyset)\rho_f c_{pf}\right]\frac{\partial T}{\partial t} + \frac{q\rho_o c_{po}}{2\pi rh}\frac{\partial T}{\partial r} - \frac{q^2 \rho_o \sigma_o \mu}{(2\pi rh)^2 k} +$$

$$\left[\emptyset s_o \rho_o \sigma_o + \emptyset s_w \rho_w \sigma_w - 1\right]\frac{\partial p}{\partial t} = 0 \quad (2.23)$$

We know that during production, fluid is flowing in a negative r-direction in cylindrical coordinate system; thus, volumetric flow rate, q, in the energy balance equation is replaced by $-q$. Thus, Eq.2.23 becomes

$$\left[\emptyset s_o \rho_o c_{po} + \emptyset s_w \rho_w c_{pw} + (1-\emptyset)\rho_f c_{pf}\right]\frac{\partial T}{\partial t} - \frac{q\rho_o c_{po}}{2\pi rh}\frac{\partial T}{\partial r} - \frac{q^2 \rho_o \sigma_o \mu}{(2\pi rh)^2 k} +$$

$$\left[\emptyset s_o \rho_o \sigma_o + \emptyset s_w \rho_w \sigma_w - 1\right]\frac{\partial p}{\partial t} = 0 \quad (2.24)$$

We multiply both sides of Eq.2.24 by $\frac{2\pi r^2 h}{q}$ to get

$$\left[\emptyset s_o \rho_o c_{po} + \emptyset s_w \rho_w c_{pw} + (1-\emptyset)\rho_f c_{pf}\right]\left(\frac{2\pi r^2 h}{q}\right)\frac{\partial T}{\partial t} - \rho_o c_{po}(r)\frac{\partial T}{\partial r} - \frac{q\rho_o \sigma_o \mu}{2\pi hk} +$$

$$[\emptyset s_o \rho_o \sigma_o + \emptyset s_w \rho_w \sigma_w - 1](\frac{2\pi r^2 h}{q})\frac{\partial p}{\partial t} = 0 \quad (2.25)$$

We assume that $\frac{\partial p}{\partial t}$ is relatively small and has an insignificant impact to the calculation. Also all fluid properties are assumed to be constant across the reservoir. Then, Eq. 2.25 can be written as

$$Ar^2\frac{\partial T}{\partial t} - Br\frac{\partial T}{\partial r} - C = 0 \quad (2.26)$$

where: $$A = \left[\emptyset s_o \rho_o c_{po} + \emptyset s_w \rho_w c_{pw} + (1-\emptyset)\rho_f c_{pf}\right]\left(\frac{2\pi h}{q}\right) \quad (2.27)$$

$$B = \rho_o c_{po} \quad (2.28)$$

$$C = \frac{q\rho_o \sigma_o \mu}{2\pi hk} \quad (2.29)$$

Note that parameters *A*, *B*, and *C* are constant for a particular reservoir.

Eq.2.26 is first order partial differential equation where fluid temperature, *T*, is a function of radial distance from wellbore into the reservoir, *r*, and producing time, *t*. An initial condition of fluid temperature in the reservoir can be expressed as

$$T(r, t=0) = T_i \quad (2.30)$$

By the method of Characteristics and the initial condition presented in Eq.2.30, Eq.2.26 can be solved. An analytical solution for flowing fluid temperature in the reservoir as a function of *r* and *t* can be expressed as

$$T(r,t) = T_i - \frac{C}{2B}\ln(\frac{r^2 A}{|r^2 A + 2Bt|}) \quad (2.31)$$

The constants *A*, *B*, and *C* are specific to a reservoir and were defined in Eq.2.27, Eq. 2.28, and Eq.2.29 respectively.

Details of derivation for this solution are presented in Appendix A. Eq.2.31 is essentially our proposed analytical model to evaluate flowing-fluid temperature distribution in the reservoir without a consideration of energy transfer between system and surroundings, which will be referred to as Model I in this study. This solution is normally applicable when production time is short and fluid temperature alteration from its original condition is not large; thus, heat transfer from reservoir is surrounding is very minimal.

Once the difference between flowing-fluid temperature and initial reservoir temperature gets bigger, energy transfer between system (reservoir) and under- and over-burden formations becomes more significant. The following subsection discusses the other analytical solution with a consideration of energy transfer across system boundary.

2.4.2 Solution with heat transfer between reservoir and surroundings (Model II)

A comprehensive energy balance equation of the system incorporating energy transfer between system and surrounding was presented in Eq.2.18:

$$\left[\emptyset s_o \rho_o c_{po} + \emptyset s_w \rho_w c_{pw} + (1-\emptyset)\rho_f c_{pf}\right]\frac{\partial T}{\partial t} + \rho_o u_r c_{po}\frac{\partial T}{\partial r} + \rho_o u_r \sigma_o \frac{\partial p}{\partial r} +$$

$$\left[\emptyset s_o \rho_o \sigma_{po} + \emptyset s_w \rho_w \sigma_{pw} - 1\right]\frac{\partial p}{\partial t} = \frac{1}{r}\frac{\partial}{\partial r}\left[\lambda r \frac{\partial T}{\partial r}\right] + \dot{Q} \qquad (2.18)$$

where $\dot{Q}$ represents net input rate of energy transferred to the system per unit volume.

Using the same assumptions and approaches described in Subsection 2.4.1, we can rewrite Eq.2.18 as

$$\left[\emptyset s_o \rho_o c_{po} + \emptyset s_w \rho_w c_{pw} + (1-\emptyset)\rho_f c_{pf}\right]\left(\frac{2\pi r^2 h}{q}\right)\frac{\partial T}{\partial t} - \rho_o c_{po}(r)\frac{\partial T}{\partial r} - \frac{q\rho_o \sigma_o \mu}{2\pi hk} = \dot{Q}\left(\frac{2\pi r^2 h}{q}\right) \quad (2.32)$$

Then, Eq.2.32 can be reduced and expressed as

$$Ar^2\frac{\partial T}{\partial t} - Br\frac{\partial T}{\partial r} - C = \left(\frac{2\pi r^2 h}{q}\right)\dot{Q} \quad (2.33)$$

The definitions of constants *A*, *B*, and *C* are the same as described in Eq.2.27, Eq. 2.28, and Eq.2.29 respectively.

Generally, net energy being transferred from surroundings to reservoir system, *Q*, can be estimated by the Newton's law of cooling:

$$Q = h_c[T_s - T] \quad (2.34)$$

Where h_c is reservoir heat transfer coefficient, T_s is temperature of surrounded formations (over- and under-burden formations), and T is fluid temperature in the reservoir.

Heat transfer to-and-from the reservoir generally happens at both surfaces: top and bottom of the reservoir. Therefore, net input rate of energy transfer across system boundary per unit volume can be expressed as

$$\dot{Q} = \frac{2(A_S)h_c[T_s - T]}{(A_S h)} \quad (2.35)$$

$$\dot{Q} = \frac{2h_c[T_s - T]}{h} = -\frac{2h_c[T - T_s]}{h} \quad (2.36)$$

Based on our assumption, temperature of under- and over-burden formations remains at initial reservoir temperature, T_i, even after heat is being transferred to/from the reservoir. We plug Eq.2.36 into Eq.2.33 to get

$$Ar^2\frac{\partial T}{\partial t} - Br\frac{\partial T}{\partial r} - C = -\frac{4h_c\pi r^2}{q}[T - T_i] \tag{2.37}$$

We assume that heat transfer coefficient of the reservoir is constant throughout the production period. Therefore, Eq.2.37 can then be simplified as

$$Ar^2\frac{\partial T}{\partial t} - Br\frac{\partial T}{\partial r} - C = -Dr^2T + Er^2 \tag{2.38}$$

Where: $$D = \frac{4h_c\pi}{q} \tag{2.39}$$

and $$E = \frac{4h_c\pi}{q}T_i \tag{2.40}$$

During production period, Ar^2, is non-zero and always positive. Thus, we divide Eq.2.38 by Ar^2 to get

$$\frac{\partial T}{\partial t} - \frac{B}{Ar}\frac{\partial T}{\partial r} - \frac{C}{Ar^2} = -\frac{D}{A}T + \frac{E}{A} \tag{2.41}$$

Eq. 2.41 is a first order partial differential equation which can be solved by the method of Characteristics. Initial condition of the system is the same as initial condition presented in Eq.2.30. An analytical solution for flowing fluid temperature in the reservoir, incorporating heat transfer between the system and surroundings, as a function of *r* and *t* can be expressed as

$$T(r,t) = T_i + \frac{C}{2B}e^{\frac{H(Ar^2+2Bt)}{2B}}Ei\left[-\frac{H(Ar^2+2Bt)}{2B}\right] - \frac{C}{2B}e^{\frac{HAr^2}{2B}}Ei\left[-\frac{HAr^2}{2B}\right] \tag{2.42}$$

Where: $$H = \frac{D}{A} \tag{2.43}$$

The other constants in Eq.2.42 were defined earlier in previous sections but will be re-stated here for convenience.

$$A = \left[\emptyset s_o \rho_o c_{po} + \emptyset s_w \rho_w c_{pw} + (1-\emptyset)\rho_f c_{pf}\right]\left(\frac{2\pi h}{q}\right) \tag{2.27}$$

$$B = \rho_o c_{po} \tag{2.28}$$

$$C = \frac{q\rho_o \sigma_o \mu}{2\pi h k} \tag{2.29}$$

and

$$D = \frac{4h_c \pi}{q} \tag{2.39}$$

Eq.2.42 is the final analytical solution for an estimation of flowing-fluid temperature distribution in the reservoir taking into account heat transfer between the pay zone and over- and under-burden formations. This analytical solution is referred to as Model II in this study. Derivation of this solution is also discussed in detail in Appendix A.

2.5 The Improved Analytical Solution: Analytical Solution with Fluid Viscosity Variation (Model III)

Eq.2.31 and Eq.2.42 are our proposed analytical models to estimate flowing-fluid temperature in the reservoir without and with a consideration of energy transport between our system (reservoir) and surroundings. Note that all rock and fluids properties are assumed to be constant in these two solutions.

This section discusses a concept and work flow for an improved version of our analytical solution where an effect of fluid viscosity alteration due to pressure and temperature variation across the reservoir is included. The ultimate goal for this

improved solution is to better estimate productivity of the well incorporating Joule-Thompson heating and/or cooling phenomena. The improved solution also allows us to better understand an impact of fluid viscosity to an estimation of flowing-fluid temperature in the reservoir. In this study, the improved solution will be referred to as Model III for convenience.

2.5.1 Well productivity index

Well productivity index is a measure of how good one well can produce from the reservoir at a given set of production constraints. Productivity index, J, is generally defined as

$$J = \frac{q}{p_r - p_{wf}} \tag{2.44}$$

where p_r is average reservoir pressure and p_{wf} is wellbore flowing pressure

Reservoir pressure as a function of *r* and *t* during different flow regimes (that is, transient, steady state, and pseudosteady state flow) can be estimated from the analytical inflow solutions presented in subsection 2.5.3. Then, a volumetric-averaged reservoir pressure can be calculated and used in productivity index calculation based on a relationship presented in Eq. 2.44.

2.5.2 Reservoir fluid viscosity

One of the key properties that have a significant impact on reservoir and well productivity is fluid viscosity, which is normally dependent on reservoir pressure and temperature. The best way to estimate fluid viscosity is collecting fluid sample from

downhole, preserving it at reservoir conditions, and having measurements in laboratory. Downhole fluid sample is normally costly and not always practical in all real situations. In most cases, empirical equations or correlations are used to approximate fluid viscosity for a specific reservoir at any given reservoir conditions. Examples of oil viscosity correlations that are available and widely used in the industry are discussed in detail in Appendix B.

When actual measurements are not available, an appropriate correlation with the closest analog should be selected and used for best estimate of fluid viscosity. A more accurate fluid viscosity approximation is resulting in a better estimate of flowing-fluid temperature in the reservoir and consequently yielding a better prediction of well productivity, which is generally useful for well performance evaluation in production engineering.

2.5.3 Reservoir analytical inflow model

Analytic reservoir inflow model for single-phase constant rate oil production has been incorporated in this study for bottomhole pressure and temperature estimation. Pressure distribution of fluid in the reservoir can also be approximated. Reservoir pressure distribution is used in an improved version of our reservoir fluid temperature analytical solution where fluid viscosity variation across the reservoir based on local pressure and temperature is incorporated.

Three analytical inflow (pressure) models for single-phase oil reservoir are used in this study and are discussed. Each model generally gives a reasonable estimate of

reservoir pressures in different flow regimes: transient flow, steady state flow, and pseudo-steady state flow periods. Although these solutions were derived from an 'isothermal' assumption, our results show that the isothermal reservoir analytical inflow model when coupled with the proposed reservoir fluid-temperature model, gives a reasonable prediction of the flowing-fluid temperature in the reservoir.

2.5.3.1 Analytical inflow model during transient period

The diffusivity equation of fluid flow in single-phase oil reservoir with constant permeability and viscosity can be written as:

$$\frac{\partial^2 p}{\partial r^2} + \frac{1}{r}\frac{\partial p}{\partial r} = \frac{\emptyset \mu c_t}{k}\frac{\partial p}{\partial t} \tag{2.45}$$

where p is reservoir pressure, μ is fluid viscosity, $c_t$is total compressibility of the reservoir, k is reservoir permeability, r is radial distance from the wellbore, and t is time after the start of production. With an appropriate set of initial and boundary conditions, Eq. 2.45 can be solved and the line source solution for diffusivity equation during infinite-acting radial flow (transient period) is defined as

$$p(r,t) = p_i + 70.6\frac{qB_o\mu}{kh}Ei(-\frac{948\emptyset\mu c_t r^2}{kt}) \tag{2.46}$$

with an initial condition of

$$p_D(r_D, t_D = 0) = 0 \tag{2.47}$$

And boundary conditions of

$$p_D(r_D \to \infty, t_D) = 0 \qquad \text{(Infinite-acting radial flow)} \tag{2.48}$$

$$(\frac{\partial p_D}{\partial r_D})_{r_D=1} = -1 \qquad \text{(Constant rate production at wellbore)} \tag{2.49}$$

where: $$t_D = \frac{0.0002637kt}{\emptyset\mu c_t r_w^2} \quad (2.50)$$

$$r_D = \frac{r}{r_w} \quad (2.51)$$

and $$p_D(r_D, t_D) = \frac{kh}{141.2qB_o\mu}[p_i - p(r,t)] \quad (2.52)$$

Generally, Eq. 2.46 gives a reasonable estimate of reservoir pressure as a function of time and distance from the wellbore during transient period before reservoir boundary is felt. Note that all parameters in Eq. 2.46 are in oilfield units.

2.5.3.2 Analytical inflow model during steady state period

Darcy's law (1856) for radial flow can be simply expressed as

$$q = -\frac{kA}{\mu}\frac{\partial p}{\partial r} \quad (2.53)$$

where A is flow area (cross-sectional area which is perpendicular to flow direction). For steady state flow regime, reservoir inflow can be directly calculated from Darcy's equation presented in Eq.2.53. Flow area at any location in the reservoir is evaluated from: $A = 2\pi rh$. Therefore, for steady state production, Eq.2.53 can be re-written as

$$q = -\frac{2\pi rhk}{\mu}\frac{\partial p}{\partial r} \quad (2.54)$$

For constant-rate production where reservoir and fluid properties are assumed to be constant, the solution to Eq. 2.54 is

$$p(r,t) = p_i - 141.2\frac{qB_o\mu}{kh}\ln(\frac{r_e}{r}) \quad (2.55)$$

All parameters in Eq. 2.55 are in oilfield units. We observe that for steady state flow, reservoir pressure is no longer time dependent; that is, reservoir pressure at any location remains constant after reservoir boundary is reached.

Normally, steady-state condition is observed in reservoirs with constant-pressure boundary. Eq. 2.55 is a reasonable inflow model for reservoirs with significant pressure maintenance, such as reservoirs in waterflood operation or reservoirs with strong gas-cap and/or aquifer support.

In case of a volumetric or closed outer-boundary system, neither Eq. 2.46 nor Eq. 2.55 is applicable for reservoir inflow calculations. Instead, pseudosteady-state inflow model can be used to evaluate reservoir pressure distribution, if production is not in the first two flow regimes.

2.5.3.3 Analytical inflow model during pseudo-steady state period

For reservoir with no-flow boundary, pseudosteady state condition is established when pressure drawdown response reaches reservoir boundary. During this flow regime, $\frac{\partial p}{\partial t}$ is constant and no longer dependent on time and distance from wellbore. Raghavan (1993) proposed a rigorous analytical solution of the diffusivity equation for single-phase, constant-rate liquid production to estimate the reservoir pressure as a function of space and time during pseudosteady state flow. He showed that at large times, the dimensionless solution for reservoir pressure during pseudosteady state flow is

$$p_D(r_D, t_D) = \frac{2}{(r_{eD}^2-1)}\left(t_D + \frac{r_D^2}{4}\right) - \frac{r_{eD}^2}{(r_{eD}^2-1)}\ln r_D - \frac{3r_{eD}^4-4r_{eD}^3\ln r_{eD}-2r_{eD}^2-1}{4(r_{eD}^2-1)^2} \qquad (2.56)$$

where the dimensionless parameters, $t_D, r_D,$ and p_D for constant rate production were defined by Eq. 2.50, Eq. 2.51, Eq. 2.52, respectively. In addition, the dimensionless parameter r_{eD} is defined as

$$r_{eD} = \frac{r_e}{r_w} \tag{2.57}$$

A simplified version of Raghavan's solution presented in Eq. 2.56 normally provides a reasonable estimation of reservoir pressure over time for single-phase liquid production during pseudosteady state condition when r_{eD} is large.

In this study, Eq. 2.46, Eq. 2.55, and Eq. 2.56 are used as reservoir inflow models for constant-rate production during transient period, steady state condition, and pseudosteady state condition, respectively. Transient inflow model is applied for production period before reservoir boundary is reached; that is, during infinite-acting radial flow. Thereafter, inflow model is switched to either steady-state or pseudosteady-state model based on the outer boundary condition.

2.5.4 Work flow: the improved-solution (Model III: analytical solution with fluid viscosity variation)

In the improved version of our analytical solution, the proposed analytical model for flowing fluid temperature in the reservoir, Model II, is coupled with analytical inflow model discussed in Subsection 2.5.3. Consequently, fluid viscosity approximation based on local pressure and temperature is included to allow better estimation of reservoir flowing-fluid temperature, reservoir pressure, and well productivity.

Reservoir fluid viscosity is actually a function of time and radial distance from the wellbore. However, in this study, viscosity is originally treated as a constant; that is, independent of *r* and *t*, in the derivation. Thus, this workflow is generated and implemented to take into account fluid viscosity variation over space and time during production for a better estimation of flowing-fluid temperature distribution in the reservoir.

General work flow for an improved solution is shown in Fig. 2.

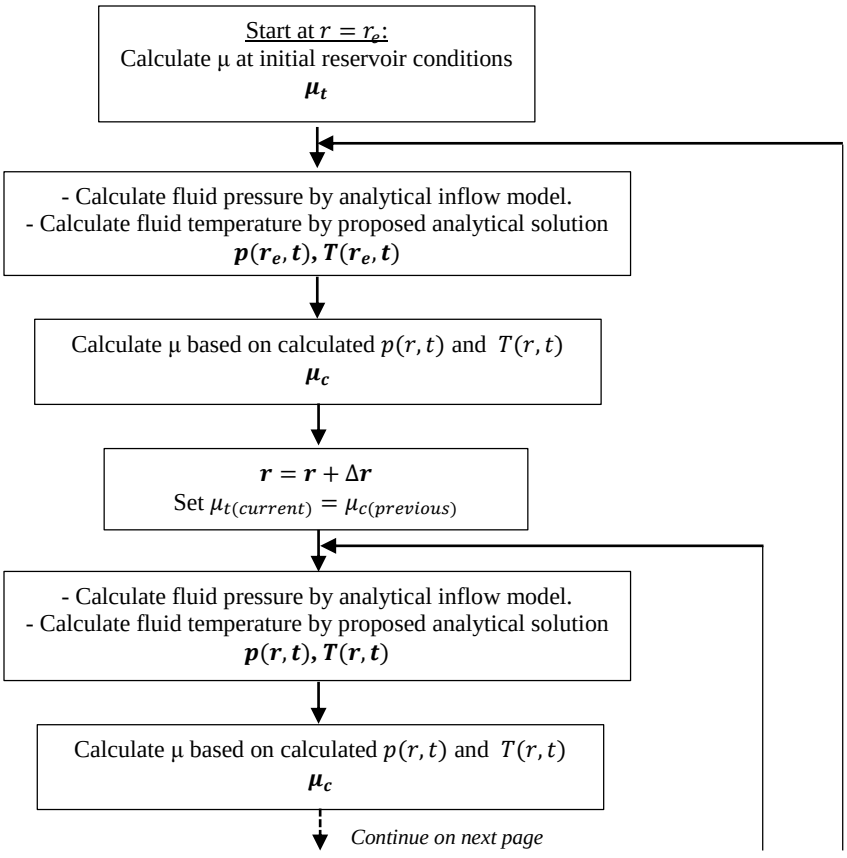

Fig. 2: Flow chart explaining work flow for the improved solution, taken into account viscosity variation across the reservoir

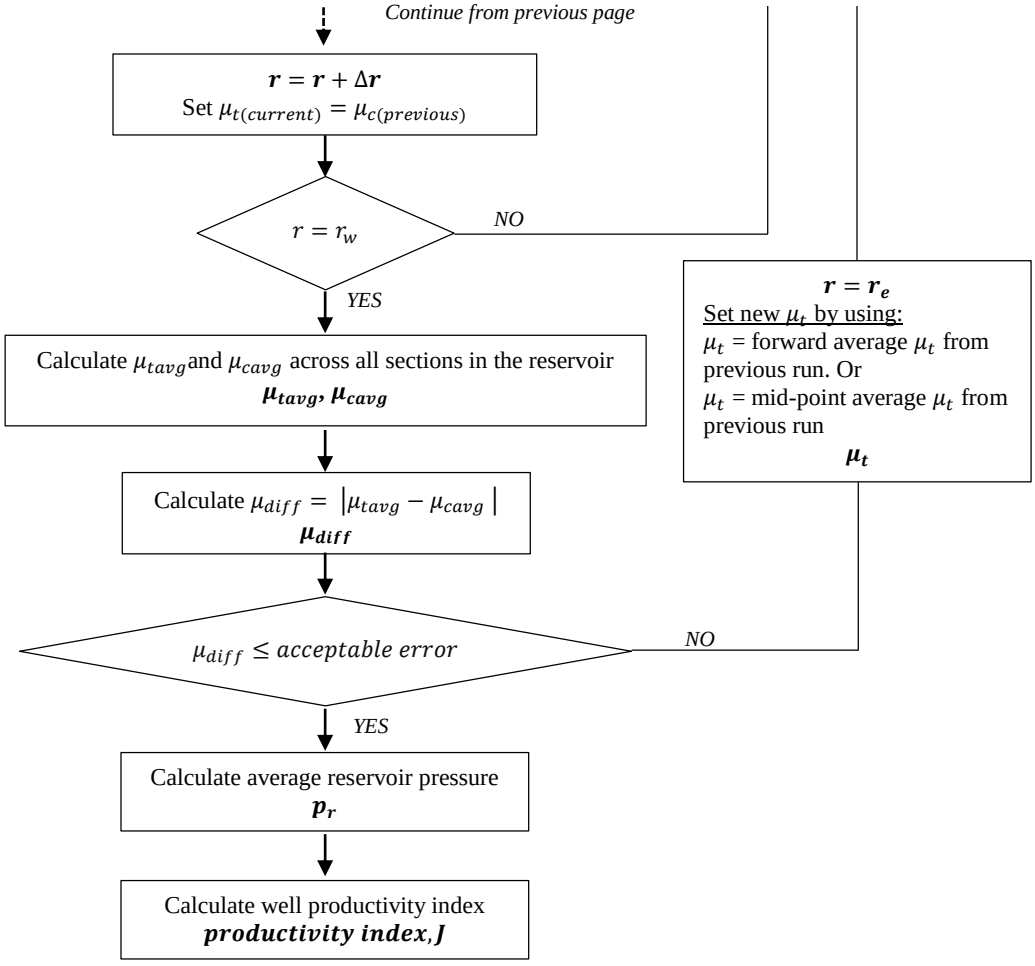

Fig. 2: Continued.

Each box in Fig. 2 explains calculation steps in the improved version of our analytical solution. Expected deliverables from each step are highlighted in bold at the bottom of each box. Details of the improved model work flow are explained as follows:

1. In an improved version of the model, reservoir is divided into sections radially to allow calculations of local pressure, temperature, and fluid viscosity.

2. Calculation starts from outer reservoir boundary, $r = r_e$. First, assume that pressure and temperature at the boundary are at initial condition, p_i and T_i, respectively. Calculate fluid viscosity at $r = r_e$ based on p_i and T_i.
3. Fluid viscosity calculated in step 2 will be referred as 'trial' viscosity, μ_t.
4. Assume $\mu = \mu_t$ and calculate $p(r_e,t)$ and $T(r_e,t)$ by applying analytical inflow model and the proposed analytical temperature model respectively.
5. Calculate fluid viscosity based on reservoir pressure and temperature calculated in step 4. The new viscosity calculated in this step will be referred as 'calculated' viscosity, μ_c.
6. Move to the next reservoir section (one grid closer to the wellbore). Let viscosity calculated in step 5 be the new 'trial' value, μ_t for the new reservoir section.
7. Similarly to step 4, calculate $p(r,t)$ and $T(r,t)$ at a location, r, based on new μ_t using analytical inflow model and the proposed analytical temperature model.
8. Calculate the new 'calculated' viscosity, μ_c, based on new $p(r,t)$ and $T(r,t)$ in step 7.
9. Move to the next reservoir section and repeat steps 6-8 until reaching the wellbore. The final calculated $p(r,t)$ and $T(r,t)$ at $r = r_w$ are p_{wf} and T_{wf} respectively.
10. Then, calculate average 'trial' and average 'calculated' viscosity, μ_{tavg} and μ_{cavg}, across the reservoir by volumetric average method.
11. Calculate μ_{diff} and compare it to our error tolerance.
    a. If μ_{diff} is smaller than the acceptable error, the trial viscosity values are reasonable and calculated $p(r,t)$ and $T(r,t)$ across the reservoir are good

representations for flowing-fluid pressure and temperature distribution in the reservoir.

b. If μ_{diff} is larger than the acceptable error, we can either
   - Use a forward average μ_t from previous run as a new 'trial' viscosity in each reservoir section and repeat steps 2-11. Or
   - Use a mid-point average μ_t from previous run as a new 'trial' viscosity in each reservoir section and repeat steps 2-11.

12. Calculate average reservoir pressure.
13. Estimate well productivity index based on average reservoir pressure, p_r, wellbore flowing pressure, p_{wf}, and a known production rate, which is held constant throughout the production period.

Model III is not really a new analytical solution, rather a new workflow to improve an estimation of flowing-fluid temperature distribution in the reservoir. In addition, well productivity approximation becomes more reasonable in this approach because fluid viscosity variation due to changes in pressure and temperature are taken into account in this approach.

An example case for reservoir flowing-fluid temperature estimation is discussed in Chapter III. Comparison of results from proposed analytical models with and without heat transfer from/to surroundings, as well as results from an improved version of the model are also presented and discussed in the same Chapter.

CHAPTER III

MODEL APPLICATIONS AND VALIDATION

3.1 Model Applications

The analytical model for fluid temperature can generally be applied to a single-phase oil reservoir to estimate flowing-fluid temperature in the reservoir, as well as fluid temperature in the wellbore at perforation depth. In a situation where significant J-T heating is expected, fluid temperature at bottomhole will be higher than the original reservoir temperature and potentially affect well equipment and tubular grade selection. The solution can be coupled with wellbore heat-transfer model to evaluate fluid temperature profile along the wellbore.

The analytical reservoir temperature model generally allows an inverse analysis for some reservoir properties, such as permeability and reservoir-drainage area. During production phase, flow rates can also be evaluated if reservoir properties are well estimated.

Additionally, a reasonable estimate of reservoir fluid temperature allows better approximation of fluid properties throughout the reservoir, which, in turn, result in better well productivity estimation. Ultimately, a more accurate productivity forecast is very beneficial for production and reservoir engineering, from the standpoint of both single-well management and full-field development planning.

3.2 Actual Field Well and Reservoir Data

In this study, reservoir rock and fluid properties from an actual well and reservoir is used to test the model. This field data is the same data set as presented in App's paper (2010). The proposed model is, therefore, later validated with the results from a rigorous numerical model that App (2010) reported. The model validation details and results are presented later in Section 3.5.

Table 1 presents the reservoir rock and fluid properties of a particular reservoir, which is considered as a base case in this study. We assumed that the reservoir is homogeneous and these parameters remain constant throughout the production period.

Table 1: Reservoir rock and fluid parameters of an actual reservoir used in the study (App, 2010)

Parameter, unit	Value
Permeability, md	20
Porosity, %	25
Thickness, ft	100
Initial Reservoir Pressure, psia	21,000
Bubblepoint Pressure, psia	7,000
Rock Compressibility, psi^{-1}	3×10^{-6}
Initial Temperature, °F	302
Wellbore Radius, ft	0.41
Reservoir Outer Radius, ft	4,000
Irreducible Water Saturation, %	15

Table 1: Continued

Parameter, unit	Value
Reservoir Heat Transfer Coefficient, BTU/hr·ft^2·°F	0.92

Table 2 shows reservoir fluid properties of the same reservoir. All formation water is considered irreducible and there is no free gas production in the reservoir system.

Table 2: Reservoir fluid parameters of an actual reservoir used in the study (App, 2010)

Parameter, unit	Value
Oil Formation Volume Factor, bbl/STB	1.05
Fluid Density – oil , lbm/ft^3	51.19
Specific Heat Capacity - oil, BTU/lbm·ft	0.53
Joule-Thompson throttling coefficient - oil, °F /psi	-0.0055
Fluid Density – water , lbm/ft^3	63.68
Specific Heat Capacity - water, BTU/lbm·ft	1.0
Joule-Thompson throttling coefficient - water, °F /psi	-0.0024
Density – formation , lbm/ft^3	165.43
Specific Heat Capacity – formation, BTU/lbm·ft	0.20
Thermal Conductivity, BTU/ hr·ft·°F	1.73

Another critical fluid property in flowing-fluid temperature and well productivity calculation is oil viscosity. The oil viscosity data from laboratory measurement for this particular reservoir fluid is also presented in App's paper. Fig. 3 demonstrates oil viscosity as a function of pressure and temperature of the base case sample.

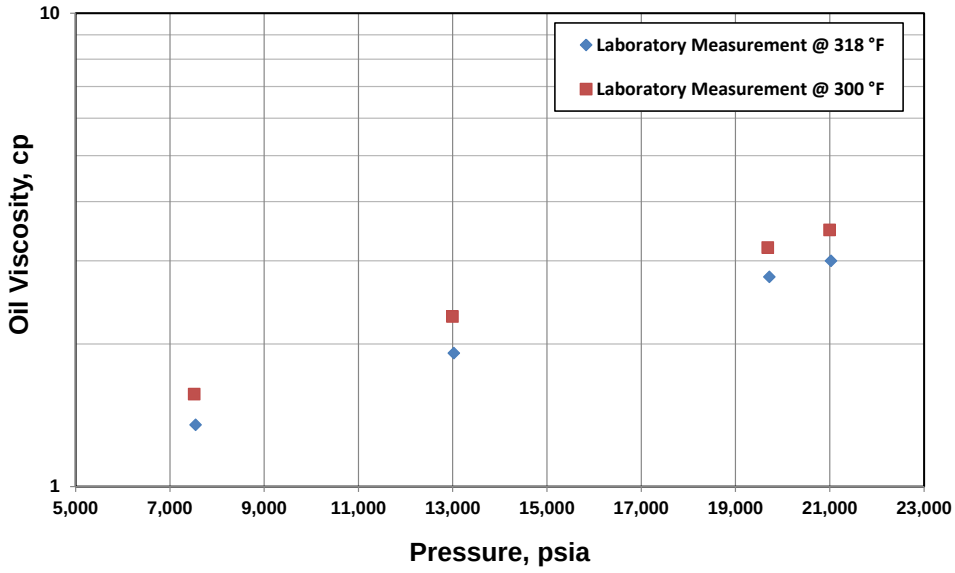

Fig. 3: Oil viscosity as a function of pressure and temperature (App, 2010)

We also calculated oil viscosity based on viscosity correlations that are available in the industry such as Beggs and Robinson's (1975) and Standing's (1947) correlations. However, estimated viscosities from those correlations do not exactly match the laboratory data presented in Fig. 3. This is because most of the widely-used correlations were developed from more 'conventional' reservoirs at lower pressures and

temperatures. The reservoir that we are considering in this study is a high-pressure, high-temperature reservoir; therefore, the conventional viscosity correlations are not directly applicable. Comparison of oil viscosity calculated from those correlations and laboratory measurement data is also shown in Appendix B for reference.

3.3 Model Results: Field Data

A version of the proposed analytical model assumes constant reservoir fluid properties throughout space and time. In this simple case, average oil viscosity, average density, and average oil formation volume factor are used in the model to calculate flowing-fluid temperature profile in the reservoir. Results from the analytical model without and with consideration of energy transfer between reservoir and over- and under-burden formations, Model I and Model II, are discussed in Subsection 3.3.1 and 3.3.2, respectively.

3.3.1 Model I: analytical model without heat transfer to over/underburden formations (constant fluid properties)

As discussed in Chapter II, an analytical solution for fluid temperature distribution in reservoir without any heat transfer from system to surroundings can be expressed as

$$T(r,t) = T_i - \frac{C}{2B}\ln\left(\frac{r^2 A}{|r^2 A + 2Bt|}\right) \tag{2.31}$$

where *A*, *B*, and *C* are lump parameters (constant) which are the products of rock and fluid properties as described in Eq. 2.27, Eq. 2.28, and Eq. 2.29.

Eq. 2.31 shows that fluid temperature in the reservoir at any time can be easily calculated from this solution. In this Subsection, results from three different study cases of the same reservoir discussed in Section 3.2 will be presented. The three cases include:

1. Evaluation of flowing-fluid temperature distribution in the reservoir at one given production rate over production period.
2. Evaluation of flowing-fluid temperature distribution in the reservoir at various production rates at a particular time of interest.
3. Evaluation of bottomhole flowing-fluid temperature at various production rates over time.

Specific input data and results for each Case Study are discussed in Subsection 3.3.1.1, 3.3.1.2, and 3.3.1.3 respectively.

3.3.1.1 Case Study 1: flowing-fluid temperature distribution in the reservoir at a given production rate over time (Model I)

In this specific case study, production rate is fixed at 6,200 STB/D. We applied Model I to estimate flowing-fluid temperature distribution in the reservoir at a different production timeframe. Fig. 4 shows flowing-fluid temperature profile in the reservoir at 0.5 hours, 3 hours, 1 day, 10 days, 100 days, and 400 days after start of production.

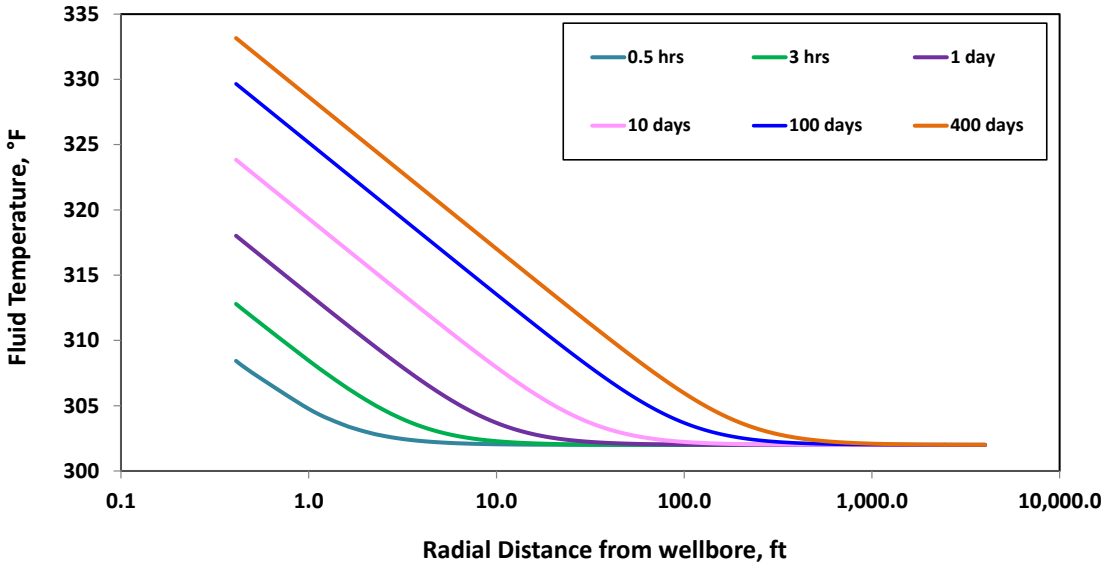

Fig. 4: Flowing-fluid temperature distribution in the reservoir over production period (constant production rate of 6,200 STB/D), estimated by Model I

From Fig. 4, we observe that the reservoir fluid gets heated up gradually over time. This heating is caused by Joule-Thomson phenomenon, where fluid temperature changes when a significant pressure drop occurs. In this specific reservoir, J-T throttling coefficient is negative in our operating pressure region (high pressure region); thus, J-T heating is expected. We also observe that the 'heated' region is mostly near the wellbore. This is because most of pressure drop in reservoir happens in a near wellbore region and J-T heating is basically proportional to the pressure drop along the flow path. As a result, fluid temperature in a near wellbore region is significantly higher than that away from the wellbore region.

Over time, the fluid temperature keeps increasing but the rate of temperature increase declines over time. Based on this model, the flowing-fluid temperature at

bottomhole can be 31°F higher than the original reservoir temperature after 400 days of continuous production. As Fig. 4 shows, the heated region generally expands from a few feet from wellbore during early production period to hundreds of feet from the wellbore after 400 days of production.

3.3.1.2 Case Study 2: flowing-fluid temperature distribution in the reservoir at various production rates at a specific timeframe (Model I)

The same analytical model (Model I) is used to estimate the flowing-fluid temperature in the reservoir when the reservoir produces at different flow rates. Fig. 5 shows fluid temperature in the reservoir after 50 days production for five different flow rate cases; that is, 970, 2,050, 3,270, 4,650, and 6,200 STB/D.

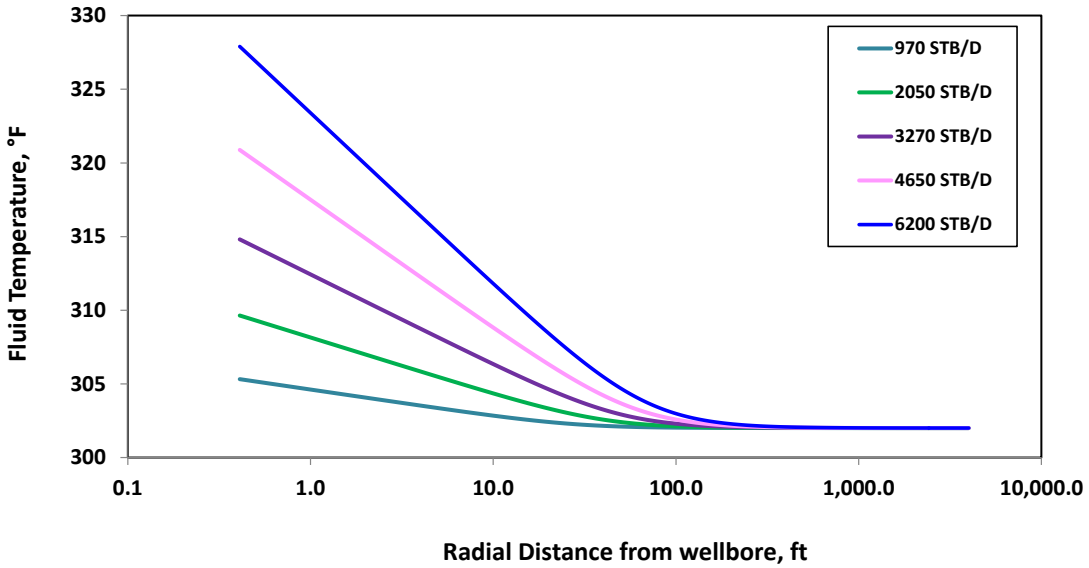

Fig. 5: Flowing-fluid temperature distribution in the reservoir after 50 days of production at various production rates, estimated by Model I

As in Fig. 4, Fig. 5 also emphasizes the fact that J-T heating is more significant in the near wellbore region. It also shows that reservoir fluid heating is increased with the rise in production rates. The 'impacted' region is also larger at higher production rates. According to the comprehensive energy-balance equation (Eq. 2.19), fluid local velocity affects energy balance of the reservoir system in several ways, particularly rate of energy transfer due to convective transport and viscous dissipation or J-T heating/cooling phenomenon. In other words, J-T heating is directly proportional to fluid flow rate; therefore, fluid flowing temperature is generally higher when reservoir is producing at higher rates.

3.3.1.3 Case Study 3: flowing-fluid temperature at bottomhole at various production rates over time (Model I)

Generally, actual fluid temperature measurement can only be made in the wellbore. Most of the time, bottomhole temperature calculated from the model is compared to actual temperature from downhole measurement to validate the temperature model. In this section, Model I is used to calculate the bottomhole flowing-fluid temperature for various production rates throughout the production period. Fig. 6 shows fluid bottomhole flowing temperature over time when reservoir is producing at 970, 2,050, 3,270, 4,650, and 6,200 STB/D (same production rates as in Case Study 2).

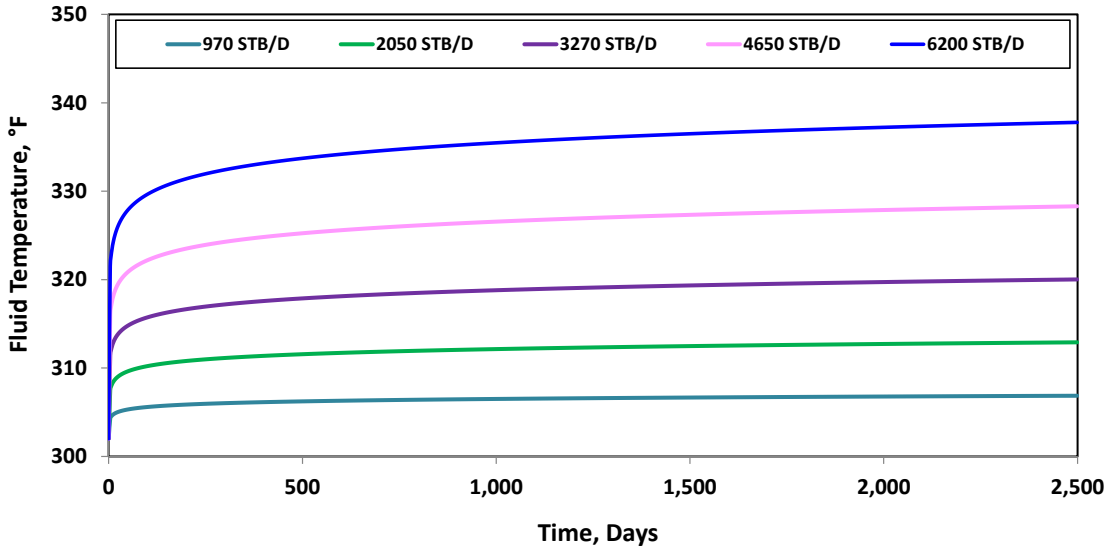

Fig. 6: Bottomhole flowing-fluid temperature at various production rates over time, estimated by Model I

Fig. 6 suggests that the bottomhole temperature gets higher with increasing production rates. This trend is consistent with the first two study cases. We also observe that the flowing-fluid temperature at bottomhole keeps increasing over time, even after a few years of production. This effect is mainly because of our assumption that there is no energy transfer from the reservoir to over-burden formations; therefore, most of the heat generated by J-T heating during production eventually translates to a rise of flowing-fluid temperature.

In all study cases, results from our analytical model without a consideration of heat transfer to over- and under-burden formations (Model I) show that the fluid temperature keeps increasing over time. This observation appears to contradict the fact that the rate of reservoir fluid temperature rise should decline over time and reach an

equilibrium temperature once heat loss (or gain) to over- and under-burden formations equal to heat gain (or loss) from J-T heating (or cooling). Additionally, reservoir fluid temperature could in fact decrease over time once energy transfer to surrounding formations increases. Subsection 3.3.2 discusses results from the other analytical temperature model, which takes into account energy transfer from reservoir to over-burden formations into the analysis.

3.3.2 Model II: analytical model with heat transfer to over/underburden formations (constant fluid properties)

Energy transfer between reservoir and over/underburden formations are included in this version of the model. Assumptions and details of the model were already discussed in Chapter II. The analytical solution for flowing-fluid temperature estimation with a consideration of heat transfer to surroundings, or Model II, is expressed as

$$T(r,t) = T_i + \frac{C}{2B} e^{\frac{H(Ar^2+2Bt)}{2B}} Ei\left[-\frac{H(Ar^2+2Bt)}{2B}\right] - \frac{C}{2B} e^{\frac{HAr^2}{2B}} Ei\left[-\frac{HAr^2}{2B}\right] \quad (2.42)$$

where *A*, *B*, *C*, and *H* are lump parameters (constant) which are products of rock and fluid properties as described in Eq. 2.27, Eq. 2.28, Eq. 2.29, and Eq. 2.43.

Results from the same study cases will be presented and discussed in this subsection. The results from this model version is compared to the results derived from analytical model without any heat transfer to surrounding (Model I) to better understand the criticality of including heat transfer across system boundary into an evaluation.

3.3.2.1 Case Study 1: flowing-fluid temperature distribution in the reservoir at a given production rate over time (Model II)

The flowing-fluid temperature distribution for reservoir that is producing at a rate of 6,200 STB/D as calculated by this version of the model is shown in Fig. 7. Results from the analytical model without heat transfer between the reservoir and over-burden formations of the same case study, presented in the previous subsection, are also shown as dash lines in Fig. 7 for comparison.

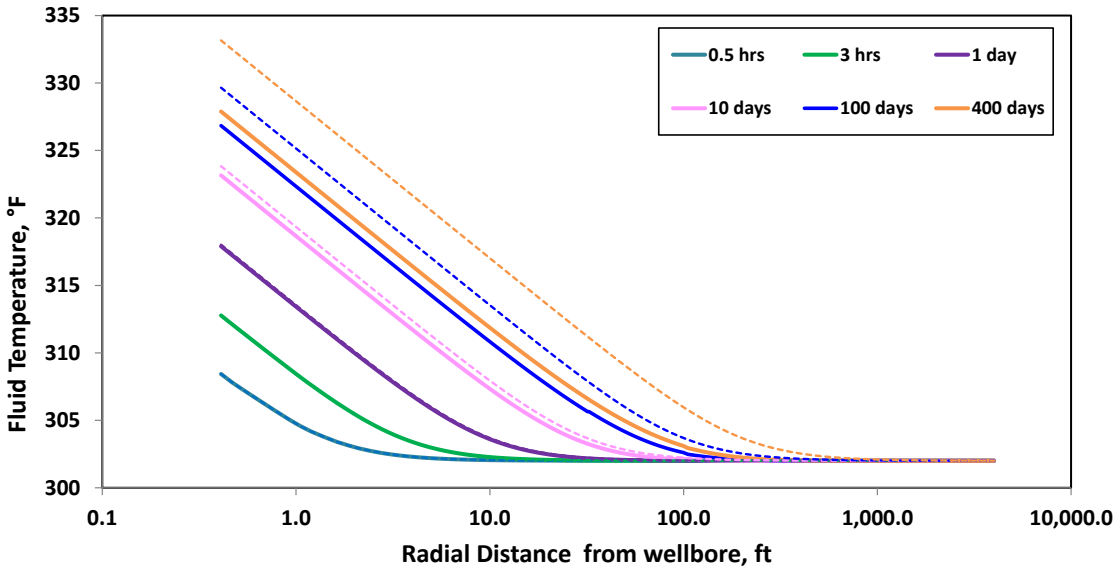

Fig. 7: Flowing-fluid temperature distribution in the reservoir over production period (constant production rate at 6,200 STB/D). Dashed and solid lines represent flowing-fluid temperature distribution estimated by Model I and Model II, respectively.

Fig. 7 shows that at early times, both models (Model I and Model II) give similar, if not the same, results. However, differences from both models are observed after 10 days of production and the differences in fluid temperature calculated from both

models get larger over time. Fluid temperatures estimated with Model II are generally lower than that calculated by the other model. Let us explore this point further.

For this specific case, reservoir fluid is heated up due to J-T heating during production. Once the flowing fluid temperature in the reservoir is significantly higher than the over- and under-burden formation temperature, energy gets transferred from the reservoir to surrounding formations. Therefore, the 'heat up' process of fluid in the reservoir due to J-T effect is slowed down. In other words, rate of reservoir fluid temperature rise is reduced when heat transfer to over- and under-burden formations is incorporated in our analysis.

During early production period, reservoir fluid temperature gets higher but reservoir fluid temperature is still not high enough to cause a significant heat transfer from reservoir to overburden formations. As a result, heat transfer to the surrounding has very minimal impact on the calculations; therefore, fluid temperatures calculated from both models are very similar.

3.3.2.2 Case Study 2: flowing-fluid temperature distribution in the reservoir at various production rates at a specific timeframe (Model II)

Fig. 8 shows fluid temperature in the reservoir after 50 days production for five different flow rate cases; that is, 970, 2,050, 3,270, 4,650, and 6,200 STB/D. The solid lines on the plot represent results estimated by Model II, whereas the dashed lines are the results from Model I.

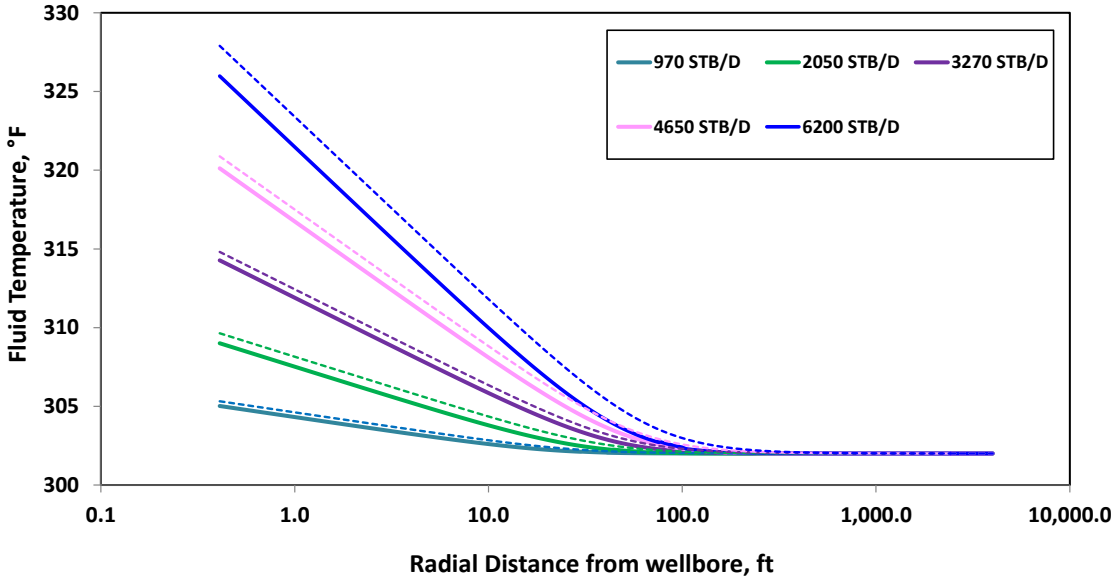

Fig. 8: Flowing-fluid temperature distribution in the reservoir after 50 days of production at various production rates. Dashed and solid lines represent flowing-fluid temperature distribution estimated by Model I and Model II, respectively.

These results convey the same massage as the first case study in that the fluid temperature estimated by an analytical solution with consideration of heat transfer from reservoir is lower than that predicted by Model I. Fig. 8 shows that discrepancy of results from the two models grows with increasing production rate. This point emphasizes the fact that discrepancies are more prominent when reservoir fluid is significantly higher than the initial temperature.

3.3.2.3 Case Study 3: flowing-fluid temperature at bottomhole at various production rates over time (Model II)

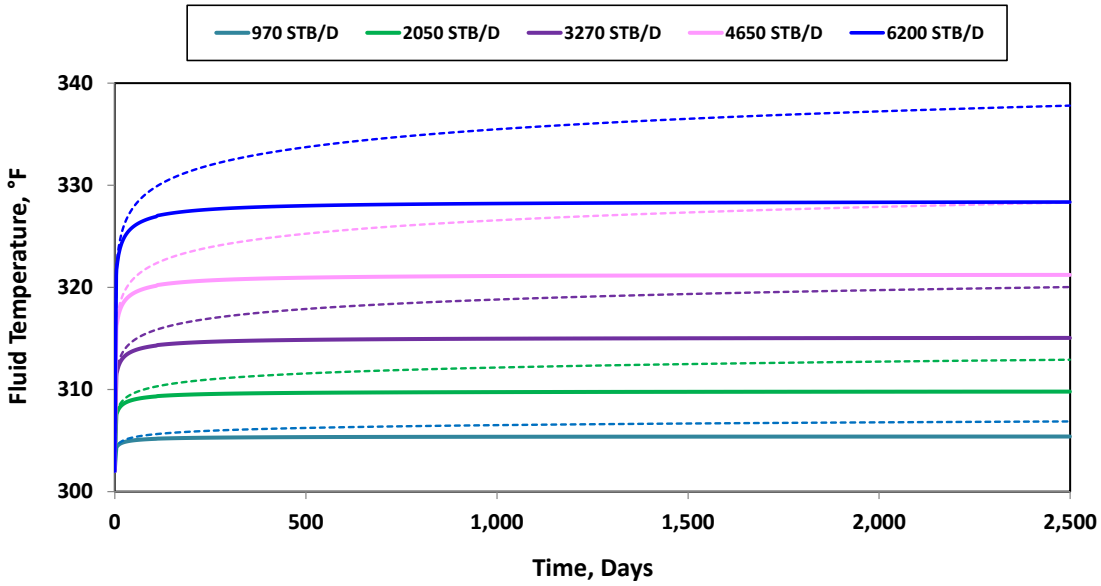

Fig. 9: Bottomhole flowing-fluid temperature at various production rates over time. Dashed and solid lines represent flowing-fluid temperature distribution estimated by Model I and Model II, respectively.

Fig. 9 shows a comparison of bottomhole fluid temperature approximated by Models I and II. The results show that fluid temperature estimated from the model without consideration of heat transfer from the reservoir is always higher. Additionally, Fig. 9 shows that change in fluid temperature is minimal at late production times, when the model with heat transfer to surroundings (Model II) is implemented. Fluid temperature reaches a steady-state condition once reservoir has been on production long enough. Fig. 9 also demonstrates that differences of results from the two models get

larger at higher production rate when the J-T phenomenon has more influence on flowing-fluid temperature in the reservoir.

During early production period, both models (Model I and II) result in similar results. This trend is explained by the small temperature differences between reservoir and over/underburden formations, meaning that heat transfer from the reservoir is insignificant. However, in reality, when the reservoir fluid is heated up to a certain point, energy will be transferred from a more 'heated' region (reservoir) to a cooler region (over/underburden formations). In addition, the heat transfer gets larger over time once fluid temperature in the reservoir reaches a certain threshold value. Therefore, an analytical model with a consideration of heat transfer to surroundings (Model II) generally gives more reasonable estimate of flowing-fluid temperature distribution in the reservoir. Both analytical solutions are relatively simple in terms of computational cost.

Results from both models are also compared to our simplified numerical solution and a more rigorous numerical solution developed by App (2010). Details for those comparisons are presented and discussed in Section 3.4 and Section 3.5, respectively.

3.4 Comparison of Results to a Simplified Numerical Solution

To verify the results from our analytical solutions, we developed simplified numerical solutions for both problems: problems with and without a consideration of energy transfer between the reservoir and its surroundings.

As discussed in Chapter II, the energy balance equation for our system can be simplified as

$$\left[\emptyset s_o \rho_o c_{po} + \emptyset s_w \rho_w c_{pw} + (1-\emptyset)\rho_f c_{pf}\right]\left(\frac{2\pi r^2 h}{q}\right)\frac{\partial T}{\partial t} - \rho_o c_{po}(r)\frac{\partial T}{\partial r} - \frac{q\rho_o \sigma_o \mu}{2\pi hk} =$$

$$\dot{Q}\left(\frac{2\pi r^2 h}{q}\right) \tag{2.32}$$

For problem without heat transfer from the reservoir, the right side of Eq. 2.32 becomes zero. We observe that this PDE can be solved numerically without any difficulties for both problem cases. Appendix C presents the concepts and steps used to develop the simplified numerical solution.

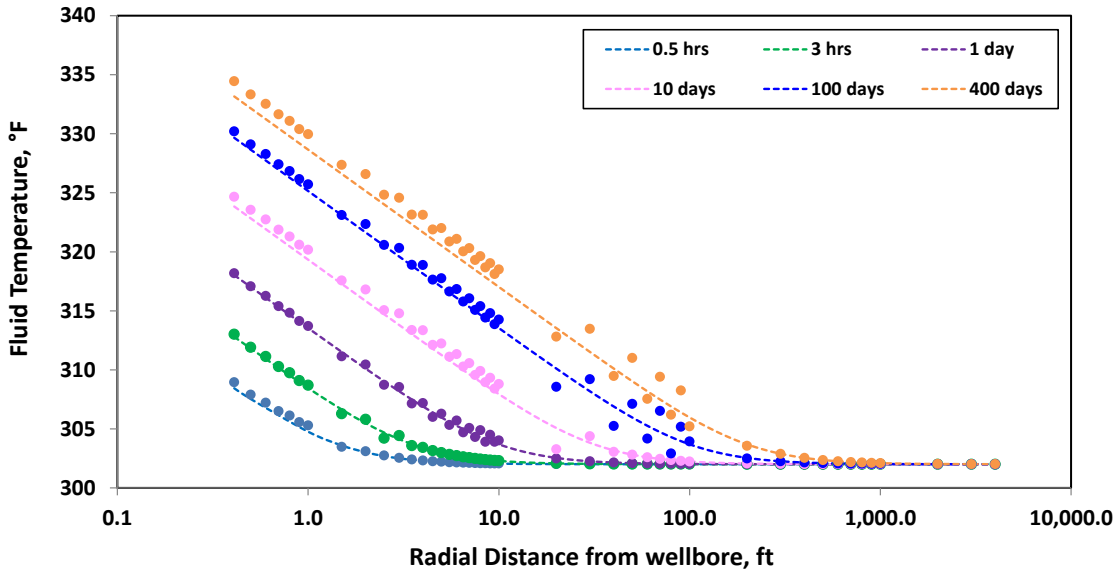

Fig. 10: Comparison of Model I (dashed lines) and simplified numerical solution (circle dots) results of flowing-fluid temperature distribution in the reservoir over production period (constant production rate at 6,200 STB/D)

Case Study 1, where fluid temperature distribution over time is calculated at a constant rate of 6,200 STB/D, is used for model verification. Fig. 10 shows a comparison of results from our analytical model and a simplified numerical solution

without consideration of heat transfer from reservoir to over- and under-burden formations. We observe that our results from the analytical model align very well with the simplified numerical solutions throughout the entire production period. This agreement indicates that our analytical solution provides a good estimation of the flowing-fluid temperature in the reservoir for this system.

Fig. 11 compares analytical and numerical results when energy transfer from the reservoir to its surroundings is incorporated. Clearly, the analytical solution aligns well with the results from the simplified numerical solution.

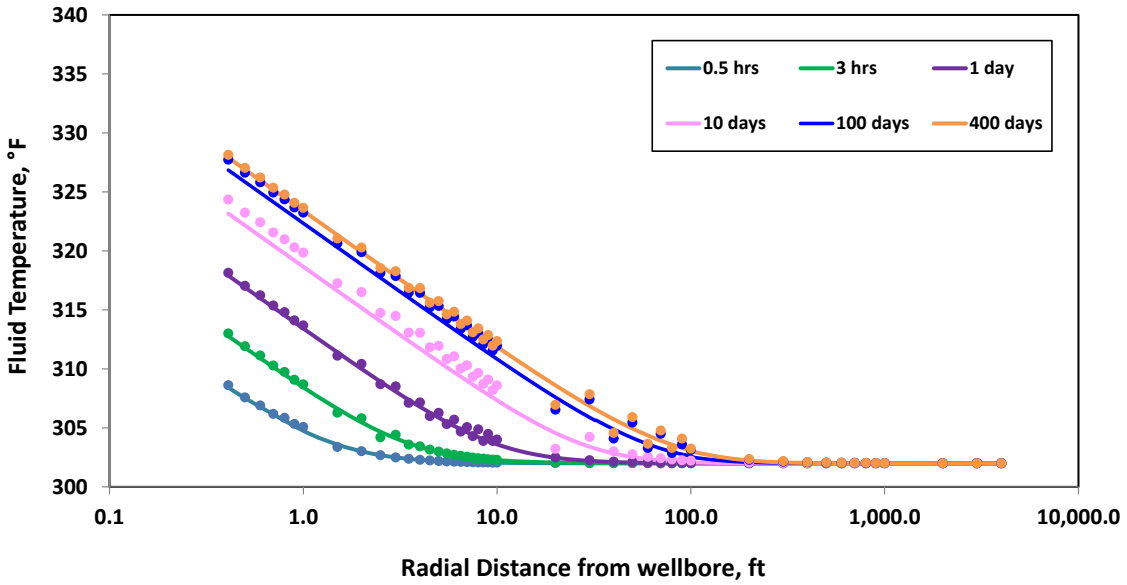

Fig. 11: Comparison of analytical and simplified numerical solution results of flowing-fluid temperature distribution in the reservoir over production period (constant production rate at 6,200 STB/D) **with** a consideration of heat transfer to surroundings.

Comparisons between analytical and simplified numerical solutions confirm that both analytical models (Model I and Model II) give a reasonable estimation of the

flowing-fluid temperature in the reservoir. However, as discussed in the previous section, a model that incorporates energy transfer from the reservoir to its surrounding formations is preferred for a more reasonable forecast of the flowing-fluid temperature in the reservoir throughout the entire production period.

3.5 Model Validation with Results from a Rigorous Numerical Solution by App (2010)

Generally, flowing-fluid temperature at bottomhole can be directly measured in the wellbore with a downhole gauge; on the other hand, fluid temperature distribution in reservoir cannot be physically measured. This fact basically implies that we cannot directly validate the whole fluid temperature profile in the reservoir with actual data. Consequently, we selected the results from App's study to validate our analytical models.

App successfully validated his work by matching bottomhole temperature and pressure from his model with continuous temperature and pressure data from downhole gauges measurement during pressure-transient analysis. In addition to evaluation of fluid temperature and pressure at bottom of the well, he also presented flowing-fluid temperature distribution in the reservoir predicted at various flow conditions. We will validate our work by comparing the analytical solutions to those results from the rigorous numerical model presented in his paper (App, 2010).

The same three case studies are used for model validation. Results from both analytical models, Models I and II, are used here. Fig. 12 shows validation of results for Case Study 1, where production rate is set at 6,200 STB/D for Model I.

Fig. 12 shows that at early production period, results from Model I match well with App's numerical solutions. However, the model overestimates reservoir fluid temperature once production time begins to grow. This outcome is not surprising because Model I does not take into account any potential heat loss from reservoir to over- and under-burden formations, when reservoir fluid is significantly heated up by the J-T effect.

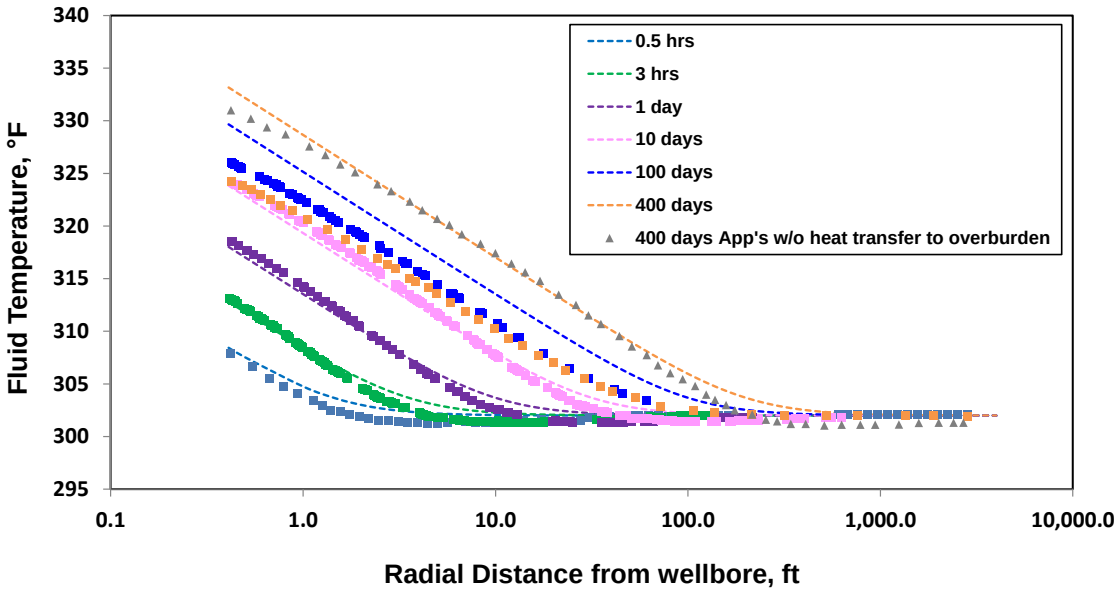

Fig. 12: Model validation: results from Model I (dash lines) VS results from rigorous numerical model by App (2010) (solid squares) - Case Study 1

Results also show that fluid temperature profile at 400 days of production matches quite well with App's model when heat transfer to surroundings is taken out from his energy-balance equation. This point emphasizes the significance of including 'heat transfer to over- and under-burden' term in our reservoir fluid temperature analysis.

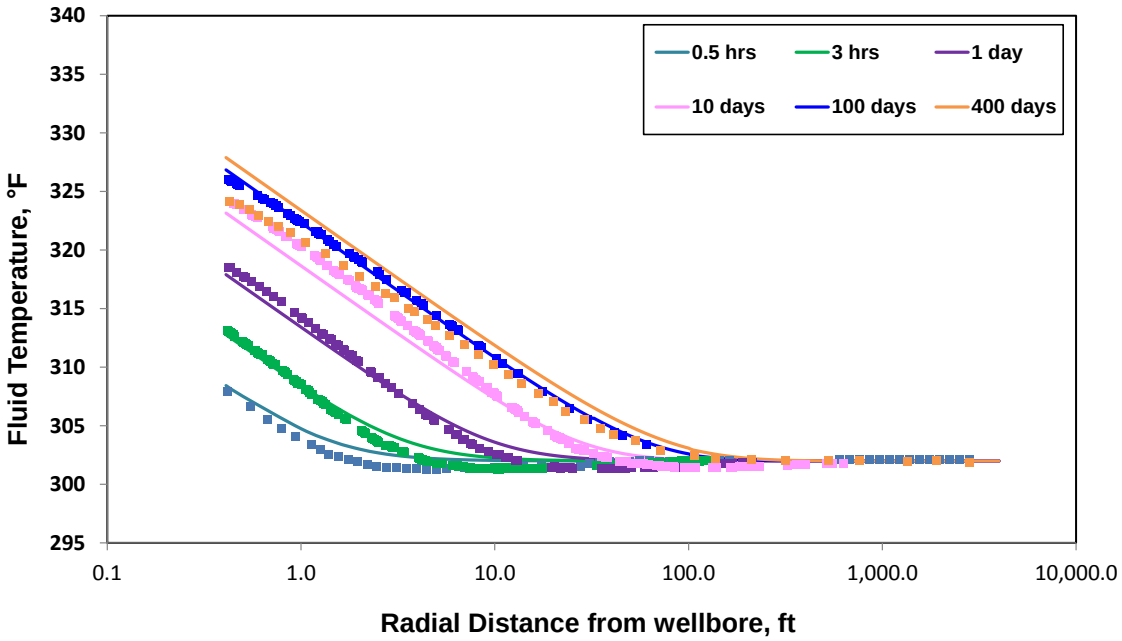

Fig. 13: Model validation: results from Model II (solid lines) VS results from rigorous numerical model by App (2010) (solid squares) - Case Study 1

Comparisons of results from Model II to App's results are shown in Fig. 13. Here, the analytical model results are reasonably close to those obtained from App's numerical simulations. In addition, the estimated fluid temperature in the reservoir at later times (> 400 days) is significantly lower, compared to those results from Model I,

when heat transfer to surroundings is incorporated in the model. This highlights our suggestion to always include the 'heat transfer to over- and under-burden formations' term in the model.

Differences in temperature profiles, especially at late times, are expected. This mismatch owes to the constant fluid viscosity assumption that is implicit in the analytical model. In contrast, App's solution allows variation of viscosity over space and time based on reservoir pressure and temperature. A sensitivity analysis is performed to allow better understanding of fluid viscosity influence to estimation of flowing-fluid temperature in reservoir. Results from this sensitivity study are discussed in the next section of this Chapter.

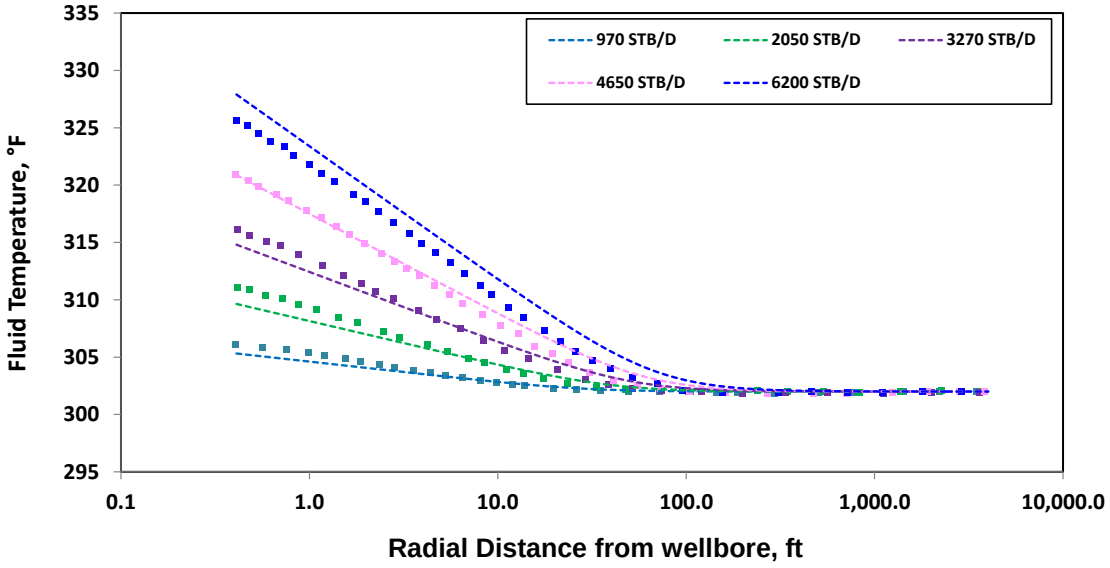

Fig. 14: Model validation: Model I (dashed lines) VS results from rigorous numerical model by App (2010) (solid squares) - Case Study 2

Case Study 2 and 3 are also looked at as part of our model validation. Figs. 14 and 15 demonstrate comparisons of results from Model I and App's numerical model for Case Study 2 and 3, respectively.

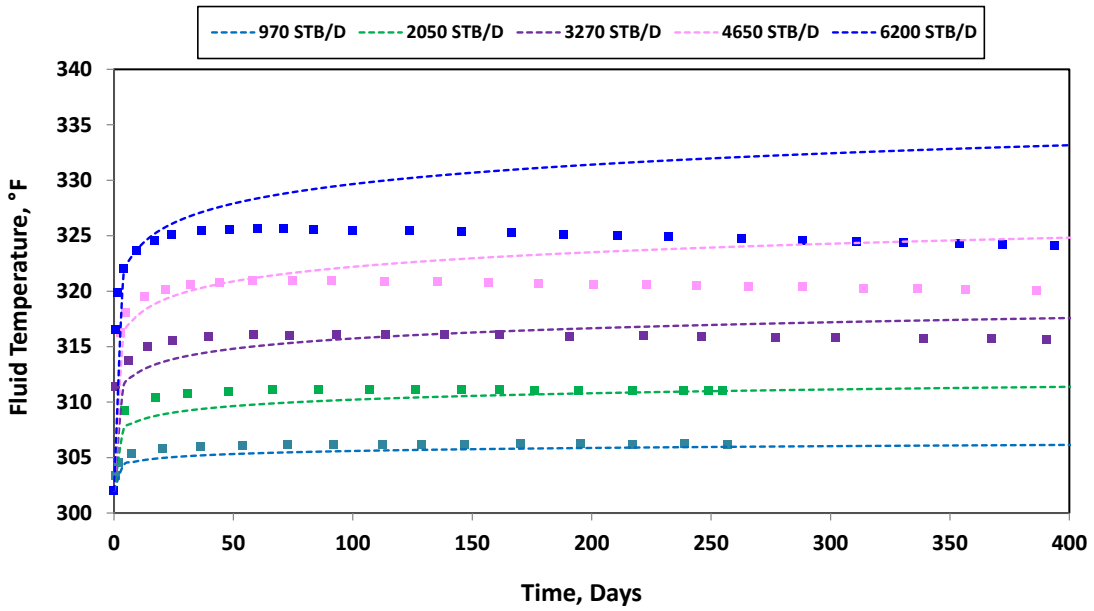

Fig. 15: Model validation: Model I (dashed lines) VS results from rigorous numerical model by App (2010) (solid squares)- Case Study 3

Both case studies show that the analytical model without consideration of heat transfer to/from surroundings (Model I) overestimates flowing-fluid temperature at later time. For example, Fig. 15 shows at 400 days of high rate production (6,200 STB/D), estimated fluid temperature at bottomhole could be up to almost 10°F higher than that obtained by App's numerical model, if reservoir-to-overburden heat transfer term is not incorporated in the model.

Figs. 16 and 17 show validation of Model II using Case Studies 2 and 3, respectively. Results from an analytical model with heat transfer from reservoir to over- and under-burden formations, Model II, are presented in solid lines whereas App's numerical results are shown in solid squares.

Clearly, Model II gives a more reasonable estimation of fluid temperature in the reservoir, compared to the model without 'heat transfer to surroundings' term (Model I). At 400 days of high-rate production (6,200 STB/D), the difference between bottomhole flowing temperature estimated by our analytical model and the numerical model is reduced to 3°F once the 'heat transfer' term is included.

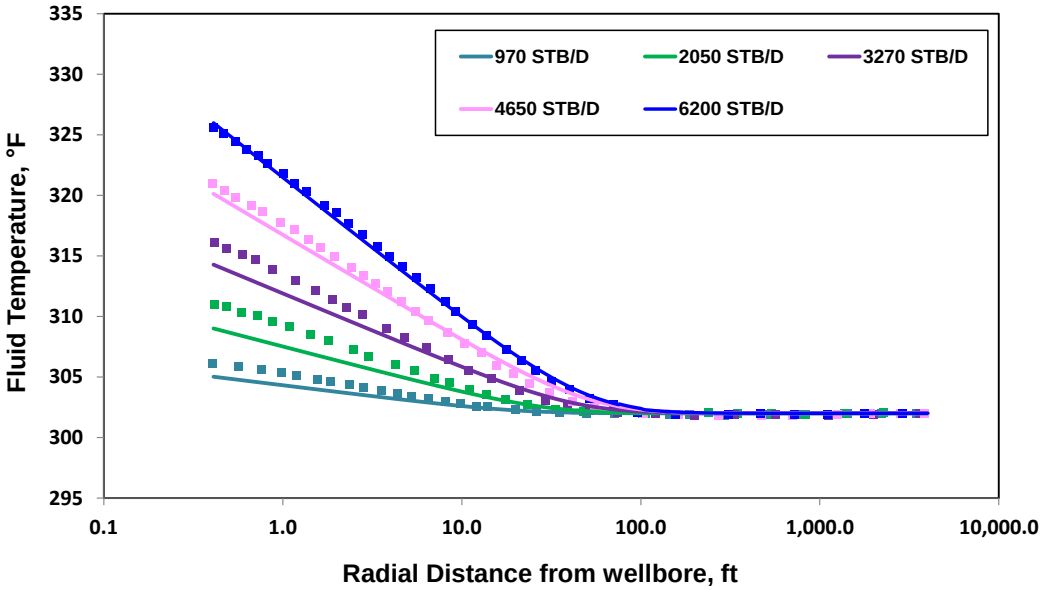

Fig. 16: Model validation: Model II (solid lines) VS results from rigorous numerical model by App (2010) (solid squares) - Case Study 2

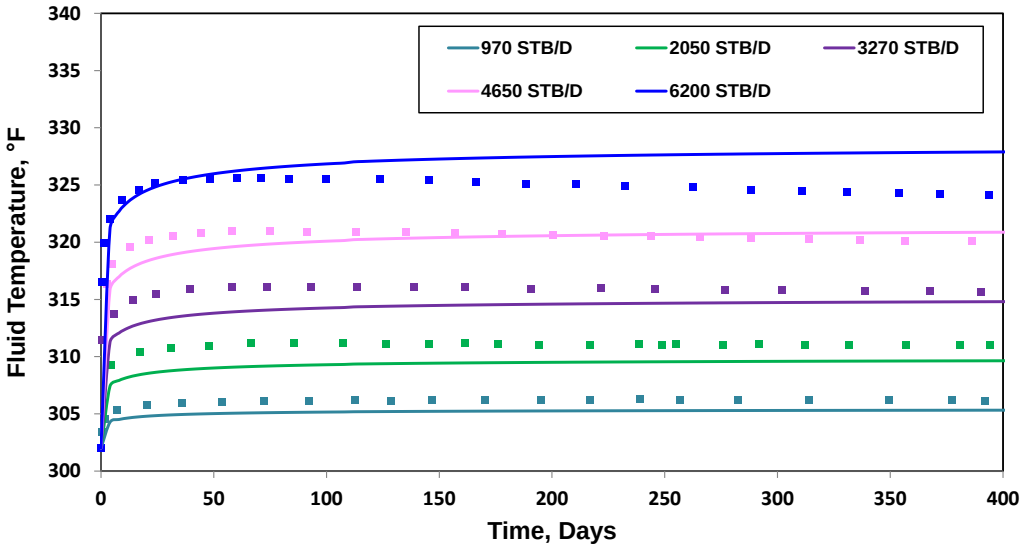

Fig. 17: Model validation: Model II (solid lines) VS results from rigorous numerical model by App (2010) (solid squares) - Case Study 3

The constant-viscosity assumption is thought to be one of the main reasons for differences in flowing-fluid temperature estimated by the proposed analytical model and App's numerical solutions. Thus, we conducted a separate analysis to understand the impact of fluid viscosity for estimating reservoir-fluid temperature. Results from that analysis are discussed in Section 3.6.

At this point, we have demonstrated that the analytical model with the incorporation of heat transfer from reservoir to the surrounding formations generally yields a better estimate of flowing fluid temperature in the reservoir. Therefore, only the model (Model II) with the 'heat transfer' term will be used for all subsequent analyses.

3.6 Impact of Fluid Viscosity to an Estimation of Flowing-Fluid Temperature in the Reservoir

Generally, the magnitude of J-T heating/cooling of fluid in reservoir depends on the amount of pressure drawdown along the flow path, as well as J-T throttling coefficient, which is normally unique to reservoir fluid. Based on Darcy's equation, pressure drop along the flow path, $\frac{\partial p}{\partial r}$,is directly proportional to fluid viscosity in the reservoir. Therefore, in theory, fluid viscosity has a direct impact in reservoir fluid temperature forecasting when the J-T effect is invoked.

To better understand the influence of fluid viscosity to flowing-fluid temperature calculations, viscosity sensitivity analysis is conducted. In this sensitivity study, four different values of fluid viscosity in the same reservoir system are considered. Thereafter, the flowing-fluid temperature profiles for each viscosity case are generated by using the analytical model (Model II: with reservoir-to-overburden formation heat transfer).

Comparisons of temperature profiles calculated for the four viscosity cases when reservoir has produced at 6,200 STB/D for 3 hours and 100 days are shown in Fig. 18. Reservoir fluid temperature profiles at 3 hours are shown in green and that at 100 days are shown in blue. Fig. 18 shows that the fluid is heated up more significantly when viscosity is higher at the same production period. In addition, fluid viscosity has more influence on reservoir fluid temperature at longer production times. An impact of temperature rise due to J-T phenomenon is greater when reservoir keeps producing and viscosity directly affects magnitude of J-T heating in reservoir. As a result, fluid

temperature is more sensitive to fluid viscosity when the J-T effect is significant; that is, at higher production rate and/or longer production period.

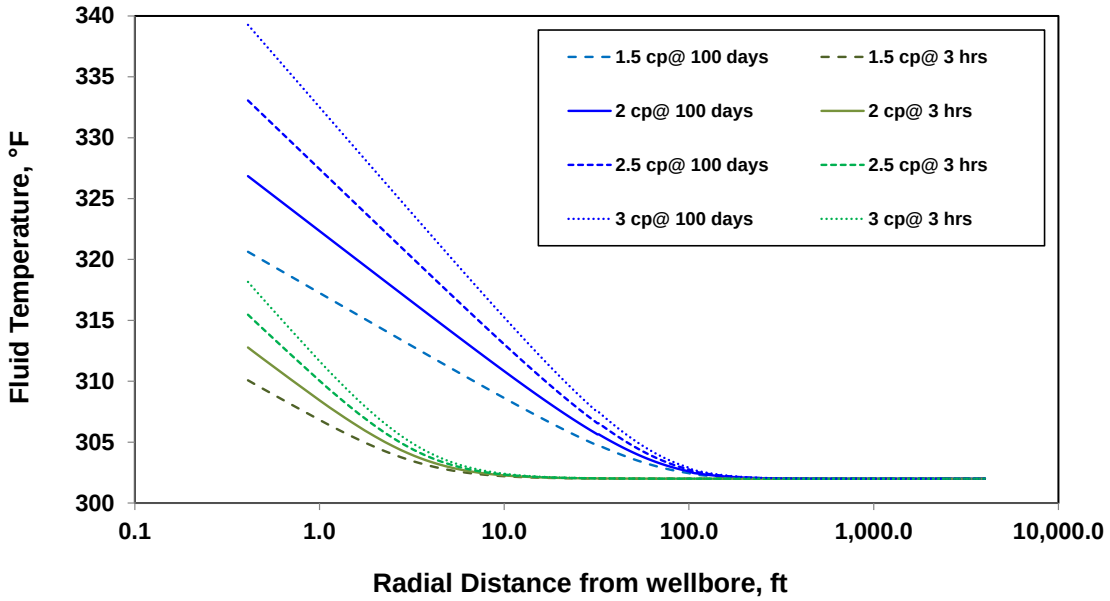

Fig. 18: Comparison of fluid temperature profiles in reservoir calculated from different fluid viscosity after 3 hours (*in green*) and 100 days (*in blue*) of 6,200 STB/D production. Fluid temperature is calculated by Model II.

Additionally, we recognized that results from Model II (shown in Fig. 13, Fig. 16, and Fig. 17 for Case Study 1, 2, and 3) can be improved if a more reasonable average viscosity value is used in the model. Better matches to App's numerical results when different values of viscosity are used are shown in Appendix D.

We can now conclude that the flowing-fluid temperature estimation is very sensitive to fluid viscosity. In our analytical model, we use constant (average) viscosity to calculate fluid temperature profile in the reservoir. Fluid viscosity in the reservoir

actually varies over time because of pressure depletion and changes in fluid temperature during production due to the J-T effect. Thus, we developed a calculation workflow to integrate our analytical temperature model and fluid viscosity variation over space and time to allow a better estimation of flowing-fluid temperature in the reservoir.

Details of improved solution workflow were discussed in Section 2.5. Results from an improved analytical solution (Model III) will be discussed in the following section.

3.7 Results from an Improved Analytical Solution (Model III)

The main difference between the original and improved analytical solution is fluid viscosity. Viscosity of reservoir fluid is assumed constant in the original models (Models I and II), whereas an improved analytical solution (Model III) incorporates viscosity variation with reservoir pressure and temperature into flowing-fluid temperature calculations. In this section, data from the same reservoir presented in Section 3.2 is used to allow comparison between results from Models I and II, discussed in Section 2.4, with the improved analytical solution, Model III discussed in Section 2.5. Additionally, results from an improved solution are compared to App's numerical results as part of model validation. All the models presented in this section take into account energy transfer between reservoir and over- and under-burden formations.

Laboratory measurements of viscosity for this particular reservoir fluid are available. Relationship between fluid viscosity and reservoir pressure and temperature is

developed. Fluid viscosity as a function of pressure and temperature is then coupled to the reservoir temperature model in an improved analytical solution.

The same three case studies are considered in model validation. First, results from improved and original analytical solutions are compared. Then, results from the improved analytical solution (Model III) are validated with results from App's rigorous numerical simulations.

3.7.1 Comparison of results from improved and original analytical solution (Model II VS Model III)

Figs. 19 and 20 show comparisons of flowing-fluid temperature in the reservoir calculated by the original and improved analytical solutions for Case Study 1 and 2, respectively. Solid lines are fluid temperature derived from the original solution (Model II) and dashed lines are fluid temperature estimated by the improved version of solution (Model III).

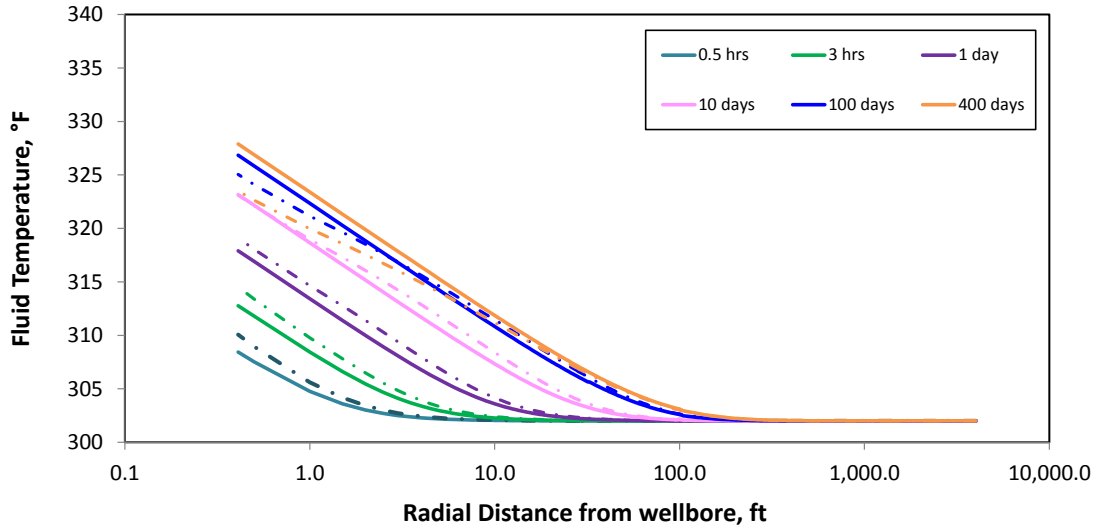

Fig. 19: Comparison of flowing-fluid temperature profiles in the reservoir calculated from Model II (solid lines) and Model III (dashed lines) - Case Study 1

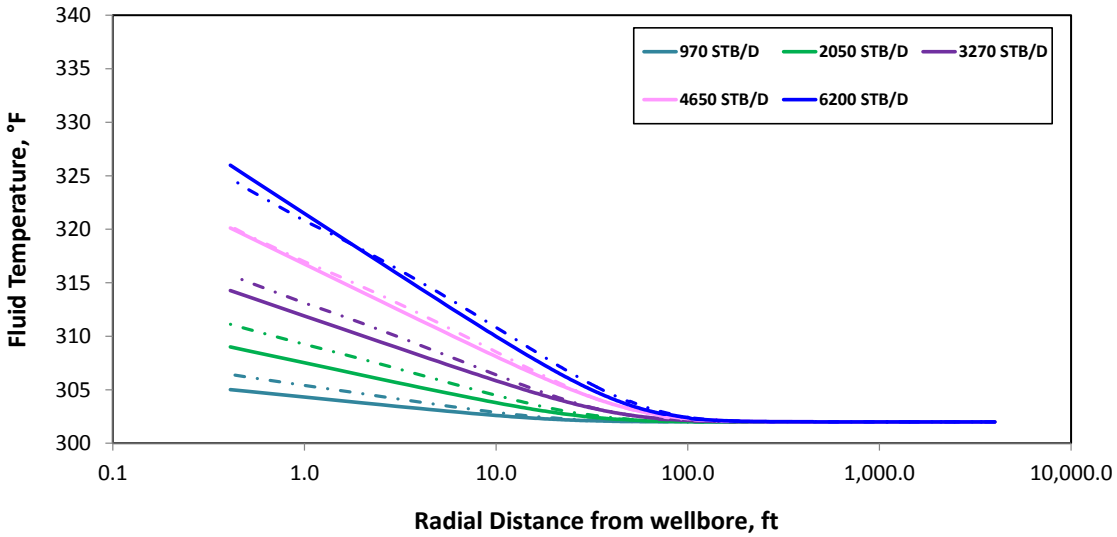

Fig. 20: Comparison of flowing-fluid temperature profiles in the reservoir calculated from an original model, Model II (solid lines) and improved model, Model III (dashed lines) - Case Study 2

Fig. 19 suggests that at early times, fluid temperature estimated by the original model is lower than that calculated from the improved model. However, the difference is in opposite direction at later times. Basically, the improved model takes into account fluid viscosity variation over time due to changes in pressure and temperature. Fluid viscosity is generally higher at early production period due to higher reservoir pressure and lower fluid temperature. Thus, J-T heating at early times in the improved solution is higher, compared to that in the original model. As a result, fluid temperature estimated by Model III is generally higher at early times.

On the other hand, fluid viscosity declines with time as production matures and reservoir gets depleted. Therefore, J-T heating calculated with Model III during depletion period is generally lower than that in the original solution, which is calculated from average viscosity.

Fig. 20 shows similar results: when production rate is small, fluid temperature forecasted by Model III is higher than that estimated by Model II. This is because at lower production rate, less fluid is drawn from the reservoir after 50 days of production; therefore, reservoir is less depleted. The J-T heating calculated by Model III is generally larger because fluid viscosity is actually higher than the average viscosity used in the original formulation. If we consider a certain production time, fluid viscosity is normally smaller when reservoir produces at higher production rate, resulting in an opposite impact to flowing-fluid temperature estimation: flowing-fluid temperature calculated by an improved model (Model III) is lower than that estimated by the previous model (Model II).

Fig. 21 shows a comparison of bottomhole flowing-fluid temperature calculated by original and improved models when reservoir is producing at different production rate (Case Study 3). Same as Case Study 2, we can see that at the same average viscosity, flowing-fluid temperature estimated from the original model is smaller at lower rate and the trends reverse for higher production rates. In this particular example, bottomhole fluid temperature estimated by Model II could be significantly higher than that calculated from Model III when production rate is 6,200 STB/D.

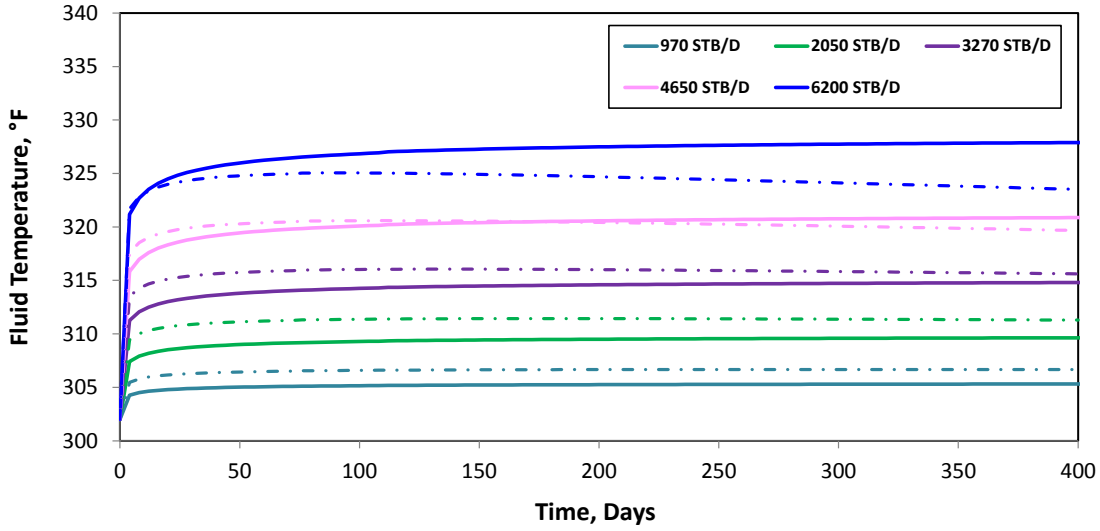

Fig. 21: Comparison of bottomhole flowing-fluid temperature calculated from Model II (solid lines) and Model III (dashed lines) - Case Study 3

We observe that at high production rates, the impact of J-T phenomenon on reservoir fluid temperature reduces over time. In fact, the estimated fluid temperature stabilizes or decreased with time at high rates, after 100 days of production once the improved solution (Model III) is applied. Both declining reservoir pressure with

depletion and reservoir heating with time influence this outcome. As a result, actual J-T heating is normally lower than that calculated by Model II, especially at late times.

In most cases, fluid temperature derived from the original and improved solutions are reasonably close to each other. However, the differences in solutions can be significant once the reservoir produces at high rates for longer duration. To better understand accuracy and applicability of both solutions, fluid temperatures estimated by the improved model are compared to that calculated from App's numerical solutions.

3.7.2 Validation of an improved analytical solution (Model III)

Results from an improved analytical solution (Model III) are validated with numerical results presented by App (2010). Comparisons of flowing-fluid temperature calculated from the improved solutions to App's numerical solutions in Case Study 1 are shown in Fig. 22.

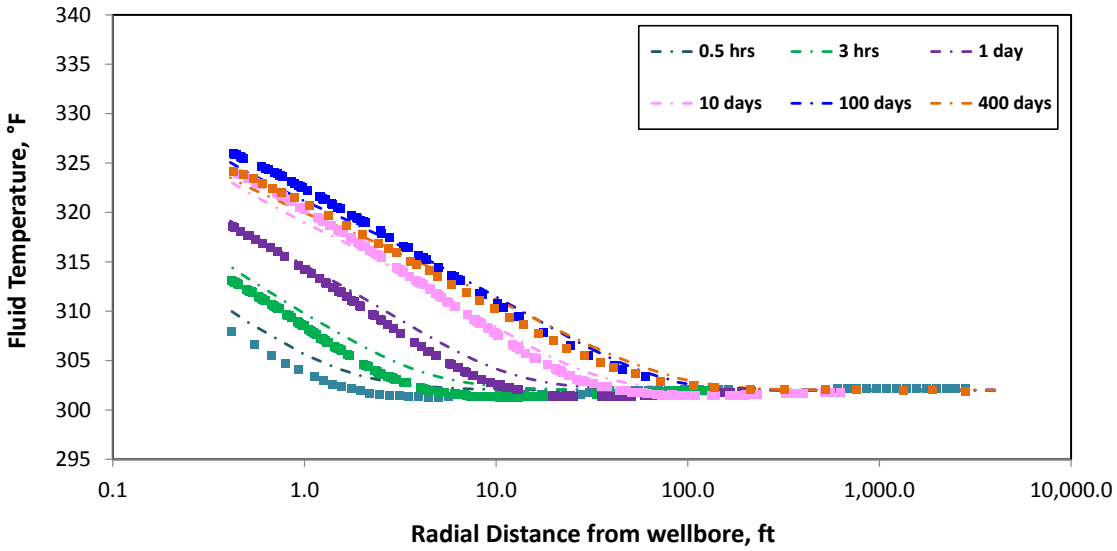

Fig. 22: Comparison of flowing-fluid temperature in the reservoir calculated from Model III (dashed lines) and App's numerical solution (solid squares)- Case Study 1

Overall, the improved solution (Model III) yield a more reasonable match with App's numerical results compared to the original analytical model (see Fig. 13), particularly at longer producing times. A better fluid viscosity approximation is the main driver for a more reasonable estimate of flowing-fluid temperature in the reservoir, which is essentially resulting in a more accurate forecast of our well and reservoir productivity.

Fluid temperature calculated by Model III in Case Study 2 and Case Study 3 are also validated with App's solutions. Results from both case studies are shown in Fig. 23 and Fig. 24, respectively.

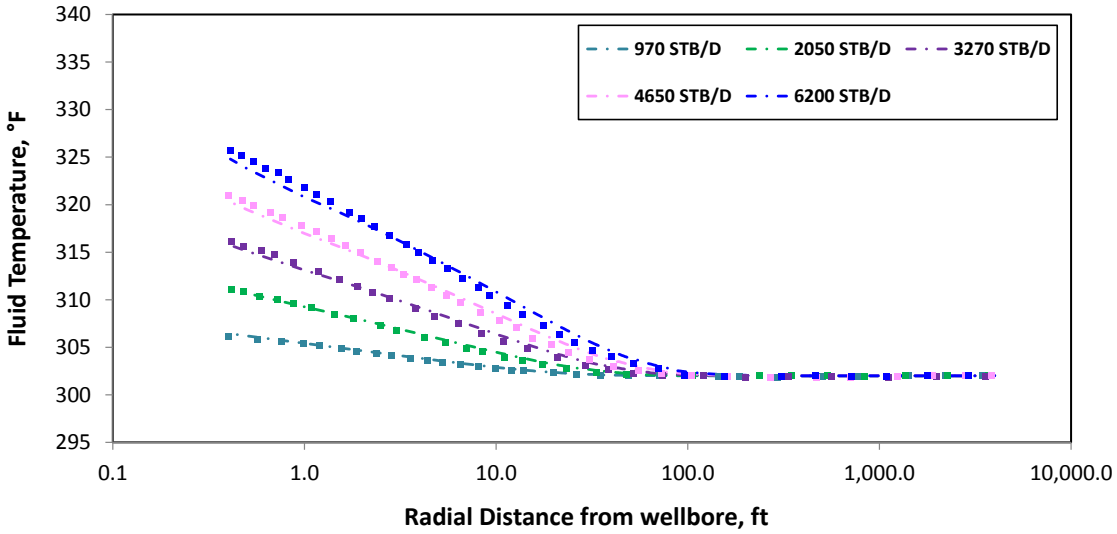

Fig. 23: Comparison of flowing-fluid temperature in the reservoir calculated from Model III (dashed lines) and App's numerical solution (solid squares) - Case Study 2

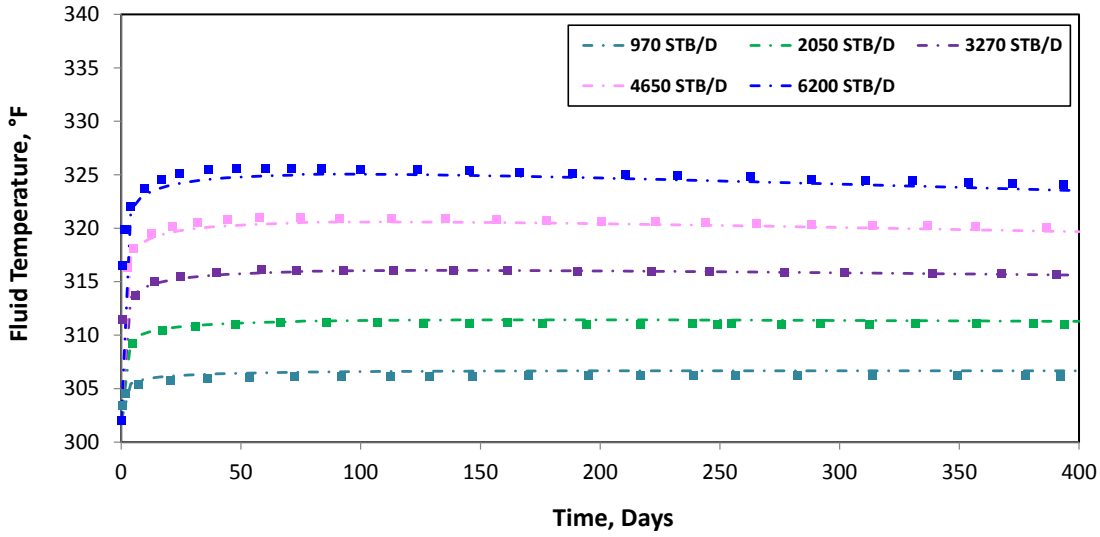

Fig. 24: Comparison of bottomhole flowing-fluid temperature calculated from Model III (dashed lines) and App's numerical solution (solid squares)- *Case Study 3*

Both case studies also show that fluid temperatures calculated from Model III are in good agreement with App's rigorous numerical simulations. With implementation of the improved solution (Model III), flowing-fluid temperature forecasts are more accurate compared to the estimates derived from our original analytical model presented in Fig. 16 and Fig. 17 for Case Study 2 and Case Study 3, respectively.

Improved analytical solution is able to capture decrease of bottomhole flowing-fluid temperature over time, especially at high production rates. As discussed earlier, reduction of reservoir fluid temperature is potentially caused by a slower J-T heating rate, compared to heat loss rate to over- and under-burden formations, due to lower fluid viscosity. The results from the improved solution agree very well with results derived with App's numerical model.

In summary, the improved analytical solution (Model III) yields the most reasonable estimate of flowing-fluid temperature distribution in the reservoir amongst all three analytical formulations. Consequently, we recommended applications of Model III.

Coupling an original analytical temperature model (Model I or Model II) to reservoir inflow model and fluid viscosity approximation (correlation) can sometimes be complicated and time consuming. In such a case, Model II is the best alternative for flowing-fluid temperature evaluation. Model II normally gives a reasonable estimation of the flowing-fluid temperature in the reservoir. A good estimate of flowing-fluid temperature in the reservoir always leads to a better forecast of well productivity because fluid viscosity approximation is generally more accurate, if fluid temperature is taken into account. In the next section, we will discuss the comparison of well productivity

index calculations with and without a consideration of viscosity variation due to change in reservoir pressure and temperature.

3.8 Well Productivity Index Forecast

In this section, we apply the improved analytical solution (Model III) to calculate reservoir pressure and temperature over production period. Then, we estimate well productivity index of the base case well and reservoir (presented in Section 3.2) for three different scenarios by using three different assumptions as follows:

1. Fluid viscosity is assumed to be constant throughout production period regardless of changes in reservoir pressure and temperature.
2. Fluid viscosity is a function of reservoir pressure only and reservoir is assumed to be isothermal.
3. Joule-Thomson heating is taken into account for reservoir flowing-fluid temperature evaluation. Reservoir is no longer isothermal. Fluid viscosity is a function of both reservoir pressure and temperature.

Five different production rates are considered. Well productivity profiles calculated for each production rate using three different assumptions are shown in Fig. 25. At each production rate, colored solid lines represent well productivity index profile when viscosity is a function of reservoir pressure only (scenario 2). Colored dash lines are well productivity index forecasts when J-T effect is incorporated in the evaluation (scenario 3). The black solid line shows the estimated well productivity index over time

when fluid viscosity is assumed constant (scenario 1). In the latter case, we observe that productivity index is totally independent of production rate.

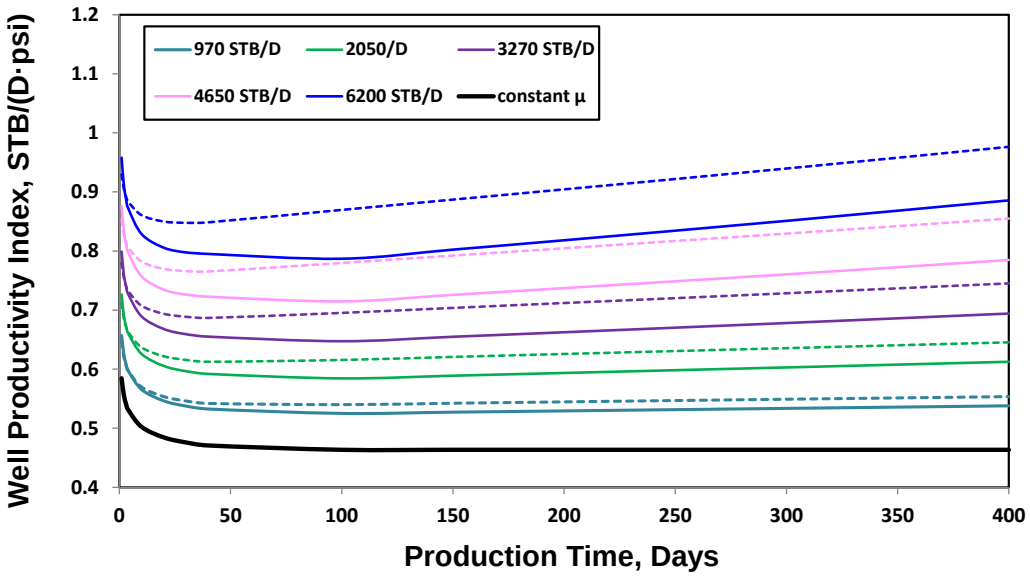

Fig. 25: Comparisons of well productivity index over production period when
i) viscosity is assumed constant (black solid line),
ii) viscosity changes as a function of pressure (colored solid lines), and
iii) viscosity changes as a function of pressure and temperature (colored dashed lines)

A more accurate productivity index estimation normally results in more efficient production optimization strategies and, eventually, a better overall field development planning. Fig. 25 emphasizes the significance of including reservoir-fluid temperature variation due to J-T phenomena in well productivity index forecast. At early times, well productivity index generally decreases during transient period. Then, well productivity index starts increasing or being constant once pseudosteady-state (PSS) flow is reached. Productivity index during PSS in scenario 1 (black solid line) does not vary over time

because viscosity is assumed constant. On the other hand, PSS productivity index for scenario 2 and 3 slightly increases over time because fluid viscosity is typically reduced when reservoir gets depleted and heated up by the J-T phenomenon.

We observe that well productivity index could be underestimated by up to 10% in high production rate cases if J-T heating is omitted. Additionally, well productivity can be totally underrated if an impact of reservoir pressure and temperature to fluid viscosity is neglected and not incorporated in the analysis.

We have showed that reservoir fluid temperature change due to J-T heating during production is very significant for this specific reservoir. The impact of J-T effect to reservoir flowing-fluid temperature is higher in a low-permeability (tight) reservoir due to significant pressure drop along the flow path. In general, J-T heating is expected in low- or high-pressure oil and high pressure gas reservoirs, whereas J-T cooling is more likely in a low-pressure gas reservoir.

Impacts of reservoir permeability, heat transfer coefficient, Joule-Thomson coefficient of reservoir fluid, oil density, and oil formation factor to flowing-fluid temperature calculation are discussed in the next Chapter. The sensitivity analysis allows better understanding of the situations where J-T heating or cooling is significant and should always be included in production- and reservoir-engineering studies.

CHAPTER IV

SENSITIVITY ANALYSIS

4.1 Focused Parameters

In Chapter III, we discussed the results from sensitivity analysis of reservoir flowing-fluid temperature to fluid viscosity and production flow rate. Results from sensitivity analysis of fluid temperature estimation to fluid viscosity was shown in Fig. 18, while the effects of production flow rate to reservoir flowing-fluid temperature were shown in several case studies in Chapter III (Figs. 23 and 24). The results clearly demonstrated that both parameters have significant impact on flowing-fluid temperature estimation in the reservoir.

In many cases, some reservoir and fluid properties cannot be directly measured or collected from the reservoir and are normally considered reservoir uncertainties. In this Chapter, variables other than viscosity and production rate that appeared in our analytical solution for temperature are looked at as part of further sensitivity analysis. This sensitivity analysis will allow a better understanding of each variable's impact to an estimate of flowing-fluid temperature in the reservoir. Understanding these critical parameters allows us to put more focus (and investment) in collecting more data, e.g. by logging, coring, and etc., to narrow down ranges of uncertainties for a more accurate and reasonable evaluation of fluid temperature in the reservoir.

Reservoir permeability, oil density, oil formation volume factor, J-T coefficient, and reservoir overall heat transfer coefficient are the focused parameters in the

sensitivity analysis in this Chapter. The same reservoir and fluid data set presented in Chapter III are used as our base case. In this sensitivity study, initial fluid viscosity and production rate are considered fixed variables because the effect of these two parameters to reservoir flowing-fluid temperature was already demonstrated in the previous Chapter. Production rate is fixed at 6200 STB/D and viscosity data presented in App's work (shown in Fig. 3) is used in this analysis.

Results from the sensitivity study are shown in the next Section. First, flowing-fluid temperature distributions in the reservoir after 50 days of continuous production (Case Study 2) derived from different sets of parameters are compared. Then, Design of Experiment (DoE) was conducted to emphasize the critical parameters which have significant influence to an estimation of flowing-fluid temperature in the reservoir.

4.2 Sensitivity Analysis Results

Model III- the improved solution incorporating heat transfer to over- and under-burden formations and viscosity variation in the reservoir- was used to calculate flowing-fluid temperature in the reservoir. The model is run for each focused variable. Results from this sensitivity analysis are shown in this section.

The results show that estimated flowing-fluid temperature after 50 days of continuous production is very sensitive to reservoir permeability and J-T coefficient, as can be seen in Fig. 26 and Fig. 27. The influence of permeability is easy to understand; lower permeability would result in higher pressure gradient and more J-T heating, leading to increased temperature. Similarly, higher J-T coefficient would definitely

contribute more to fluid temperature change. In contrast, Fig. 28 shows that oil formation volume factor has limited impact to an evaluation of flowing-fluid temperature in the reservoir.

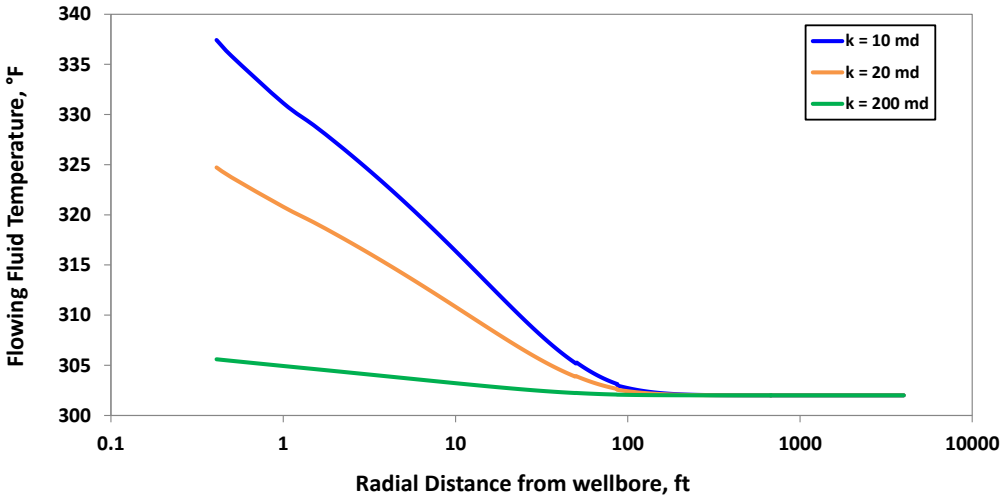

Fig. 26: A sensitivity analysis of flowing-fluid temperature in the reservoir to reservoir permeability– at 50 days of production

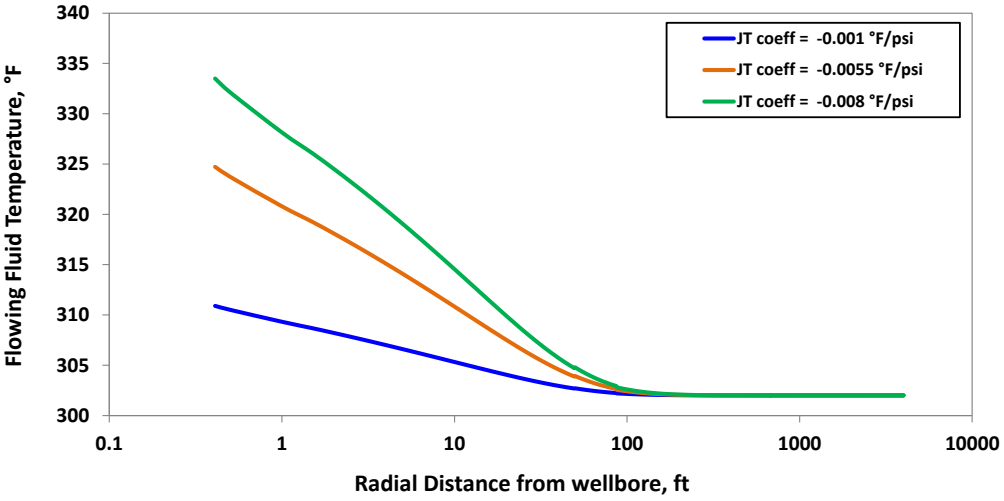

Fig. 27: A sensitivity analysis of flowing-fluid temperature in the reservoir to Joule-Thomson coefficient for oil– at 50 days of production

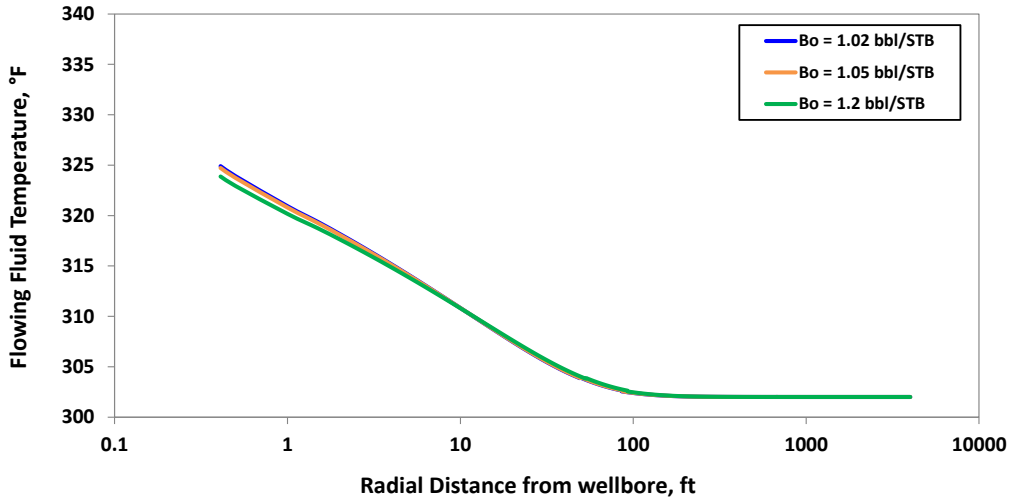

Fig. 28: A sensitivity analysis of flowing-fluid temperature in the reservoir to oil formation volume factor– at 50 days of production

Fig. 29 and Fig. 30 show that reservoir radius and oil density have some influence to reservoir flowing-fluid temperature estimation but the influence is minor compared to other critical parameters i.e. reservoir permeability, J-T coefficient, fluid viscosity, and production flow rate. From Fig. 29, we see that flowing-fluid temperature after 50 days of production is lower in the small reservoir case. At the same production rate, small reservoir gets depleted more quickly than the larger reservoir. In other words, at 50 days, average reservoir pressure is lower in a smaller reservoir; therefore, oil density and oil viscosity are smaller so that the effect from J-T heating is less, compared to the other two cases. As a result, flowing-fluid temperature in a smallest reservoir is the lowest amongst all cases.

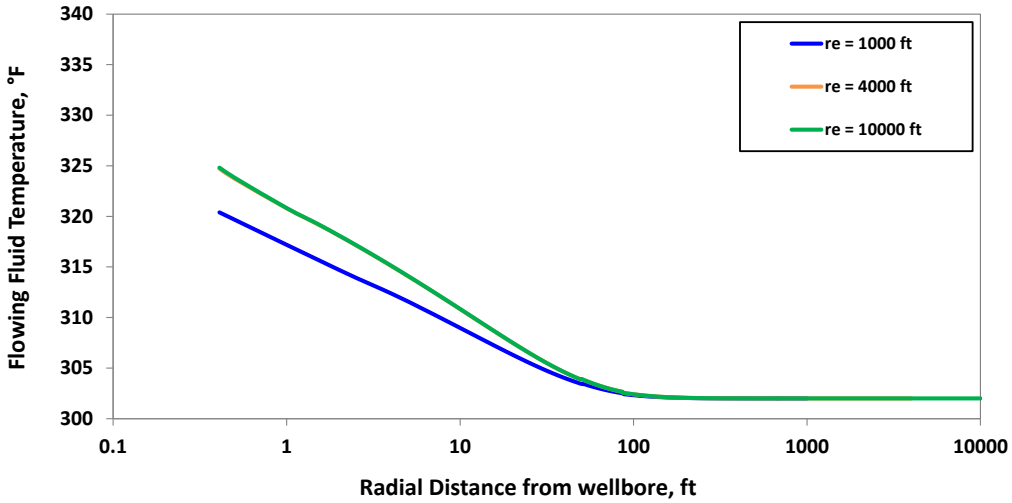

Fig. 29: A sensitivity analysis of flowing-fluid temperature in the reservoir to reservoir external radius– at 50 days of production

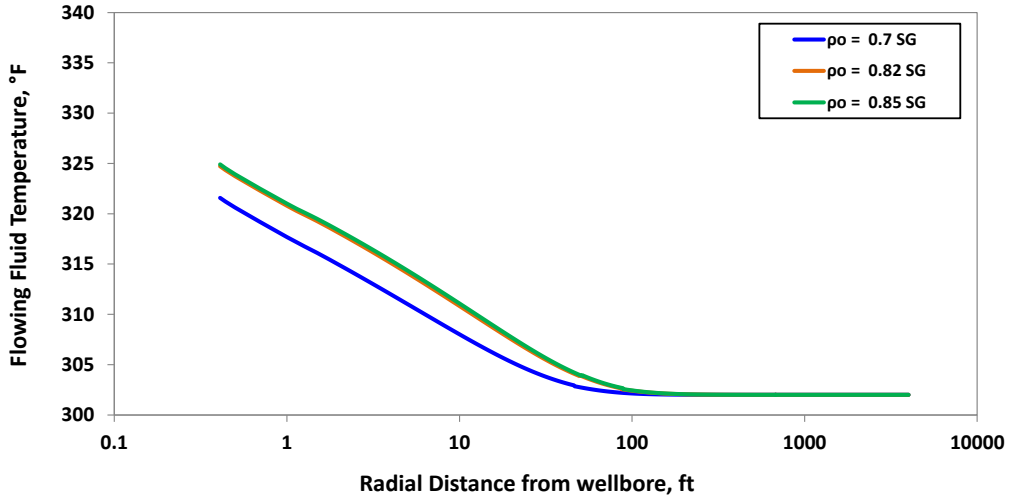

Fig. 30: A sensitivity analysis of flowing-fluid temperature in the reservoir to oil density– at 50 days of production

Reservoir heat transfer coefficient is another property which has an impact on reservoir fluid temperature. Fig. 31 shows that the impact of this parameter to fluid temperature is small in the base case (after 50 days of production rate of 6200 STB/D); however, heat transfer coefficient could become more critical when the fluid is heated up more significantly after a longer period of production. To demonstrate this, the sensitivity analysis of flowing-fluid temperature to heat transfer coefficient after 400 days of 6200 STB/D production is presented in Fig. 32.

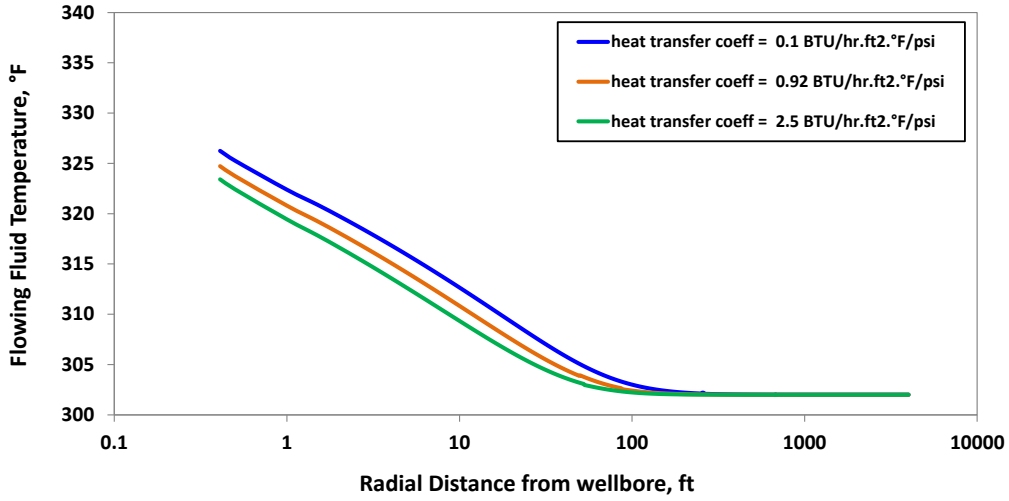

Fig. 31: A sensitivity analysis of flowing-fluid temperature in the reservoir to overall heat transfer coefficient– at 50 days of production

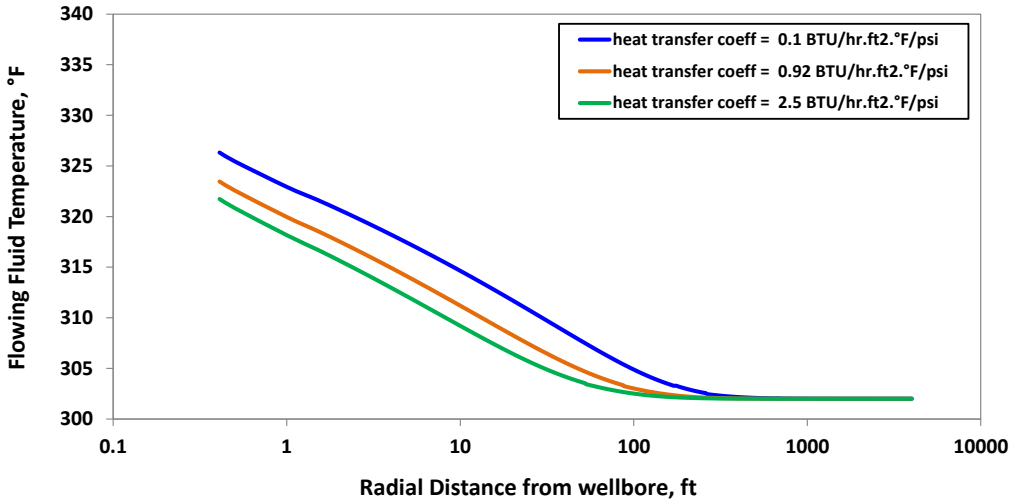

Fig. 32: A sensitivity analysis of flowing-fluid temperature in the reservoir to reservoir overall heat transfer coefficient– 400 days of production

Comparing results in Fig. 32 to Fig. 31, we can see that the significance of heat transfer coefficient to flowing-fluid temperature increases over time. This is because heat transfer from reservoir to over- and under-burden formations gets higher once the fluid gets heated up more and more throughout production time. This agrees very well with results and discussions presented in the previous chapters regarding the significance of including the 'heat transfer to overburden formations' term into the comprehensive energy balance equation of our system and therefore, our analytical solution.

Design of Experiment (DoE) was applied to the six variables which are of interest, namely: reservoir permeability, reservoir radius, oil formation volume factor, oil density, J-T coefficient, and reservoir overall heat transfer coefficient. The DoE allows us to pinpoint the critical parameters, as well as non-critical variables, which have influence(s) on an estimation of flowing-fluid temperature in the reservoir.

Model III is implemented in this DoE analysis. Fluid temperature calculated at three different locations: at well bottom, 10-ft from the wellbore, and 100-ft from the wellbore are considered as dependent variables in this DoE study. Pareto charts demonstrating effects of each focused parameter to flowing-fluid temperature at each location after 50 days of 6200 STB/D production are shown in Fig. 33, Fig. 34, and Fig. 35. In each Pareto chart, **k** is reservoir permeability, **J-T** represents J-T coefficient, **re** is reservoir external radius, **Bo** is oil formation volume factor, **hc** is overall heat transfer coefficient of the reservoir, and **ρo** is oil density.

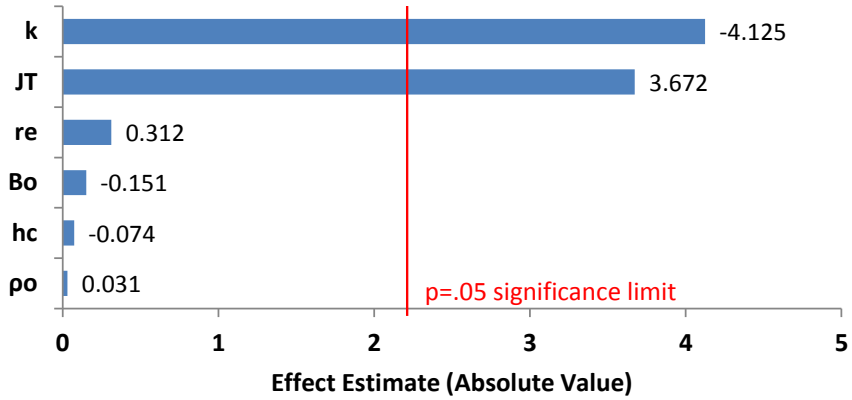

Fig. 33: Pareto chart of standardized effects for fluid temperature at **well bottom** after 50 days of 6200 STB/D production

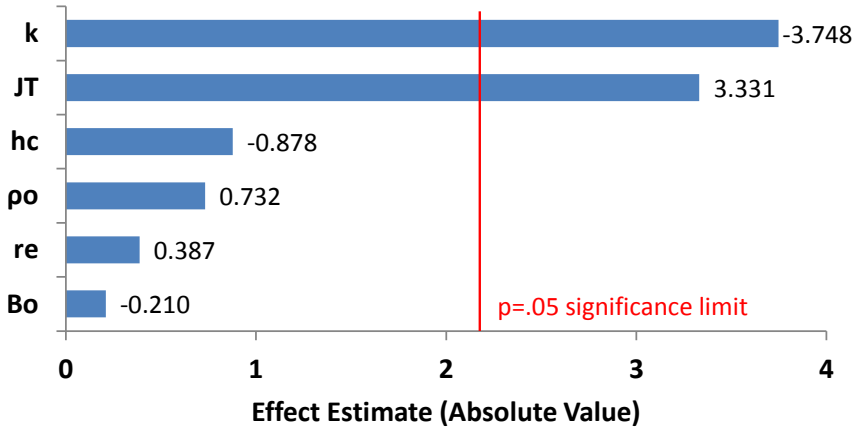

Fig. 34: Pareto chart of standardized effects for reservoir fluid temperature at **10 ft from the wellbore** after 50 days of 6200 STB/D production

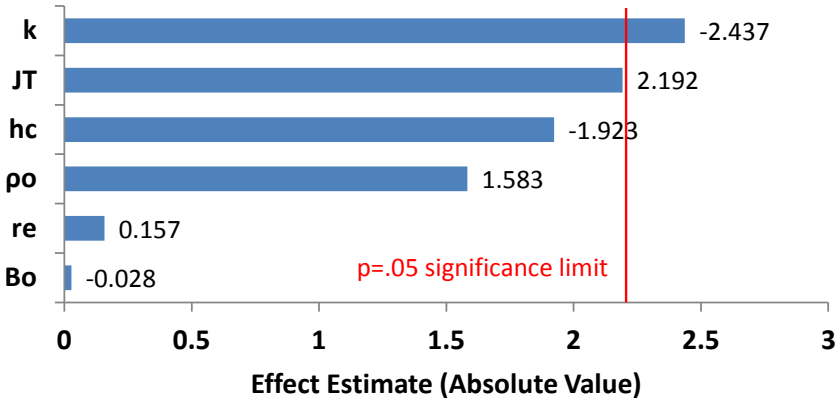

Fig. 35: Pareto chart of standardized effects for reservoir fluid temperature at **100 ft from the wellbore** after 50 days of 6200 STB/D production

DoE results confirm that reservoir permeability and J-T coefficient are the two parameters that are critical to an estimation of flowing-fluid temperature in the reservoir. The impact of these parameters is very prominent at well bottom and getting less significant when we move further into the reservoir. According to the results shown in

Fig. 35, fluid temperature at 100-ft away from the wellbore is almost independent from any of the input parameters. Basically, fluid heating from J-T phenomena is minimal further in the reservoir because pressure gradient along the flow at that location is not as large as pressure gradient in the near wellbore region.

Sensitivity analysis and DoE for low rate production (500 STB/D) are also performed. The results are very similar to the base case DoE study, Fig. 33 to Fig. 35, that the two critical parameters for flowing-fluid temperature calculation are reservoir permeability and J-T coefficient. However, the magnitude of flowing-fluid temperature alteration in each sensitivity case is not significantly different, compared to the base case sensitivity study. In addition, both parameters have totally no significant impact to reservoir fluid temperature at 100-ft away from the wellbore. In other words, the 'impacted' region is relatively smaller. At low production rates, J-T heating generally has less impact to flowing-fluid temperature in the reservoir because of smaller pressure drop along the flow. The sensitivity analysis results and Pareto charts showing low rate DoE results are included in Appendix E for reference.

From the sensitivity analysis study, we observe that reservoir permeability, J-T coefficient, fluid viscosity, and production rate are the four parameters which have significant influence on flowing-fluid temperature in the reservoir. Another way to verify the sensitivity of flowing-fluid temperature to these parameters is to develop a tornado chart. The tornado chart showing the impact of each parameter to reservoir fluid temperature estimation, based on Model III, is presented in Fig. 36. It is clear from the tornado chart that the four critical parameters to reservoir flowing-fluid temperature are

production rate, reservoir permeability, oil viscosity, and J-T coefficient. This generally confirms the significance of these four parameters to flowing-fluid temperature calculation. Other parameters are less critical at the production time that we consider (50 days of continuous production).

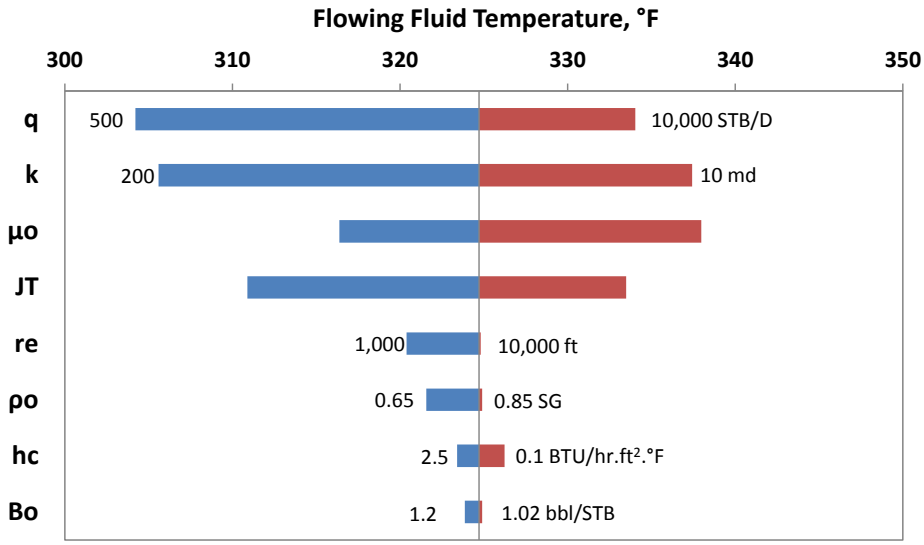

Fig. 36: Tornado chart showing impact of input parameters to flowing-fluid temperature in the reservoir at 50 days of 6,200 STB/D production

Production rate is actually controlled by an operator and is not really considered a reservoir uncertainty. However, it is included in this analysis because precise flow rate acquisition and measurement is crucial for reservoir fluid temperature analysis. An operator should always ensure that the recorded production flow rate at the job site is reasonably accurate and reflecting actual performance of the well. Estimated flowing-fluid temperature could be totally off if the production rate is extremely inaccurate.

In a reservoir where knowledge of flowing-fluid temperature is critical, e.g. high pressure and tight oil reservoir; more focus should also be put to reservoir fluid compositional and PVT tests. A better knowledge of fluid viscosity and J-T coefficient is very useful in a meaningful evaluation of reservoir flowing-fluid temperature. The more reasonable estimate of reservoir fluid temperature would, in turn, lead to a better approximation of well productivity, which is important in field development planning, as well as production optimization.

A reasonable reservoir permeability estimate is also a key to decent evaluation of reservoir flowing-fluid temperature. Sometimes, more investment is put on coring operation where a reservoir core test can be performed so that reservoir permeability is directly measured. Coring operation could be very expensive and the measured permeability from a core test generally represents only a local value as opposed to the average permeability of the reservoir. Most of the time, reservoir permeability is, instead, indirectly interpreted from certain types of test. Pressure transient and rate transient analyses are the two tests that are widely used in the industry to reasonably estimate an average permeability of the reservoir. Therefore, these two tests are strongly recommended in a 'more challenging' reservoir where J-T heating is significant. This is to narrow down reservoir permeability ranges for a better estimation of flowing-fluid temperature in the reservoir. In contrast, in absence of transient-pressure tests, the proposed analytical solution may be used for an inverse analysis to estimate an average-reservoir permeability. Of course, the flowing-fluid pressure and temperature at well bottom, as well as production flow rate, are required.

The sensitivity analyses presented in this chapter yield a better understanding of each input parameter's influence to flowing-fluid temperature estimation in the reservoir. Though only Model III is used in this sensitivity analysis, the sensitivity analysis results are expected to be the same even if Model I and Model II is used. This is because all models- Model I, II, and III- were derived from the same comprehensive energy balance equation; but with slightly different assumptions.

The analysis also raises our awareness in the impact(s) of reservoir uncertainties to flowing-fluid temperature, and therefore, well productivity forecast. Results from this sensitivity study allow us to make a decision to put more effort (and money) to acquire more data that is critical to the reservoir fluid temperature evaluation for better planning in production optimization, as well as reservoir management and full-field development, especially in a 'more challenging' reservoir environment.

CHAPTER V

CONCLUSIONS AND RECOMMENDATIONS

5.1 Conclusions

In this study, a robust analytical model for flowing-fluid temperature estimation in a single-phase oil reservoir was developed. The concepts of energy balance, momentum balance, and conservation of mass were applied to arrive at an analytical formulation for estimating fluid temperature in an oil reservoir producing at a constant rate. Fluid temperature change due to heat convection, Joule-Thomson effect, as well as energy exchange between system (reservoir) and surroundings (overburden formations), were incorporated in this study. The proposed analytical solution was successfully validated with the results from a rigorous numerical solution based on actual field data.

The advantage of this analytical model over other analytical solutions for reservoir temperature estimation is that heat transfer from/to over- and under-burden formations, $\dot{Q}$, is incorporated into this analysis. We have demonstrated that $\dot{Q}$ is crucial in the estimation of flowing-fluid temperature in the reservoir, especially at later times when reservoir fluid is heated (by J-T effect) significantly and fluid temperature in the reservoir is very different from that of over and under-burden formations. Compared to Model I ($\dot{Q}$=0, μ constant), Model II ($\dot{Q}\neq$0, μ constant), generally yields a better estimate of fluid temperature in the reservoir, especially during late production periods. Therefore, we strongly recommended that the analytical solution with a consideration of

heat transfer from reservoir to over- and under-burden formations (Model II) be applied to reservoir problems, where an evaluation of flowing-fluid temperature is needed.

Fluid viscosity turned out to be one of the variables that are critical to estimating temperature of flowing-fluid in a reservoir. An improved version of our analytical solution (Model III) incorporates fluid viscosity variation during production. Compared to the original analytical solutions (Model I and Model II), results from the improved model showed a better match with the results from a rigorous numerical model developed by App (2010). Therefore, Model III is recommended for reservoir flowing-fluid temperature calculation when fluid viscosity data (or correlation) are available and coupling the proposed temperature model to analytical inflow model(s) and fluid viscosity correlation is not too complicated.

The sensitivity analysis identified fluid viscosity, production flow rate, reservoir permeability, and J-T coefficient as variables that have significant impact on the estimation of flowing-fluid temperature in the reservoir. Results from the sensitivity analysis allow us to focus on the relevant variables to manage uncertainties of the outcome. A more reasonable estimate of the flowing-fluid temperature during production leads to a better well-productivity index assessment, especially in low-PI reservoirs, where pressure drop is significant. Additionally, a more accurate flowing-fluid temperature at well bottom is very useful for well design and well equipment selection, as well as pressure-transient analysis interpretation.

In summary, the proposed analytical model provides comparable reservoir flowing-fluid temperature estimation as the rigorous numerical simulator developed by

App (2010). Generally, an analytical model is relatively simpler and allows the calculations to be performed in a spreadsheet. Therefore, the proposed model is recommended when the reservoir can be conformed to a simpler flow problem, because its computational cost is significantly less compared to a full-fledged numerical solution.

5.2 Recommendations for Future Work

In this study, we successfully developed a robust analytical model to estimate flowing-fluid temperature in the reservoir during production. We envision that the technical basis and approach implemented in this study can be applied to more complicated reservoir (and wellbore) flow problems. The recommendations for future work and potential to expand applications of this work are as follows:

1. Expand the study to single-phase gas and two-phase gas-oil reservoirs.
2. Expand the work to a linear flow production system to accommodate an estimation of flowing-fluid temperature in unconventional reservoirs.
3. Include an actual calculation of J-T coefficient, based on fluid properties and pressure and temperature, in the analysis. A calculation of J-T coefficient could be coupled with the proposed temperature model in a way similar to that for fluid viscosity to the analytical solution shown in this study. The actual calculation of J-T coefficient can be critical in flowing-fluid temperature calculation in gas and two-phase flow.
4. Conduct a detailed study to evaluate the 'heat transfer to overburden' term, $\dot{Q}$, in a comprehensive energy-balance equation. In this study, we simplified the problem

and handled this term by applying Newton's law of cooling. However, the actual heat-transfer mechanism between the reservoir and under- and over-burden formations is conduction into an infinite sink.

5. Perform an analysis to evaluate the impact of pressure transient term, $\frac{\partial p}{\partial t}$, to flowing-fluid temperature calculation. In this study, we assumed that the impact of this term to reservoir fluid temperature is negligible. However, this term may become significant in more complex reservoir problems and/or in gas and two-phase reservoirs.
6. Evaluate if the proposed model is applicable when fluid injection occurs into a reservoir.
7. Apply superposition of pressure and temperature to the model to allow flowing-fluid temperature calculation during multirate production or in more complex cases where the well is intermittently shut-in during production.
8. Apply the proposed analytical solution in an inverse analysis to estimate average-reservoir permeability in the situation where production flow rate, as well as bottomhole fluid pressure and temperature, are known.
9. Apply the proposed analytical solution in an inverse analysis to approximate production rate in the situation where reservoir and fluid properties, as well as bottomhole flowing fluid pressure and temperature, are known.

REFERENCES

Al-Hadhrami, A.K., Elliott, L., and Ingham, D.B. 2003. A New Model for Viscous Dissipation in Porous Media Across a Range of Permeability Values. *Transport in Porous Media* **53** (1): 117–122. http://dx.doi.org/ 10.1023/A:1023557332542.

App, J.F. 2009. Field Cases: Nonisothermal Behavior Due to Joule-Thomson and Transient Fluid Expansion/ Compression Effects. Paper SPE 124338 presented at the 2009 SPE Annual Technical Conference and Exhibition, New Orleans, Louisiana, 4-7 October. http://dx.doi.org/10.2118/124338-MS.

App, J.F. 2010. Nonisothermal and Productivity Behavior of High-Pressure Reservoirs. *SPE J.* **15** (1): 50-63. SPE-114705-PA. http://dx.doi.org/10.2118/114705-PA.

Avdomin, N.A. 1964a. Some Formulas for Calculating the Temperature Field of a Stratum Subject to Thermal Injection. *Neft'i Gaz* **7** (3): 37.

Avdomin, N. A. 1964b. On the Different Methods of Calculating the Temperature Fields of a Stratum during Thermal Injection. *Neft'i Gaz* **7** (8): 39.

Beggs, H. D. and Robinson, J. R. 1975. Estimating the Viscosity of Crude Oil Systems. *Journal of Petroleum Technology* **27** (9): p.1140-1141. SPE-5434-PA. http://dx.doi.org/10.2118/5434-PA.

Darcy, H. 1856. *Les Fontaines Publiques de la Ville de Dijon*. Victor Dalmont, Paris.

Dawkrajai, P., Lake, L.W., Yoshioka, K. et al. 2006. Detection of Water or Gas Entries in Horizontal Wells From Temperature Profiles. Paper SPE 100050 presented at the 2006 SPE/DOE Symposium on Improved oil Recovery, Tulsa, Oklahoma, 22-26 April. Society of Petroleum Engineers. http://dx.doi.org/10.2118/100050-MS.

Duru, O.O. and Horne, R.N. 2010. Modeling Reservoir Temperature Transients and Reservoir-Parameter Estimation Constrained to the Model. *SPE Res Eval* & Eng **13** (6): 873-883. SPE-115791-PA. http://dx.doi.org/10.2118/115791-PA.

Izgec, B., Kabir, C.S., Zhu, D. et al. 2007. Transient Fluid and Heat Flow Modeling in Coupled Wellbore/Reservoir Systems. *SPE Res Eval & Eng* **10** (3): 294–301. SPE-102070-PA. http://dx.doi.org/10.2118/102070-PA.

Kabir, C.S., Izgec, B., Hasan, A.R. et al. 2012. Computing flow profiles and total flow rate with temperature surveys in gas wells. 2012. *Journal of Natural Gas Science & Engineering* **4** (1): 1–7. http://dx.doi.org/10.1016/j.jngse.2011.10.004.

Lauwerier, H.A. 1955. The Transport of Heat in an Oil Layer Caused by Injection of Hot Fluid. *Applied Scientific Research* **5** (2-3): 145-150.

Malofeev, G.E. 1960. Calculation of the Temperature Distribution in a Formation when Pumping Hot Fluid Into a Well (in Russian). *Neft'I Gaz* **37** (1): 59-64.

Raghavan, R. 1993. *Well Test Analysis*. Englewood Cliffs, New Jersey: A Simon & Schuster Company.

Ramazanov A.Sh. and Nagimov V.M. 2007. Analytical Model for the Calculation of Temperature Distribution in the Oil Reservoir during Unsteady Fluid Inflow. *Oil and Gas Business* **1** (1).

Ramazanov A.Sh., Nagimov V.M., and Akhmetov. R.K. 2013. Analytical Model of Temperature Prediction for a Given Production History. *Oil and Gas Business* **1** (1): 537-546.

Rubenstein, L.I. 1959. The Total Heat Losses in Injection of a Hot Fluid into a Stratum. *Neft'i Gaz* **2** (9): 41.

Spillette, A. G. 1965. Heat Transfer During Hot Fluid Injection Into an Oil Reservoir. *PETCO Journal Paper* **4** (4): 213-218. PETSOC-65-04-06. http://dx.doi. org/10.211 8/65-04-06.

Satman, A.; Brigham, W. E.; Zolotukhin, A. B. 1979. A New Approach for Predicting the Thermal Behavior in Porous Media During Fluid Injection. *Geothermal Resources Council Transactions* **3** (1): 621-624.

Standing, M.B. 1947. A Pressure-Volume-Temperature Correlation for Mixtures of California Oils and Gases. Paper API 47-275 presented at the Spring Meeting of the Pacific Coast District, Division of Production, Los Angeles, California, 15 May.

Steffensen, R. J. and Smith, R. C. 1973. The Importance of Joule-Thomson Heating (or Cooling) in Temperature Log Interpretation. Paper SPE 4636 presented at the SPE-AIME 48th Annual Fall Meeting, Las Vegas, Nevada, 1-3 October. http://dx.doi.org/10.2118/4636-MS.

Vazquez, M. and Beggs, H. D. 1980. Correlations for Fluid Physical Property Prediction. *Journal of Petroleum Technology* **32** (6)*:* 968-970. SPE-6719-PA. http://dx.doi. org/10.2118/6719-PA.

Yoshioka, K., Zhu, D., Hill A.D. et al. 2005. A Comprehensive Model of Temperature Behavior in a Horizontal Well. Paper SPE 95656 presented at the 2005 SPE Annual

Technical Conference and Exhibition, Dallas, Texas, 9-12 October. http://dx.doi.org/10.2118/95656-MS.

Yoshioka, K., Zhu, D., Hill, A.D. et al. 2006. Detection of Water or Gas Entries in Horizontal Wells from Temperature Profiles. Paper SPE 100209 presented at the SPE Europec/EAGE Annual Conference and Exhibition, Vienna, Austria, 12-15 June. http://dx.doi.org/10.2118/100209-MS.

APPENDIX A

DERIVATIONS OF THE ANALYTICAL SOLUTIONS

A.1 Analytical solution without heat transfer between reservoir and surroundings

A comprehensive energy balance equation for the system without a consideration of heat transfer between reservoir and surroundings is

$$\left[\emptyset s_o \rho_o c_{po} + \emptyset s_w \rho_w c_{pw} + (1-\emptyset)\rho_f c_{pf}\right]\frac{\partial T}{\partial t} + \rho_o u_r c_{po}\frac{\partial T}{\partial r} + \rho_o u_r \sigma_o \frac{\partial p}{\partial r} +$$

$$\left[\emptyset s_o \rho_o \sigma_o + \emptyset s_w \rho_w \sigma_w - 1\right]\frac{\partial p}{\partial t} = \frac{1}{r}\frac{\partial}{\partial r}\left[\lambda r \frac{\partial T}{\partial r}\right] \quad \text{(A.1)}$$

Based on our assumption that radial heat conduction during constant rate production is negligible, the term on right side of Eq.A.1 becomes zero. Therefore, Eq.A.1 is reduced to

$$\left[\emptyset s_o \rho_o c_{po} + \emptyset s_w \rho_w c_{pw} + (1-\emptyset)\rho_f c_{pf}\right]\frac{\partial T}{\partial t} + \rho_o u_r c_{po}\frac{\partial T}{\partial r} + \rho_o u_r \sigma_o \frac{\partial p}{\partial r} +$$

$$\left[\emptyset s_o \rho_o \sigma_o + \emptyset s_w \rho_w \sigma_w - 1\right]\frac{\partial p}{\partial t} = 0 \quad \text{(A.2)}$$

We can write fluid velocity, u_r, in term of flow rate as $\frac{q}{2\pi r h}$ rewrite the $\frac{\partial p}{\partial r}$ term in term of flow rate as $-\frac{\mu q}{2\pi r h k}$ to get

$$\left[\emptyset s_o \rho_o c_{po} + \emptyset s_w \rho_w c_{pw} + (1-\emptyset)\rho_f c_{pf}\right]\frac{\partial T}{\partial t} + \frac{q\rho_o c_{po}}{2\pi r h}\frac{\partial T}{\partial r} - \frac{q^2 \rho_o \sigma_o \mu}{(2\pi r h)^2 k} +$$

$$\left[\emptyset s_o \rho_o \sigma_o + \emptyset s_w \rho_w \sigma_w - 1\right]\frac{\partial p}{\partial t} = 0 \quad \text{(A.3)}$$

Then, we replace q by $-q$ since production occurs in a negative r-direction. Therefore, we get

$$\left[\emptyset s_o \rho_o c_{po} + \emptyset s_w \rho_w c_{pw} + (1-\emptyset)\rho_f c_{pf}\right]\frac{\partial T}{\partial t} - \frac{q\rho_o c_{po}}{2\pi r h}\frac{\partial T}{\partial r} - \frac{q^2 \rho_o \sigma_o \mu}{(2\pi r h)^2 k} +$$

$$\left[\emptyset s_o \rho_o \sigma_o + \emptyset s_w \rho_w \sigma_w - 1\right]\frac{\partial p}{\partial t} = 0 \qquad \text{(A.3)}$$

Multiply both sides of the above equation by $\frac{2\pi r^2 h}{q}$:

$$\left[\emptyset s_o \rho_o c_{po} + \emptyset s_w \rho_w c_{pw} + (1-\emptyset)\rho_f c_{pf}\right]\left(\frac{2\pi r^2 h}{q}\right)\frac{\partial T}{\partial t} - \rho_o c_{po}(r)\frac{\partial T}{\partial r} - \frac{q\rho_o \sigma_o \mu}{2\pi h k} +$$

$$\left[\emptyset s_o \rho_o \sigma_o + \emptyset s_w \rho_w \sigma_w - 1\right]\left(\frac{2\pi r^2 h}{q}\right)\frac{\partial p}{\partial t} = 0 \qquad \text{(A.4)}$$

We assume that $\frac{\partial p}{\partial t}$ has minimal impact to temperature calculation. Thus, Eq.A.4 becomes

$$\left[\emptyset s_o \rho_o c_{po} + \emptyset s_w \rho_w c_{pw} + (1-\emptyset)\rho_f c_{pf}\right]\left(\frac{2\pi r^2 h}{q}\right)\frac{\partial T}{\partial t} - \rho_o c_{po}(r)\frac{\partial T}{\partial r} -$$

$$\frac{q\rho_o \sigma_o \mu}{2\pi h k} = 0 \qquad \text{(A.5)}$$

Rock and fluid properties, e.g. porosity, saturations, density, specific heat capacity and etc., are assumed to be constant. Hence, we can condense Eq.A.5 to

$$Ar^2\frac{\partial T}{\partial t} - Br\frac{\partial T}{\partial r} - C = 0 \qquad \text{(A.6)}$$

Where: $$A = \left[\emptyset s_o \rho_o c_{po} + \emptyset s_w \rho_w c_{pw} + (1-\emptyset)\rho_f c_{pf}\right]\left(\frac{2\pi h}{q}\right) \qquad \text{(A.7)}$$

$$B = \rho_o c_{po} \qquad \text{(A.8)}$$

$$C = \frac{q\rho_o \sigma_o \mu}{2\pi h k} \qquad \text{(A.9)}$$

Note that parameters *A*, *B*, and *C* are constants that are specific for particular reservoir.

Eq.A.6 is first order partial differential equation (PDE) where fluid temperature, *T*, is a function of radius from wellbore into the reservoir, *r*, and producing time, *t*.

Ar^2 is always positive. We divide both sides of Eq.A.6 by Ar^2 and rearrange the equation to get

$$\frac{\partial T}{\partial t} - \frac{B}{Ar}\frac{\partial T}{\partial r} = \frac{C}{Ar^2} \tag{A.10}$$

We apply the method of Characteristics to solve this first order PDE. First, we consider

$$dT = \frac{\partial T}{\partial t}dt + \frac{\partial T}{\partial r}dr \tag{A.11}$$

Or Eq.A.11 can be written as

$$\frac{dT}{dt} = \frac{\partial T}{\partial t} + \frac{\partial T}{\partial r}\frac{dr}{dt} \tag{A.12}$$

By the method of Characteristics, comparing terms on left side of Eq.A.10 to Eq.A.12, we can see that we can rewrite our PDE presented in Eq.A.10 as

$$\frac{dT}{dt} = \frac{C}{Ar^2} \tag{A.13}$$

Along the characteristic curve

$$\frac{dr}{dt} = -\frac{B}{Ar} \tag{A.14}$$

Rearranging Eq.A.14 to get

$$rdr = -\frac{B}{A}dt \tag{A.15}$$

Integrating both sides of Eq.A.15:

$$\int rdr = -\frac{B}{A}\int dt \tag{A.16}$$

We can bring $\frac{B}{A}$ outside the integration since both *A* and *B* are constant and are not a function of time, *t*. Then, Eq.A.16 becomes

$$r^2 = -\frac{2B}{A}t + \varepsilon_1 \tag{A.17}$$

And thus,

$$\varepsilon_1 = r^2 + \frac{2B}{A}t \tag{A.18}$$

Now, we plug r^2 from Eq.A.17 into Eq.A.13 and get

$$\frac{dT}{dt} = \frac{C}{A(\varepsilon_1 - \frac{2B}{A}t)} \tag{A.19}$$

$$\frac{dT}{dt} = \frac{C}{\varepsilon_1 A - 2Bt} \tag{A.20}$$

Eq.A.20 is a first order ordinary differential equation (ODE) that can be simply solved. We rearrange Eq.A.20 and integrate both sides of the equations with respect to time to get

$$dT = \frac{C}{\varepsilon_1 A - 2Bt}dt \tag{A.21}$$

$$\int dT = \int \frac{C}{\varepsilon_1 A - 2Bt}dt \tag{A.22}$$

C is a constant; therefore, Eq.A.22 is rearranged as

$$\frac{1}{C}\int dT = \int \frac{1}{\varepsilon_1 A - 2Bt}dt \tag{A.23}$$

Therefore,

$$T = -\frac{C}{2B}\ln(\varepsilon_1 A - 2Bt) + f(\varepsilon_1) \quad \text{;where } f(\varepsilon_1) \text{ is a function of } \varepsilon_1 \tag{A.24}$$

Eq.A.24 is a general solution to our PDE for flowing fluid temperature calculation. An initial condition of fluid temperature in the reservoir can be generally expressed by

$$T(r, t = 0) = T_i \tag{A.25}$$

Applying initial condition to the general solution in Eq.A.24, we get

$$T_i = -\frac{C}{2B}\ln(\varepsilon_1 A) + f(\varepsilon_1) \tag{A.26}$$

According to Eq.A.18, $\varepsilon_1 = r^2 + \frac{2B}{A}t$. At initial condition, *t =0*, ε_1 is essentially r^2. Plugging $\varepsilon_1 = r^2$ into Eq.24, we get

$$T_i = -\frac{C}{2B}\ln(Ar^2) + f(r^2) \tag{A.27}$$

Rearranging the above equation to get

$$f(r^2) = T_i + \frac{C}{2B}\ln(Ar^2) \tag{A.28}$$

Let *x* be any random variables. Eq.A.28 can be written in term of *f(x)* as

$$f(x) = T_i + \frac{C}{2B}\ln(|Ax|) \tag{A.29}$$

Therefore,

$$f(\varepsilon_1) = T_i + \frac{C}{2B}\ln(|A\varepsilon_1|) \tag{A.30}$$

Now, we can plug $f(\varepsilon_1)$ from Eq.A.30 into the general solution presented in Eq.A.24 to obtain a final solution:

$$T = -\frac{C}{2B}\ln(\varepsilon_1 A - 2Bt) + \left\{T_i + \frac{C}{2B}\ln(|A\varepsilon_1|)\right\} \tag{A.31}$$

Since $\varepsilon_1 = r^2 + \frac{2B}{A}t$, Eq.A.31 can be written as

$$T = -\frac{C}{2B}\ln\left(A(r^2 + \frac{2B}{A}t) - 2Bt\right) + \left\{T_i + \frac{C}{2B}\ln\left(\left|A(r^2 + \frac{2B}{A}t)\right|\right)\right\} \tag{A.32}$$

$$T = T_i + \frac{C}{2B}\ln(|Ar^2 + 2Bt)|) - \frac{C}{2B}\ln(Ar^2) \tag{A.33}$$

The final form of our analytical solution without a consideration of heat transfer to surroundings is presented in Eq.A.34 below:

$$T(r,t) = T_i - \frac{C}{2B}\ln\left(\frac{r^2 A}{|r^2 A + 2Bt)|}\right) \tag{A.34}$$

where *A*, *B*, and *C* are constant parameters described in Eq.A.7, Eq.A.8, and Eq.A.9 respectively

A.2 Analytical Solution with heat transfer between reservoir and surroundings

A comprehensive energy balance equation for the system with a consideration of heat transfer between the system and surroundings is expressed as

$$\left[\emptyset s_o \rho_o c_{po} + \emptyset s_w \rho_w c_{pw} + (1-\emptyset)\rho_f c_{pf}\right]\frac{\partial T}{\partial t} + \rho_o u_r c_{po}\frac{\partial T}{\partial r} + \rho_o u_r \sigma_o \frac{\partial p}{\partial r} +$$

$$\left[\emptyset s_o \rho_o \sigma_{po} + \emptyset s_w \rho_w \sigma_{pw} - 1\right]\frac{\partial p}{\partial t} = \frac{1}{r}\frac{\partial}{\partial r}\left[\lambda r \frac{\partial T}{\partial r}\right] + q_c \qquad \text{(A.35)}$$

Based on our general assumptions, radial heat conduction during constant rate production is negligible. Additionally, $\frac{\partial p}{\partial t}$ term is assumed to be minimal and can be neglected. Thus, Eq.A.35 becomes

$$\left[\emptyset s_o \rho_o c_{po} + \emptyset s_w \rho_w c_{pw} + (1-\emptyset)\rho_f c_{pf}\right]\frac{\partial T}{\partial t} + \rho_o u_r c_{po}\frac{\partial T}{\partial r} + \rho_o u_r \sigma_o \frac{\partial p}{\partial r} = q_c \qquad \text{(A.36)}$$

We rewrite fluid velocity, u_r, in term of flow rate as $\frac{q}{2\pi rh}$ and rewrite the $\frac{\partial p}{\partial r}$ in term of flow rate as $-\frac{\mu q}{2\pi rhk}$.

$$\left[\emptyset s_o \rho_o c_{po} + \emptyset s_w \rho_w c_{pw} + (1-\emptyset)\rho_f c_{pf}\right]\frac{\partial T}{\partial t} + \frac{q\rho_o c_{po}}{2\pi rh}\frac{\partial T}{\partial r} - \frac{\mu q^2 \rho_o \sigma_o}{(2\pi rh)^2 k} = q_c \qquad \text{(A.37)}$$

Replacing q by $-q$ in Eq.A.37 because flow occurs in a negative r-direction during production, Eq.A.37 becomes

$$\left[\emptyset s_o \rho_o c_{po} + \emptyset s_w \rho_w c_{pw} + (1-\emptyset)\rho_f c_{pf}\right]\frac{\partial T}{\partial t} - \frac{q\rho_o c_{po}}{2\pi r h}\frac{\partial T}{\partial r} - \frac{\mu q^2 \rho_o \sigma_o}{(2\pi r h)^2 k} = q_c \tag{A.38}$$

As discussed in Chapter II, net input rate of energy between reservoir and under/overburden formations, q_c, can be approximated by Newton's law of Cooling:

$$q_c = -\frac{2h_c[T-T_s]}{h} \tag{A.39}$$

Where $h_c$is heat transfer coefficient of the reservoir, *T* is fluid temperature in reservoir, T_s is temperature of the surroundings, and *h* is reservoir thickness. Then, we plug in q_c from Eq.A.39 into Eq.A.38 to get

$$\left[\emptyset s_o \rho_o c_{po} + \emptyset s_w \rho_w c_{pw} + (1-\emptyset)\rho_f c_{pf}\right]\frac{\partial T}{\partial t} - \frac{q\rho_o c_{po}}{2\pi r h}\frac{\partial T}{\partial r} - \frac{\mu q^2 \rho_o \sigma_o}{(2\pi r h)^2 k} = -\frac{2h_c[T-T_s]}{h} \tag{A.40}$$

Multiply both sides of Eq.A.40 by $\frac{2\pi r^2 h}{q}$, we obtain

$$\left[\emptyset s_o \rho_o c_{po} + \emptyset s_w \rho_w c_{pw} + (1-\emptyset)\rho_f c_{pf}\right]\left(\frac{2\pi r^2 h}{q}\right)\frac{\partial T}{\partial t} - \rho_o c_{po}(\mathrm{r})\frac{\partial T}{\partial r} - \frac{q\mu\rho_o\sigma_o}{2\pi h k} = -\frac{4\pi r^2 h_c}{q}(T-T_s) \tag{A.41}$$

Eq.A.41 can be written in terms of constants *A*, *B*,and *C* defined in Eq.A.7, Eq.A.8, Eq.A.9 as

$$Ar^2\frac{\partial T}{\partial t} - Br\frac{\partial T}{\partial r} - C = -\frac{4\pi r^2 h_c}{q}(T-T_s) \tag{A.42}$$

$$Ar^2\frac{\partial T}{\partial t} - Br\frac{\partial T}{\partial r} - C = -\frac{4\pi r^2 h_c}{q}T + \frac{4\pi r^2 h_c}{q}T_s \tag{A.43}$$

We assume that heat transfer coefficient, h_c, is constant. In addition, we assume that surrounding temperature remains at initial condition throughout production period, even after heat transfer takes place. Eq.A.43 can then be written as

$$Ar^2\frac{\partial T}{\partial t} - Br\frac{\partial T}{\partial r} - C = -Dr^2T + Er^2 \tag{A.44}$$

Where: $$D = \frac{4h_c\pi}{q} \tag{A.45}$$

and $$E = \frac{4h_c\pi}{q}T_i \tag{A.46}$$

$Ar^2$is always positive. We divide both sides of Eq.A.44 by Ar^2 to get

$$\frac{\partial T}{\partial t} - \frac{B}{Ar}\frac{\partial T}{\partial r} + \frac{D}{A}T = \frac{E}{A} + \frac{C}{Ar^2} \tag{A.47}$$

We apply the method of Characteristics to solve first order PDE presented in Eq.A.47. Based on the method of Characteristics, Eq.A.47 can be written as

$$\frac{dT}{dt} + \frac{D}{A}T = \frac{E}{A} + \frac{C}{Ar^2} \tag{A.48}$$

Along the characteristic curve

$$\frac{dr}{dt} = -\frac{B}{Ar} \tag{A.49}$$

We can integrate both sides of Eq.A.49 to get a relationship between *r* and *t* as follows:

$$r^2 = -\frac{2B}{A}t + \varepsilon_1 \tag{A.50}$$

And,

$$\varepsilon_1 = r^2 + \frac{2B}{A}t \tag{A.51}$$

Plugging r^2 from Eq.A.50 to Eq.A.48, we arrive

$$\frac{dT}{dt} + \frac{D}{A}T = \frac{C}{A\varepsilon_1 - 2Bt} + \frac{E}{A} \tag{A.52}$$

Eq. A.52 is a first order ODE that can be solved. First, let $H = \frac{D}{A}$ and $\mu = e^{Ht}$. Then, we multiply both sides of Eq.A.52 by μ to obtain

$$(e^{Ht})\frac{dT}{dt} + (e^{Ht})HT = (e^{Ht})\frac{C}{A\varepsilon_1 - 2Bt} + (e^{Ht})\frac{E}{A} \tag{A.53}$$

Consider the left side of Eq.A.53, we can see that

$$(e^{Ht})\frac{dT}{dt} + (e^{Ht})HT = \frac{d}{dt}(Te^{Ht}) \tag{A.54}$$

Thus, another way to express Eq.A.53 is

$$\frac{d}{dt}(Te^{Ht}) = (e^{Ht})\frac{C}{A\varepsilon_1 - 2Bt} + (e^{Ht})\frac{E}{A} \tag{A.55}$$

Rearranging and integrating both sides of Eq.A.55 with respect to time, *dt*, we get

$$\int d(Te^{Ht}) = \int \left\{(e^{Ht})\frac{C}{A\varepsilon_1 - 2Bt} + (e^{Ht})\frac{E}{A}\right\} dt \tag{A.56}$$

$$\int d(Te^{Ht}) = \int \frac{C}{A\varepsilon_1 - 2Bt} e^{Ht} dt + \int \frac{E}{A} e^{Ht} dt \tag{A.57}$$

$$Te^{Ht} = -\frac{C}{2B} e^{\frac{AH\varepsilon_1}{2B}} Ei[-\frac{H(A\varepsilon_1 - 2Bt)}{2B}] + \frac{E}{AH} e^{Ht} + g'(\varepsilon_1) \tag{A.58}$$

Since e^{Ht} is not zero, we divide both sides of Eq.A.58 by e^{Ht} and a general solution of our ODE becomes

$$T = -\frac{C}{2B} e^{\left(\frac{AH\varepsilon_1}{2B} - Ht\right)} Ei[-\frac{H(A\varepsilon_1 - 2Bt)}{2B}] + \frac{E}{AH} + g(\varepsilon_1) \tag{A.59}$$

Where $g(\varepsilon_1)$ is a function of ε_1.

As mentioned in Eq.A.25, an initial condition of fluid temperature in the reservoir can be expressed as

$$T(r, t = 0) = T_i \tag{A.25}$$

Applying an initial condition to evaluate $g(\varepsilon_1)$ of the general solution presented in Eq.A.59, we get

$$T_i = -\frac{C}{2B} e^{\frac{AH\varepsilon_1}{2B}} Ei[-\frac{H(A\varepsilon_1)}{2B}] + \frac{E}{AH} + g(\varepsilon_1) \quad \text{(A.58)}$$

At initial condition (*t=0*), $r^2 = \varepsilon_1$. Thus, Eq.A.58 can be expressed as

$$T_i = -\frac{C}{2B} e^{\frac{AHr^2}{2B}} Ei[-\frac{H(Ar^2)}{2B}] + \frac{E}{AH} + g(r^2) \quad \text{(A.58)}$$

$$g(r^2) = T_i + \frac{C}{2B} e^{\frac{AHr^2}{2B}} Ei\left[-\frac{H(Ar^2)}{2B}\right] - \frac{E}{AH} \quad \text{(A.59)}$$

Eq.A.59 can be written in term of a function of any variable, *g(x)* as

$$g(x) = T_i + \frac{C}{2B} e^{\frac{AHx}{2B}} Ei\left[-\frac{HAx}{2B}\right] - \frac{E}{AH} \quad \text{(A.60)}$$

Therefore,

$$g(\varepsilon_1) = T_i + \frac{C}{2B} e^{\frac{AH\varepsilon_1}{2B}} Ei\left[-\frac{HA\varepsilon_1}{2B}\right] - \frac{E}{AH} \quad \text{(A.61)}$$

Now, we replace $g(\varepsilon_1)$ in the general solution expressed in Eq.A.59 by its definition in Eq.A.61 to get

$$T = -\frac{C}{2B} e^{\left(\frac{AH\varepsilon_1}{2B} - Ht\right)} Ei[-\frac{H(A\varepsilon_1 - 2Bt)}{2B}] + \frac{E}{AH} + \left\{T_i + \frac{C}{2B} e^{\frac{AH\varepsilon_1}{2B}} Ei\left[-\frac{HA\varepsilon_1}{2B}\right] - \frac{E}{AH}\right\} \quad \text{(A.62)}$$

$$T = -\frac{C}{2B} e^{\left(\frac{AH\varepsilon_1}{2B} - Ht\right)} Ei[-\frac{H(A\varepsilon_1 - 2Bt)}{2B}] + \left\{T_i + \frac{C}{2B} e^{\frac{AH\varepsilon_1}{2B}} Ei\left[-\frac{HA\varepsilon_1}{2B}\right]\right\} \quad \text{(A.63)}$$

Plugging $\varepsilon_1 = r^2 + \frac{2B}{A}t$ into Eq.A.63, we obtain

$$T = -\frac{C}{2B} e^{\left(\frac{HAr^2}{2B}\right)} Ei[-\frac{HAr^2}{2B}] + \left\{T_i + \frac{C}{2B} e^{\frac{H(Ar^2+2Bt)}{2B}} Ei\left[-\frac{H(Ar^2+2Bt)}{2B}\right]\right\} \quad \text{(A.64)}$$

Therefore, a final form of an analytical solution for flowing fluid temperature in the reservoir with a consideration of energy transfer between system and surroundings can be expressed as

$$T(r,t) = T_i + \frac{C}{2B} e^{\frac{H(Ar^2+2Bt)}{2B}} Ei\left[-\frac{H(Ar^2+2Bt)}{2B}\right] - \frac{C}{2B} e^{\left(\frac{HAr^2}{2B}\right)} Ei[-\frac{HAr^2}{2B}] \quad \text{(A.65)}$$

Definitions of all constant parameters are re-stated here for convenience:

$$A = \left[\emptyset s_o \rho_o c_{po} + \emptyset s_w \rho_w c_{pw} + (1-\emptyset)\rho_f c_{pf}\right]\left(\frac{2\pi h}{q}\right) \quad \text{(A.7)}$$

$$B = \rho_o c_{po} \quad \text{(A.8)}$$

$$C = \frac{q\rho_o \sigma_o \mu}{2\pi h k} \quad \text{(A.9)}$$

$$D = \frac{4h_c \pi}{q} \quad \text{(A.45)}$$

And $$H = \frac{D}{A} \quad \text{(A.66)}$$

APPENDIX B

FIELD CASE: COMPARISON OF FLUID VISCOSITY FROM CORRELATIONS VS LABORATORY MEASUREMENT

Generally, oil viscosity correlations are developed from a specific set of test data for certain types of reservoir. In other words, one correlation might be only applicable in a reservoir whose conditions are very analogous to the sample set being used in original correlation development. Some of oil viscosity correlations that are available and widely used in the industry are:

Beggs and Robinson (1975): This correlation was developed from 460 dead oil viscosity measurements whose oil density is ranging from 16 ^{o}API to 58 ^{o}API with a temperature between 70 ^{o}F and 295 ^{o}F. According to Beggs and Robinson's work, oil viscosity can be calculated from

$$\text{For } p_r \leq p_b: \ \mu_o = A_v \mu_{oD}^{B_v} \tag{B.1}$$

For pressure above bubble point pressure, oil viscosity can be calculated from Vazquez and Beggs (1980) correlation as follows

$$\text{For } p_r > p_b: \ \mu_o = \mu_{ob} \left(\frac{p_r}{p_b}\right)^m \tag{B.2}$$

Where:

$$A_v = 10.715(R_s + 150)^{-0.515} \tag{B.3}$$

$$B_v = 5.44(R_s + 150)^{-0.338} \tag{B.4}$$

$$m = 2.6 p_r^{1.187} e^{(-11.513 - 8.98 \cdot 10^{-5} p_r)} \tag{B.5}$$

All parameters in Eq.B.1 through Eq.B.5 are in field units. Dead oil viscosity, μ_{oD}, can be obtained directly from laboratory measurement or can be calculated from a dead oil viscosity correlation as follows:

$$\mu_{oD} = 10^{X} - 1.0 \tag{B.6}$$

Where:
$$X = YT^{-1.163} \tag{B.7}$$

$$Y = 10^{Z} \tag{B.8}$$

$$Z = 3.0324 - 0.0203(^{o}\text{API}) \tag{B.9}$$

Standing (1947): This correlation was developed in 1981 based on laboratory data of California crude oil samples. Standing's oil viscosity correlations are expressed in Eq.B.10 to Eq.B.13 below:

For $p_r \leq p_b$: $\mu_o = 10^{a}\mu_{oD}^{b}$ (B.10)

For $p_r > p_b$: $\mu_o = \mu_{ob} + 0.001(p_r - p_b)(0.024\mu_{ob}^{1.6} + 0.38\mu_{ob}^{0.56})$ (B.11)

Where:
$$a = R_s(2.2 \cdot 10^{-7}R_s - 7.4 \cdot 10^{-4}) \tag{B.12}$$

$$b = \frac{0.68}{10^{8.62 \cdot 10^{-5}R_s}} + \frac{0.25}{10^{1.10 \cdot 10^{-3}R_s}} + \frac{0.062}{10^{3.74 \cdot 10^{-3}R_s}} \tag{B.13}$$

All parameters in Eq.B.10 to Eq.B.13 are also in field units.

The accuracy of oil viscosity correlations is generally not high and most of the correlations were developed for conventional reservoirs where reservoir temperature and pressure are within a certain range and not extreme. When possible, actual laboratory measurements are preferred, especially when reservoirs are not conventional e.g. high pressure and high temperature reservoirs.

Laboratory measurements for viscosity of reservoir fluid in actual field case presented in Chapter III are available (see Fig. 3). However, an attempt to calculate fluid viscosity from oil viscosity correlations has been made. In this analysis, calculated viscosity from those correlations is compared to the actual data. Then, fluid temperature calculated from those viscosities is compared to the base model where laboratory viscosity is used. Both aforementioned correlations, i.e. Begg and Robinson's and Standing's viscosity correlations, are considered.

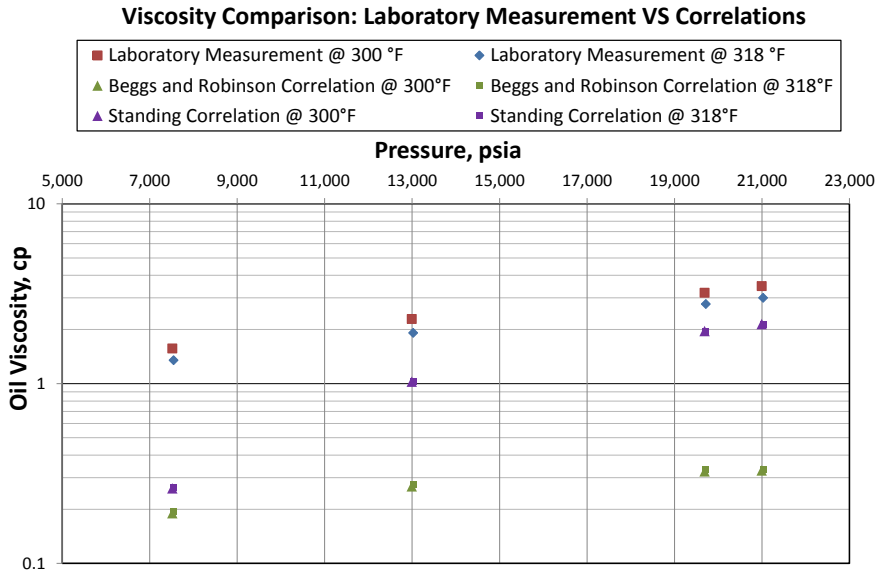

Fig. B1: Comparison of fluid viscosity from laboratory measurement and two different oil viscosity correlations at high pressure and high temperature

Fig. B1 demonstrates a comparison of oil viscosity calculated from the two correlations versus laboratory measurement at different pressure and temperature. We

can see that both correlations underestimate oil viscosity under pressure and temperature ranges of this particular reservoir.

Most of 'conventional' oil viscosity correlations were developed from laboratory tests of fluids from reservoirs at lower pressure and temperature, compared to reservoir of our interest. Beggs and Robinson's viscosity correlation was developed from 460 dead oil and 2,073 live oil samples from 600 different oil reservoirs. All reservoir systems in their study have reservoir pressure between 0 to 5,250 psig and reservoir temperature between 70 to 295 °F. Similarly, Standing's data set comprises of oil samples from reservoirs whose pressures are between 400 to 5,000 psig and temperature ranges from 100 to 258 °F. It can be clearly seen that pressure and temperature of our sample reservoir presented in Chapter III is outside these ranges; thus, these correlations are not very accurate in our analysis.

In summary, an appropriate viscosity correlation should be selected and applied to the proposed analytical solution for accurate reservoir fluid temperature estimation. The best option is actually to use viscosity data measured in a laboratory in an analysis; however, laboratory measurements are not always available because of time and cost constraints. We have to realize a range of uncertainty of fluid viscosity and/or viscosity correlation that are used in the analysis for a better understanding of accuracy and possible range of fluid temperature in our reservoir system.

Fig. B2 shows a comparison of flowing fluid temperature in reservoir estimated by our analytical model using laboratory viscosity data and viscosity approximated from Standing's correlation.

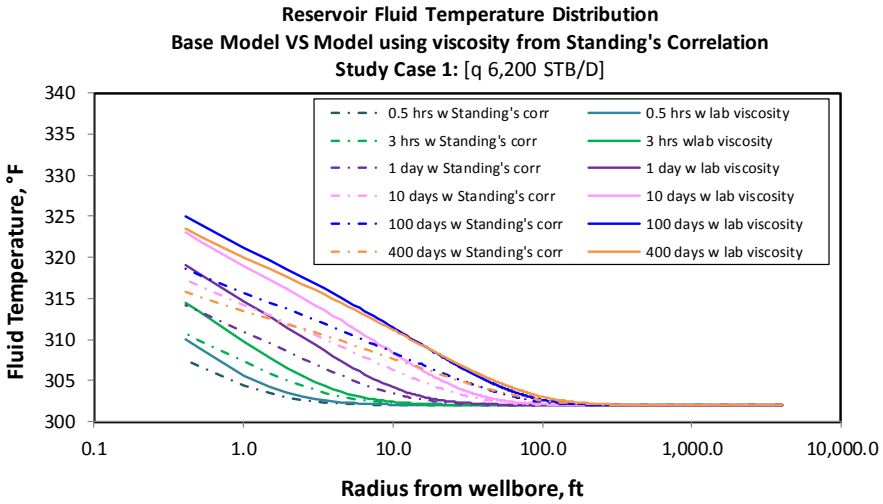

Fig. B2: Comparison of fluid temperature distribution in reservoir calculated from base model, using viscosity from laboratory measurement (solid lines), VS an analytical model using viscosity estimated from Standing's viscosity correlation (dash lines)

Standing's correlation underestimates fluid viscosity for this specific reservoir; thus, estimated flowing fluid temperature is generally underrated when his correlation is used in our analytical reservoir temperature model. At high production rate, estimated bottomhole fluid temperature could be up to 7-8°F lower than that calculated from actual viscosity data if Standing's correlation is used. This emphasizes the significance of good understanding of a possible fluid viscosity range to reservoir fluid temperature forecast when an analytical temperature model is implemented.

APPENDIX C

SIMPLIFIED NUMERICAL SOLUTION

Reservoir parameters are assumed to be constants in the simplified version of numerical solution of the comprehensive energy balance equation for our reservoir system. This allows a fair verification of our analytical solution to results obtained by the numerical approach. The simplified numerical solution for the system without and with a consideration of heat transfer between reservoir and surrounded formation are discussed separatelly in this Appendix. Our analytical solutions were successfully validated by these simplified numerical solutions and the results were already shown and discussed in Chapter III.

C.1 Simplified numerical solution without heat transfer between reservoir and surroundings

Recall a final form of comprehensive energy balance equation without a consideration of heat transfer between reservoir and over- and underburden formations (discussed in Appendix A):

$$Ar^2\frac{\partial T}{\partial t} - Br\frac{\partial T}{\partial r} - C = 0 \tag{A.6}$$

where:

$$A = \left[\emptyset s_o \rho_o c_{po} + \emptyset s_w \rho_w c_{pw} + (1-\emptyset)\rho_f c_{pf}\right]\left(\frac{2\pi h}{q}\right) \tag{A.7}$$

$$B = \rho_o c_{po} \tag{A.8}$$

$$C = \frac{q\rho_o \sigma_o \mu}{2\pi h k} \tag{A.9}$$

Then, we rearrange Eq.A.6 to allow one to solve the equation numerically:

$$\frac{\partial T}{\partial t} = \frac{1}{Ar^2}\left[Br\frac{\partial T}{\partial r} + C\right] \quad \text{(C.1)}$$

As stated earlier, an initial condition for the problem is

$$T_f(r, t = 0) = T_i \quad \text{(A.25)}$$

The initial condition implies that at $t = 0$, $\frac{\partial T}{\partial r} = 0$. Then, $\frac{\partial T}{\partial t}$ at each location in the reservoir can be calculated. Consequently, fluid temperature at each location at the next time step can be calculated from

$$T_f(r, t) = T_{f\ previous\ time\ step} + \Delta t \frac{\partial T}{\partial t}_{current\ time\ step}$$

The process to solve for flowing-fluid temperature at a particular time numerically is shown in Fig. C1.

C.2 Simplified Numerical solution with heat transfer between reservoir and surroundings

The comprehensive energy balance equation of the system when heat transfer from reservoir to surrounded formations are incorporated is

$$Ar^2\frac{\partial T}{\partial t} - Br\frac{\partial T}{\partial r} - C = -Dr^2 T + Er^2 \quad \text{(A.44)}$$

where *A, B,* and *C* were defined in Eq.A.7, A.8, and A.9 respectively and *D* and *E* are defined in Eq.A.45 and Eq.A.46 as followed:

$$D = \frac{4h_c\pi}{q} \quad \text{(A.45)}$$

$$E = \frac{4h_c\pi}{q}T_i \quad \text{(A.46)}$$

Then, we rearrange Eq.A.44 to solve for $\frac{\partial T}{\partial t}$:

$$\frac{\partial T}{\partial t} = \frac{1}{Ar^2}\left[Br\,\frac{\partial T}{\partial r} + C - Dr^2\,T + Er^2\right] \qquad \text{(C.2)}$$

With the same initial condition (Eq.A.25), we can solve for $\frac{\partial T}{\partial t}$ at any location in the reservoir at each time step. The process to numerically solve for flowing-fluid temperature at any time of interest is the same as the process described in Appendix C.1. The only difference is that Eq.C.2, as oppose to Eq.C.1, is used in step 3 when heat transfer to overburden formations is incorporated in the analysis.

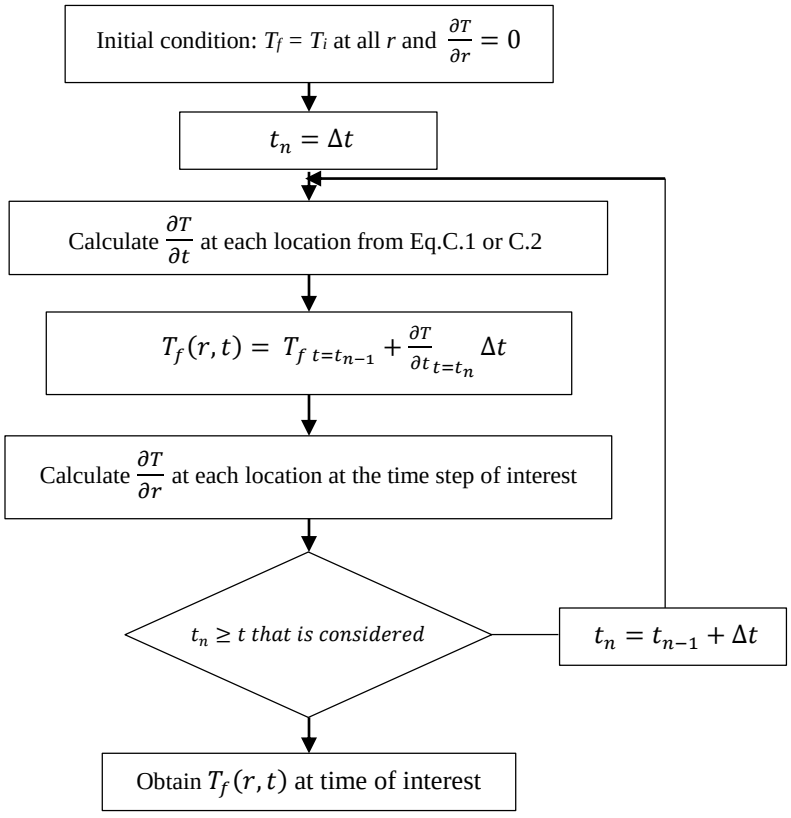

Fig. C1: A flow chart explaining the process for simplified numerical solutions being used in this study

APPENDIX D

RESULTS WITH MORE REASONABLE AVERAGE VISCOSITY VALUES

This appendix section is a part of the sensitivity analysis of flowing-fluid temperature to average fluid viscosity. As discussed in Chapter III, fluid viscosity plays a significant role in reservoir fluid heat-up (or cool-down) due to J-T phenomena. In this section, different values of average viscosity are used to estimate flowing-fluid temperature in the reservoir when flow conditions are varied such as when production rates or production times are different. Fig. D1,Fig. D2, and Fig. D3 show reservoir flowing-fluid temperature estimated by Model II using more reasonable values of fluid viscosity.

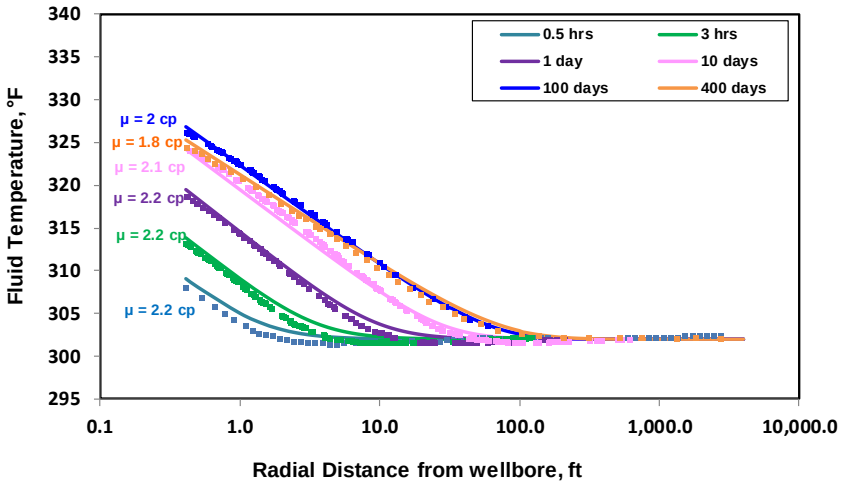

Fig. D1: Results from the Proposed Analytical Model (Model II) using Different Viscosities in each Production Rate Case VS Results from Rigorous Numerical Model by App (2010) - Study Case 1

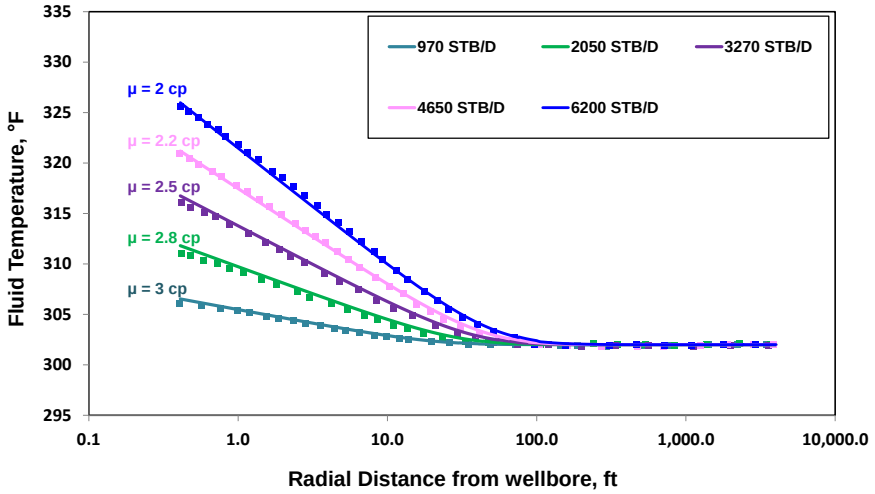

Fig. D2: Results from the Proposed Analytical Model (Model II) using Different Viscosities in each Production Rate Case VS Results from Rigorous Numerical Model by App (2010) - Study Case 2

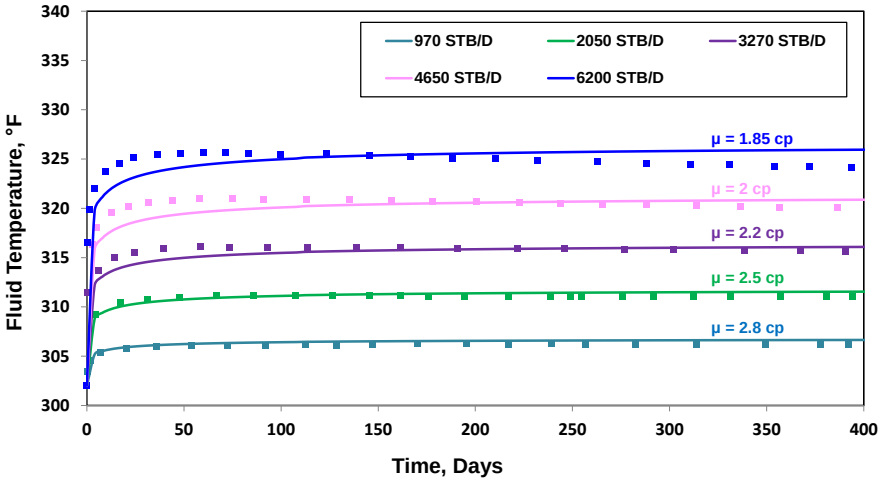

Fig. D3: Results from the Proposed Analytical Model (Model II) using Different Viscosities in Each Production Rate Case VS Results from Rigorous Numerical Model by App (2010) - Study Case 3

Compared to the results from a single-viscosity calculation (shown in Fig. 13, Fig. 16, and Fig. 17), we observe that the match of our results to App's numerical results are significantly improved if more reasonable average viscosity values are used. The results from this sensitivity strongly support our conclusion that fluid viscosity is very critical to an estimation of flowing-fluid temperature in the reservoir.

APPENDIX E

SENSITIVITY RESULTS- LOW RATE CASE

Sensitivity analysis and DoE are repeated for low production rate case in order to see the impact of each parameter to flowing-fluid temperature when production rate is varied. In this study, 500 STB/D production rate is used instead of the 6200 STB/D rate in the base case. Results from sensitivity analysis, using Model III, are shown in Fig. D1 through Fig. D6.

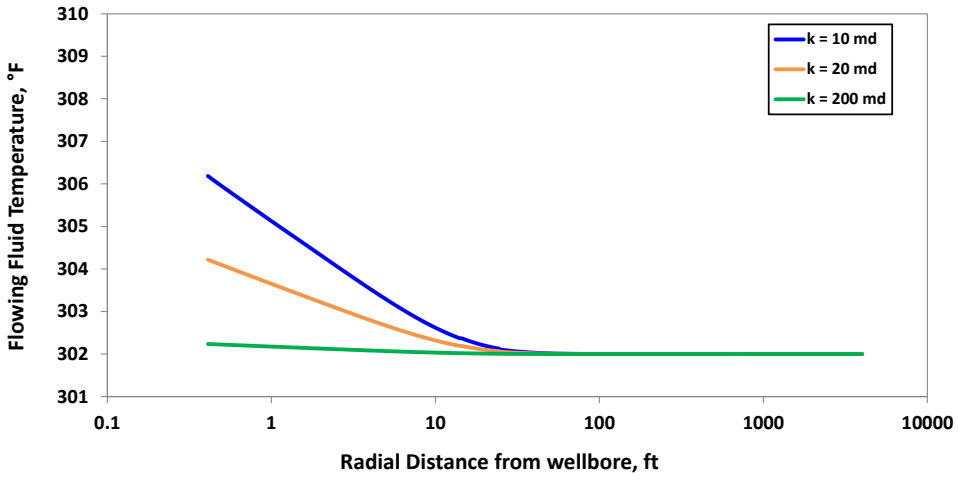

Fig. D1: A sensitivity analysis of flowing-fluid temperature in the reservoir to reservoir permeability– at 50 days of 500 STB/D production

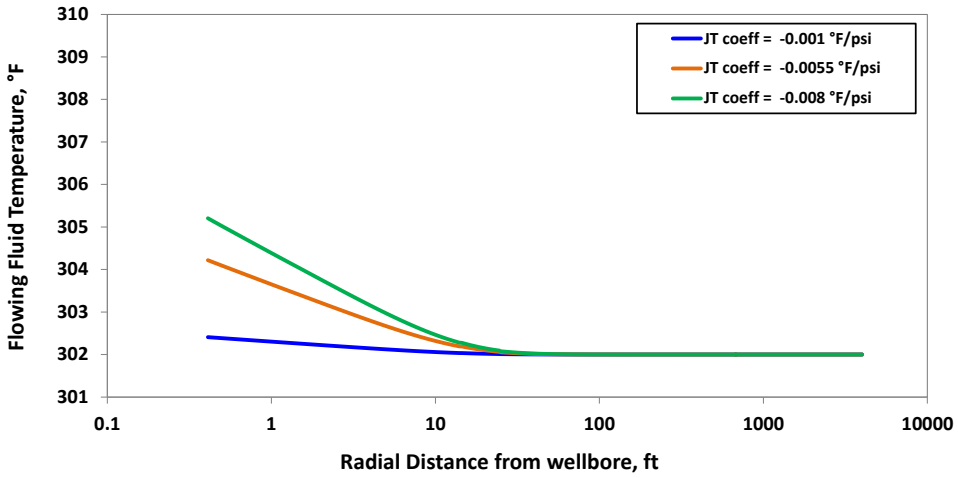

Fig. D2: A sensitivity analysis of flowing-fluid temperature in the reservoir to J-T coefficient– at 50 days of 500 STB/D production

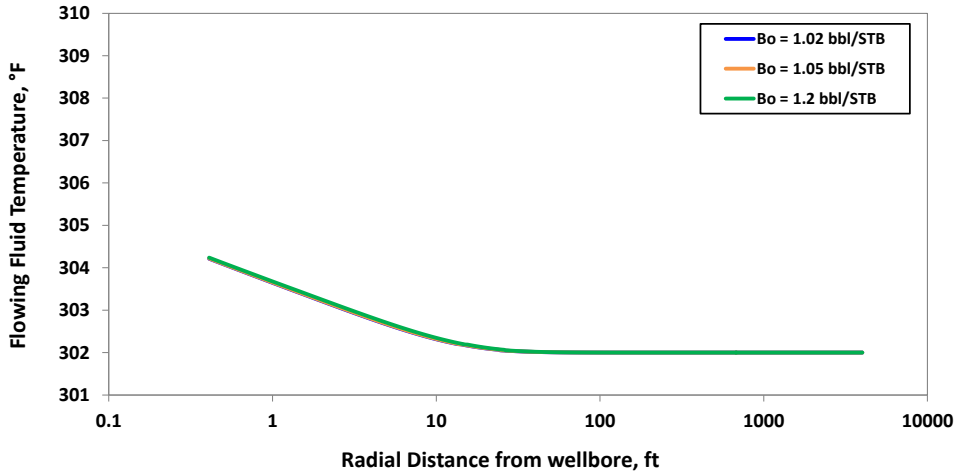

Fig. D3: A sensitivity analysis of flowing-fluid temperature in the reservoir to oil formation volume factor– at 50 days of 500 STB/D production

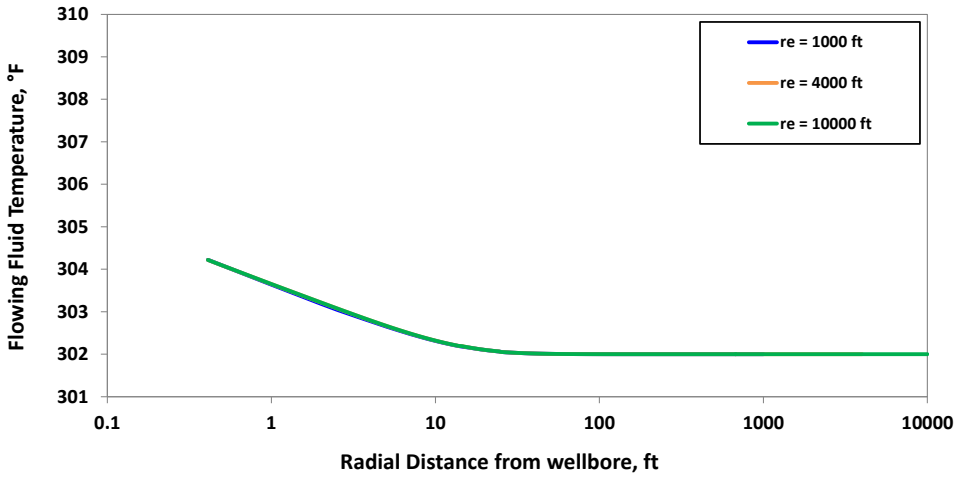

Fig. D4: A sensitivity analysis of flowing-fluid temperature in the reservoir to reservoir radius– at 50 days of 500 STB/D production

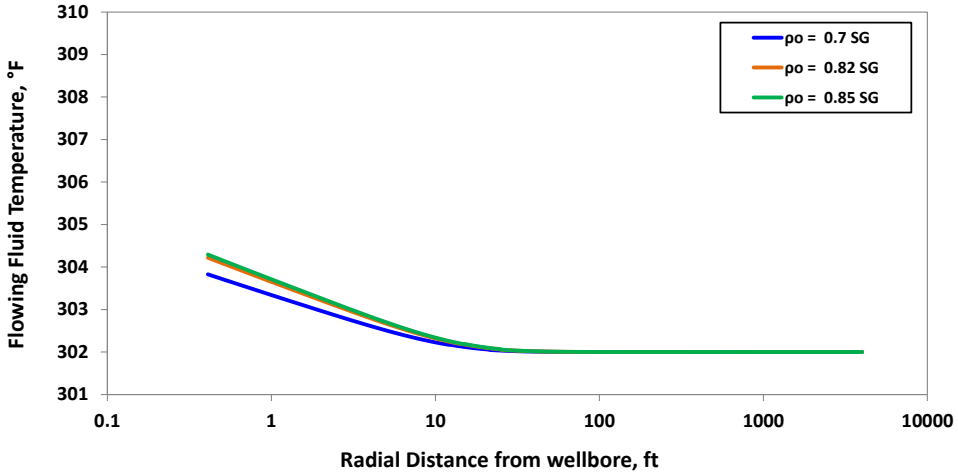

Fig. D5: A sensitivity analysis of flowing-fluid temperature in the reservoir to oil density– at 50 days of 500 STB/D production

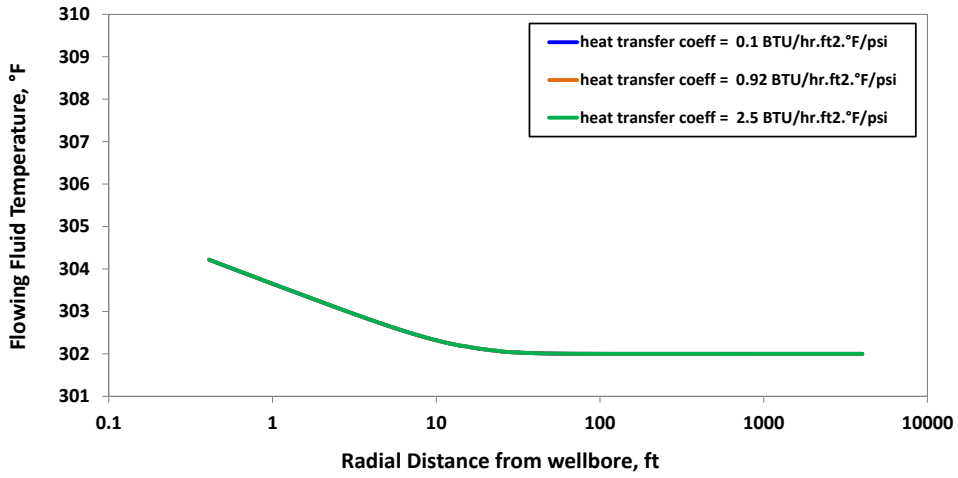

Fig. D6: A sensitivity analysis of flowing-fluid temperature in the reservoir to reservoir overall heat transfer coefficient– at 50 days of 500 STB/D production

We observe from the results that the parameters that are critical to flowing-fluid temperature estimation are reservoir permeability and J-T coefficient. The results from low rate sensitivity study perfectly agree with results from the base case study presented in Chapter IV. However, the range of possible outcomes is narrower when production rate is lower, compared to higher rate case. This is because effect of J-T heating is generally smaller in a low rate reservoir as demonstrated and discussed in Chapter III.

Heat transfer coefficient has minimal impact to flowing-fluid temperature in the low rate case and its impact at late time is no longer significant because fluid is not heated up enough to allow heat transfer from reservoir to over- and underburden formations when production rate is low. The results from the low rate sensitivity analysis assure our knowledge and findings in the base case sensitivity study, presented in Chapter IV, that fluid viscosity, production rate, reservoir permeability and J-T coefficient are critical parameters in reservoir flowing-fluid temperature evaluation.

Results from DoE analysis for low rate production case are demonstrated inFig. D7 to Fig. D9. In general, the results align very well with the sensitivity analysis and the base case DoE. As mentioned in Chapter III, at 100-ft away from the wellbore, no parameter has a significant impact on reservoir flowing-fluid temperature because J-T phenomena is less prominent in low rate production reservoir.

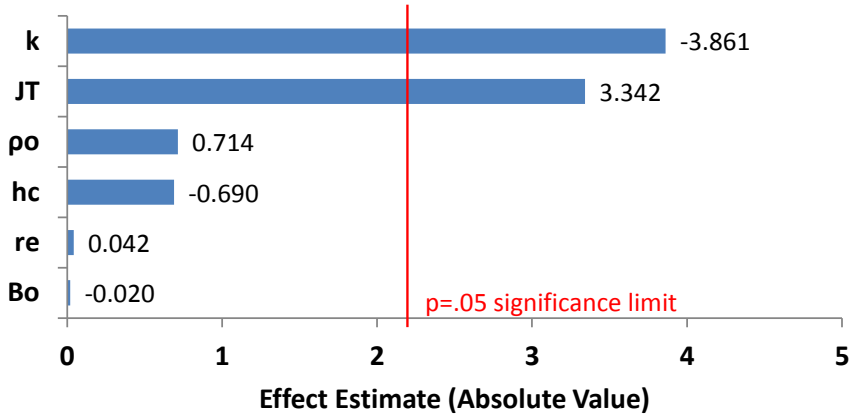

Fig. D7: Pareto chart of standardized effects for fluid temperature at **well bottom** after 50 days of 500 STB/D production

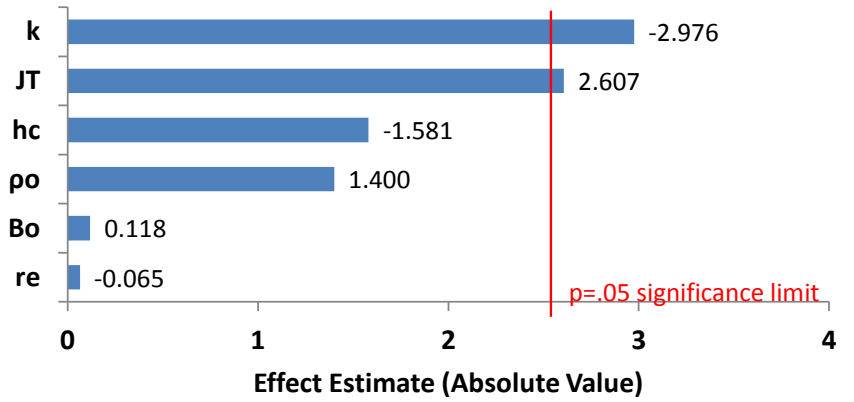

Fig. D8: Pareto chart of standardized effects for fluid temperature at **10 ft from the wellbore** after 50 days of 500 STB/D production

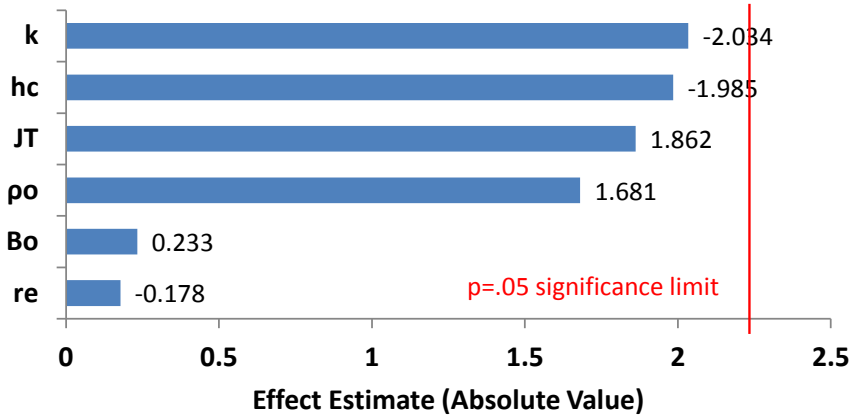

Fig. D9: Pareto chart of standardized effects for fluid temperature at **100 ft from the wellbore** after 50 days of 500 STB/D production